

3D STEM MODELLING IN TROPICAL FOREST: TOWARDS IMPROVED BIOMASS AND BIOMASS CHANGE ESTIMATES



Sébastien Bauwens
2022

COMMUNAUTÉ FRANÇAISE DE BELGIQUE
UNIVERSITÉ DE LIÈGE – GEMBLoux AGRO-BIO TECH

**3D STEM MODELLING IN TROPICAL FOREST:
TOWARDS IMPROVED BIOMASS AND BIOMASS CHANGE ESTIMATES**

Sébastien BAUWENS

Dissertation originale présentée en vue de l'obtention du grade de docteur en
sciences agronomiques et ingénierie biologique

Promoteurs : Pr Philippe LEJEUNE, Dr Sylvie GOURLET-FLEURY
Année civile : 2022

Copyright

Auteur : BAUWENS Sébastien

Dépôt de la thèse : 2022

Citation : BAUWENS Sébastien, 2022. 3D stem modelling in tropical forest: towards improved biomass and biomass change estimates. Thèse de doctorat, Gembloux Agro-Bio Tech – Université de Liège, Gembloux, 85 p.

Crédits photographiques : /

Cette œuvre est sous licence Creative Commons. Vous êtes libre de reproduire, de modifier, de distribuer et de communiquer cette création au public selon les conditions suivantes :

- Paternité (BY) : vous devez citer le nom de l'auteur original de la manière indiquée par l'auteur de l'œuvre ou le titulaire des droits qui vous confère cette autorisation (mais pas d'une manière qui suggérerait qu'ils vous soutiennent ou approuvent votre utilisation de l'œuvre) ;
- Pas d'utilisation commerciale (NC) : vous n'avez pas le droit d'utiliser cette création à des fins commerciales ;
- Partage des conditions initiales à l'identique (SA) : si vous modifiez, transformez ou adaptez cette création, vous n'avez le droit de distribuer la création qui en résulte que sous un contrat identique à celui-ci. À chaque réutilisation ou distribution de cette création, vous devez faire apparaître clairement au public les conditions contractuelles de sa mise à disposition. Chacune de ces conditions peut être levée si vous obtenez l'autorisation du titulaire des droits sur cette œuvre. Rien dans ce contrat ne diminue ou ne restreint le droit moral de l'auteur.

Abstract

Tropical forests are the main contributors of CO₂ emissions between the biosphere and the atmosphere in the land use sector. The deforestation and degradation of these forests are the main sources of emissions from this sector, which accounts for 15% of the world's CO₂ emissions. The monitoring of CO₂ emissions and removals from tropical forests requires fine measurements of their trees. These measurements are then used as inputs in allometric model to predict the tree aboveground biomass and thus indirectly their equivalent in CO₂. However, a significant proportion of trees in tropical forests show morphological singularities on the stem such as buttresses or other irregularities. The height (H_{POM}) of the diameter measured (D_{POM}) is therefore commonly raised above the buttresses to reach a circular part of the stem. The standard of measuring the diameter at breast height (DBH) is then lost. In this context, this thesis aims to improve the monitoring of tropical trees with stem irregularities by using recent three-dimensional (3D) measurement tools and developing a model-based approach to harmonize height measurements of the diameterdo.

First, we evaluated the potential of the close-range terrestrial photogrammetric approach (CRTP) to measure irregular shaped stems. The advantage of this 3D approach is its low cost and ease of implementation as it only requires a camera and targets. Following the convincing results of this approach, we studied the quality of the allometric relationship between variables extracted from the stem cross-section at 1.3 m height and above-ground biomass. We found that the equivalent diameter of the basal area at 1.3 m height (DBH') correlates better with aboveground tree biomass and thus its carbon content than does diameter above buttress (D_{POM}). Therefore, harmonization of H_{POM} to 1.3 m height should be further studied to improve biomass estimates.

Secondly, we investigated the potential of a hand-held mobile lidar scanner (HMLS) to measure in 3D not only one tree at a time but many trees from forest plots with a 15 m radius in Belgian temperate forest. To assess the HMLS, we compared it to 3D measurements made with a more commonly used static terrestrial laser scanning (TLS) and with conventional forest inventory diameter and position measurements. The HMLS has a better 3D spatial coverage of the stems than the TLS and the precision of the stem diameter measurements is also better with the HMLS. Setting up the plot and scanning it from five locations with the TLS takes three times longer than scanning with HMLS. This pioneering work shows us the potential of using HMLS in tropical forests through its speed of execution and its important spatial coverage at the stem level, an important issue for irregular shaped tree stems.

Thirdly, we developed and assessed a model-based approach for harmonizing H_{POM} to correct the bias induced by irregular stems in the aboveground biomass estimates of forest inventory plots. Following the estimation of DBH' using a taper model proposed in our study, we find that conventional aboveground biomass estimates (i.e.

with only D_{POM}), compared to estimates made with DBH', show an increasing divergence with the increase of irregular stems proportion within plots and going up to -15% in our study. These results show the importance of considering H_{POM} when estimating aboveground biomass in tropical forests, especially in forests with many irregular stems. Estimates of the evolution of plot above-ground biomass over time should also be revised to better consider the biomass growth of irregular shaped tree stems, which has been underestimated until now.

Finally, based on the results of this research, we summarize the 3D measurement tools currently available and describe their advantages and disadvantages in the case of irregular stems. Based on available human and technical resources, we also give recommendations on the harmonization method to use in permanent sampling plots to correct the bias induced by irregular stems. Improved monitoring of these tropical trees may provide a better understanding of some of the residual, i.e. unexplained, terrestrial ecosystem CO_2 sink currently noted in IPCC reports.

Résumé

Les forêts tropicales sont les principales contributrices des émissions de CO₂ entre la biosphère et l'atmosphère dans le secteur de l'affectation des terres. La destruction et dégradation des ces forêts sont les principales sources d'émissions de ce secteur qui représente 15 % des émissions mondiales de gaz à effet de serre. Le suivi des émissions et absorptions de CO₂ des forêts tropicales passe par des mesures fines des arbres qui les constituent et l'utilisation de ces mesures dans des modèles allométriques prédisant la biomasse aérienne de ces arbres et donc indirectement leurs équivalents CO₂. Cependant, une part importante d'arbres en forêt tropicale présente des singularités morphologiques sur le tronc telles que des contreforts ou d'autres irrégularités, ce qui complexifie la transformation des mesures de terrain via ces modèles allométriques. En effet, sur ces arbres, la hauteur (H_{POM}) de mesure du diamètre (D_{POM}) est classiquement rehaussée pour atteindre une partie circulaire du tronc. Le caractère standard du diamètre mesuré à hauteur de poitrine (DHP) est donc perdu. Dans ce contexte, cette thèse a pour objectif d'améliorer le suivi des arbres tropicaux présentant des irrégularités sur le tronc par l'usage d'outils de mesure en trois dimensions (3D), et de proposer une méthode qui prenne mieux en compte ces singularités morphologiques.

Tout d'abord, nous avons évalué le potentiel de l'approche photogrammétrique terrestre (CRTP) pour mesurer les troncs irréguliers. L'avantage de cette approche 3D est son faible coût et sa facilité de mise en œuvre car elle ne nécessite qu'un appareil photo et des cibles. Suite aux résultats concluants de cette approche, nous avons étudié la qualité de la relation allométrique entre des variables calculées sur la base de la surface de sections de troncs à 1,3 m de hauteur et la biomasse aérienne. Il en ressort que le diamètre équivalent à la surface de la section à 1.3 m de hauteur (DHP') présente une meilleure corrélation avec la biomasse aérienne des arbres que la mesure du diamètre au-dessus des contreforts (D_{POM}). Par conséquent une harmonisation permettant de ramener les mesures faites au-dessus des contreforts à 1,3 m est à envisager pour améliorer les estimations de biomasse.

Ensuite, nous avons étudié le potentiel d'un scanner lidar mobile (HMLS) pour mesurer en 3D non plus un seul arbre à la fois mais des placettes forestières de 15 m de rayon en forêt tempérée belge. Pour évaluer cet outil, nous l'avons comparé à des mesures 3D faites avec un scanner lidar terrestre statique (TLS) plus communément utilisé et, avec des mesures de diamètre et de position classiques d'inventaire forestier. Le HMLS présente une meilleure couverture spatiale des troncs en 3D que le TLS et la mesure du diamètre des troncs est également meilleure avec le HMLS. Le temps de mise en place et d'acquisition d'une placette en HMLS est 3 fois inférieur au temps d'acquisition de cinq scans TLS. Ce travail précurseur nous montre le potentiel de l'usage du HMLS en forêt tropicale au travers de l'importante couverture spatiale qu'il procure à hauteur des troncs et sa rapidité de mise en œuvre.

Enfin, nous avons développé et évalué une méthode d'harmonisation du H_{POM} afin de corriger le biais induit par les troncs irréguliers dans les estimations de biomasse aérienne de placettes d'inventaire. Suite à l'estimation du DHP', grâce à l'équation de défilement proposée dans notre étude, nous constatons que les estimations de biomasse aérienne faites de manière conventionnelle (c'est à dire avec uniquement D_{POM}) sont inférieures aux estimations faites avec les DHP'. Cette divergence augmente avec la proportion d'arbres à tronc irrégulier au sein des parcelles et va jusqu'à -15 % dans le cas de notre étude. Ces résultats dévoilent l'importance de la prise en compte de H_{POM} dans les estimations de biomasse aérienne des forêts tropicales, plus particulièrement dans les forêts présentant une proportion importante de troncs irréguliers. Les estimations sur l'évolution de cette biomasse aérienne au cours du temps devront également être revues afin de mieux prendre en compte la croissance en biomasse des arbres à tronc irrégulier qui est jusqu'à présent sous-estimée.

Finalement, sur base des résultats de cette recherche nous synthétisons les outils de mesures 3D actuellement disponibles et présentons leurs avantages et inconvénients respectifs dans le cas des arbres à tronc irrégulier. Des recommandations sont également données sur la manière de corriger le biais induit par ces arbres sur les estimations de stock et de changements de stocks de carbone des parcelles de suivi de croissance en fonction des moyens humains et techniques disponibles. L'amélioration du suivi de ces arbres tropicaux permettra peut-être de mieux comprendre une partie du puits de CO_2 résiduel, c'est à dire non expliqué, de l'écosystème terrestre actuellement constaté dans les rapports du GIEC.

Remerciements

Tout d'abord, je remercie tous les organismes qui ont contribué au financement de cette thèse et de mes travaux de terrain : le Fonds Français pour l'Environnement Mondial (FFEM) et l'Agence Française du Développement (AFD) qui ont co-financé le projet DynafFor par lequel mes deux premières années de thèse ont été financées ainsi que le travail de terrain à Loundoungou en République du Congo (Conventions CZZ 1636.01 D and CZZ 1636.02 E). Je remercie également les organismes CIFOR (Center for International Forestry Research), R&SD (Ressources and Synergies Development) et l'UNIKIS (Université de Kisangani), partenaires du projet REFORCO financé par l'Union Européenne et qui ont contribué au financement et à la préparation logistique de mon travail de terrain à Yangambi et à Biaro en République Démocratique du Congo. La Banque Mondiale au travers du projet PREREDD+ piloté par Nature+ qui a également financé mon travail de thèse pendant quelques mois et l'Institut de Recherche pour le Développement (IRD) pour leur support financier et logistique à Mindourou II au Cameroun.

Je tiens également à remercier celles et ceux qui m'ont accompagné et ont joué un rôle important durant le très long périple de cette thèse. Au-delà du travail scientifique que représente une thèse, c'est également une aventure humaine un peu particulière pour celui qui la mène.

Un grand merci Sylvie pour ta supervision, ton soutien et ta patience. Ce n'était pas évident de me suivre à distance. Tu étais toujours disponible dès que j'en exprimais le besoin.

Merci Philippe, c'est au travers de ton enthousiasme débordant que je me suis lancé dans cette aventure et que j'ai exploré ces outils innovants dans notre discipline initialement peu technologique. J'ai toujours eu plaisir à travailler à tes côtés, ta jovialité et ton énergie sont communicatives. Eviter la dispersion fût notre plus grand défi.

Merci Adeline, toujours présente, à l'écoute, réactive, structurante, directe et efficace. Merci pour tes relectures toujours très pertinentes. La qualité de mon travail scientifique aurait été bien moindre sans les scans de tes yeux de lynx. Ton coaching humain m'a également permis de tenir la distance.

Merci Jean-Louis pour ton soutien au lancement de ma thèse. J'ai toujours eu un profond respect pour le travail que tu mènes dans ces belles forêts tropicales.

Merci Alexandre pour ta présence et ton accueil à ton bureau. J'étais un peu perdu avec tous ces gigas de données 3D et tes conseils techniques m'ont permis de me sortir de l'ornière !

Merci Quentin pour ton accueil chaleureux en RDC et toutes les facilités que tu m'as permises dans ce pays.

Merci Coralie pour ton investissement et ta rigueur dans la mission de terrain difficile que tu as menée à Loundoungou et pour les différents moments partagés.

Merci Alain pour le travail d'ombre de nettoyage des données que tu as réalisé avec rigueur.

Merci Pierre pour ton appui et les verres qui suivirent notre travail de terrain à Mindourou II.

Thanks to Kim and Bart for your collaboration on this valuable scientific paper!

Merci à Nature+ de m'avoir permis de prolonger, de plusieurs mois, le financement de cette thèse en son début.

Merci aux sociétés forestières qui nous ont accueillis pour ces recherches, plus particulièrement Alpica et CIB-OLAM. Merci également aux professeurs F. Boyemba, L. Ndjele, C. Lomba de l'UNIKIS pour les facilités offertes en RDC.

Je tiens également à remercier toute l'équipe de forêt tempérée que j'ai côtoyée durant toutes ces années au sein de ces vieux murs de Gembloux et avec qui j'ai passé d'excellents moments. J'ai peur de vous citer au risque d'en oublier... Marie, Marie-Ange, Adrien, Gauthier, Cédric, Hugues, Jo, Nico, Peter, Steph, François 3x, Mikhail, Jérôme, Sam, Atchoum, Corentin, Chloé, Jacques... Mais également les tropicaux : Jean-Yves, Grace, Cédric et tous les autres ;)

Je terminerai ces remerciements par ma petite famille, Anne, Noah, Simon et Louis, pour m'avoir permis de ne jamais oublier le vrai ordre des priorités. Anne, merci d'avoir été là durant tout ce long processus qui ne fût pas de tout repos dans mon esprit !

Table of contents

ABSTRACT	VII
RÉSUMÉ	IX
REMERCIEMENTS	XI
TABLE OF CONTENTS	XIII
LIST OF FIGURES	XV
LIST OF TABLES	XX
ABBREVIATIONS	XXI

GENERAL INTRODUCTION

1.1 THE TROPICAL FORESTS IN THE GLOBAL CARBON BUDGET	3
1.1.1 HOW FORESTS FIT INTO THE GLOBAL CARBON BUDGET?	3
1.1.2 HOW IMPORTANT IS THE ROLE OF TROPICAL FORESTS IN THE GLOBAL CARBON BUDGET?	4
1.1.3 HOW PRECISE ARE THE CARBON STOCKS AND STOCK CHANGE ESTIMATES IN TROPICAL FORESTS?	5
1.2. THE STEM DIAMETER, A KEY FEATURE IN TROPICAL FORESTS MONITORING	7
1.2.1 WHY AND HOW MEASURING THE STEM DIAMETER?	7
1.2.2. HOW TO MEASURE THE DIAMETER ON IRREGULAR STEMS?	7
1.3. THE CURRENT METHODS TO MEASURE IRREGULAR STEM CROSS-SECTIONS	10
1.3.1 DIRECT MEASUREMENTS IN THE FIELD	10
1.3.2 MODEL-BASED APPROACHES	12
1.4. RESEARCH STRATEGY	13
1.4.1. RESEARCH GAPS AND OBJECTIVES	13
1.4.2. STRUCTURE OF THE THESIS	14

3D MEASUREMENTS OF IRREGULARLY SHAPED STEMS

2.1. PREAMBLE	18
2.2. THE SCIENTIFIC PEER-REVIEWED PAPER	19

3D STEM MEASUREMENTS AT THE PLOT-LEVEL

3.1. PREAMBLE	34
3.2. THE SCIENTIFIC PEER-REVIEWED PAPER	35

MAKING TROPICAL FOREST PLOTS COMPARABLE

4.1. PREAMBLE	54
4.2. THE SCIENTIFIC PEER-REVIEWED PAPER	55
DISCUSSION	68
<hr/>	
5.1. THE MAJOR FINDINGS	70
5.1.1 THE EFFECTIVENESS OF DIRECT 3D MEASURING TOOLS IN TROPICAL FORESTS	70
5.1.2 THE MODEL-BASED APPROACH TO OVERCOME THE CURRENT LIMITS OF 3D MEASURING TOOLS	71
5.2. THE PERSPECTIVES	72
5.2.1 WHICH 3D MEASUREMENT TOOL IN WHICH CASE FOR PERMANENT FOREST INVENTORY PLOTS?	72
5.2.2 THE CLOSE-RANGE 3D MEASUREMENT TOOLS IN OPERATIONAL PRECISION FORESTRY	74
5.2.3 THE MODEL-BASED APPROACHES TO OVERCOME THE CURRENT LIMITS OF 3D MEASURING TOOLS	75
5.3. PRACTICAL RECOMMENDATION FOR MEASURING IRREGULARLY SHAPED TREE STEMS IN PERMANENT FOREST INVENTORY PLOTS	77
REFERENCES	80
<hr/>	
APPENDICES	92
<hr/>	
APPENDIX 1 – SUPPLEMENTARY INFORMATION OF SCIENTIFIC PAPER OF CHAPTER 2: <i>TERRESTRIAL PHOTOGRAMMETRY: A NON-DESTRUCTIVE METHOD FOR MODELLING IRREGULARLY SHAPED TROPICAL TREE TRUNKS</i>	93
SI 1: DESCRIPTION OF THE LOUNDOUNGOU SITE (REPUBLIC OF CONGO).	93
SI 2: METHODOLOGY AND VALIDATION OF THE PHOTOGRAMMETRIC PROCESS.	94
SI 3: POM DEFINITION, FORMATTING BIOMASS DATA AND $D_{AREA130}$ (IE DBH')-FIELD VARIABLE RELATIONSHIPS	99
APPENDIX 2 - SUPPLEMENTARY INFORMATION OF THE SCIENTIFIC PAPER OF CHAPTER 3: <i>FOREST INVENTORY WITH TERRESTRIAL LIDAR: A COMPARISON OF STATIC AND A HAND-HELD MOBILE LASER SCANNING</i>	104
APPENDIX 3 – SUPPLEMENTARY INFORMATION OF THE SCIENTIFIC PAPER OF CHAPTER 3: <i>A 3D APPROACH TO MODEL THE TAPER OF IRREGULAR TREE STEMS: MAKING PLOTS BIOMASS ESTIMATES COMPARABLE IN TROPICAL FORESTS</i>	109

List of figures

Figure 1.1: Schematic representation of the overall perturbation of the global carbon cycle caused by anthropogenic activities, averaged globally for the decade 2009-2018. The budget imbalance is also shown in grey. This figure is from Le Quéré et al. (2017; 2009) and has been updated with data from Friedlingstein et al. (2019)..3

Figure 1.2: Error propagation from the data sources (light blue rectangles) up to the region-wide AGB estimates (light orange rectangle) by using tree aboveground biomass model (Tree AGB model) and remote sensing model (RS model). The region-wide AGB density (Mg/ha) is then used as emission factor (EF) in eq. 1.6

Figure 1.3: The international standard of the point of measurement (POM): the breast height, i.e.:1.3 m, and the practical diameter POM (D_{ref}) measured in a tropical forest with irregularly shaped tree stems such as buttresses trees. The copyright of the forest drawing belongs to Andreja Brule.8

Figure 1.4: The distribution of HPOM values higher than 1.3 m in 1 ha tropical forest plots of Central Africa (data from Ploton et al., 2020).9

Figure 1.5: Wire method to estimate the basal area of a cross-section (left: shaping the wire, right: counting the number of squares with a reference area).10

Figure 1.6: Example of a convex-concave method with measurements of the cylindrical and buttresses components (modified figure of Henry et al., 2010)..... 11

Figure 1.7: The use of Terrestrial Laser Scanning (TLS) to measure irregularly shaped tree stems (modified figure of Nölke et al., 2015)..11

Figure 1.8: Example of a model based approach based on a taper model. Measured taper data of the regular part of the stem with optical denrometer (points) and fitted taper models (lines) for individual trees. Solid lines show the best-fit curves to the measured data for each stem (solid), dashed lines show the taper curves obtained by extrapolating from the 2010 diameter measurement for each tree using the best-fit taper value for the stem, and dotted lines show the extrapolation from the 2010 diameter using the general model applied to that stem. The horizontal dashed line is the standard height at 1.3 m (modified figure of Cushman et al., 2014).....12

Figure 1.9: Conceptual framework of the thesis. Biomass changes are derived from biomass stocks estimated at two different years ($t_n = n$ years after the year t_0).....14

Figure 2.1: Workflow of the non-destructive method for the three-dimensional tree modelling suitable for large and irregularly shaped tropical trees. The main steps are (1) acquisition of photographs all around the tree, (2) location of the photographs in the three-dimensional space based on the structure-from-motion process (the blue squares in sub-Figure 2 corresponds to the photographs), (3) scaling the project with reference points and (4) generating a dense three-dimensional point cloud of the stem.

In the post-processing phase, the tree skeleton is computed (step 5) by slicing the point cloud along the z-axis and estimating the centre of each cross-section. Then, measurements of cross-sections are carried out perpendicular to the skeleton (step 6). Finally, in step 7, based on the cross-sectional measurements, the stem morphology is analysed by computing shape indices and fitting taper curves.23

Figure 2.2: Variation of the shape index DeBA (Basal Area Deficit) along the stem for 14 *C. mildbraedii* and 20 *E. cylindricum*. The coloured lines correspond to trees with contrasted diameters, and the black dots, as well as the intersection between the solid and dashed lines, indicate the position of the diameter above buttresses (DAB). Cross-sections with a DeBA below the 0.05 reference value are considered circular.25

Figure 2.3: Relationship between the shape index D_{eBA} (Basal Area Deficit) at 1.3 m height and the diameter of a disc with the same area as the basal area at 1.3 m height ($D_{area130}$).26

Figure 2.4: Biomass error of different allometric models according to the diameter used. The model m1 is the model fitted with DAB, the model m2 is the model fitted with $D_{area130}$, the Chave et al. (2005, 2014) model without height is the model for moist forest which is fitted with a mixed of DBH and DAB data, the Fayolle et al. (2013a, b) model is a local multispecies model which is fitted with a mixed of DBH and DAB data, the Chave et al. (2005, 2014) model with height is the model for moist forest requiring the height in addition to diameter and basal wood density (also fitted with a mixed of DBH and DAB data) and the Chave et al. (2014) model with height is a model requiring the height in addition to diameter and basal wood density (also fitted with a mixed of DBH and DAB data). The solid and dashed lines are local fitted lines (loess fitting with a span of 2/3), the solid line is fitted on biomass data predicted with DAB (cross symbols) and the dashed line on biomass data predicted with $D_{area130}$ (square symbols). DAB, diameter above buttresses.27

Figure 2.5: Relationships between the diameter of a disc with the same area as the basal area at 1.3 m height ($D_{area130}$) and field measurements including the diameter of the convex hull measured at 1.3 m height ($D_{ConvexHull130}$) around the buttresses (a); the height of the diameter above buttresses (H_{DAB}) (b); and the diameter above buttresses (DAB) at a variable height (c).28

Figure 3.1: Overview of the study area, with the locations of the plots (IR orthoimage with contour intervals of 20 m of elevation).37

Figure 3.2: Locations of the TLS and the spheres (left) and walking pattern for the HMLS data acquisitions (starting in red and ending in dark.39

Figure 3.3: Comparison of a 1.3 m height slice of the point cloud (thickness of 10 cm) of one *Picea abies* stem scanned with the hand-held mobile laser scanning ZEB1 and with the multiscan method (FARO5). From the left, we have the top view of the

slices, the 3D density graph of the slices, histograms of transects within the slices with bins of 5 mm (red dotted lines are transects following the x-axis and the yellow dotted line transects following the y axis) and, finally, on the right, we have an overlay of the ZEB1 slice and the FARO5 slice.42

Figure 3.4: Percentage of the cross-section closure between the three different scanning methods according to the visual interpretation of the point cloud slices at 1.3 m height (thickness of 10 cm) of the eight plots.42

Figure 3.5: DTM differences comparing different scan setups. The bias is generally low, but the slope and understory lead to variation in the generated DTMs (note that the y-axis scale is different for the two graphs).43

Figure 3.6: CHM differences comparing different scan setups.44

Figure 3.7: CHM illustration of two plots with the three different scanning methods.44

Figure 3.8: On the left, scatterplots of the DBH measured with the tape versus the DBH derived from the different LiDAR data. The dashed line shows the 1:1 line and the solid line the trend-line. On the right, the diameter difference between DBH estimates from LiDAR and DBH measured in the field with a tape (the y scale of the residual plot of FARO 1 is different to the other residual plots). The solid grey curve is composed of local fitted lines (LOESS fitting with a span of 2/3) for the species classified as smooth bark species and the long dashed red curve shows local fitted lines for the rough bark species. The y values of the horizontal dotted lines are, respectively, 3 cm and -3 cm, which are threshold values discussed in the results. ...46

Figure 4.1: Conventional (left) and original (right) workflows for plot-level aboveground biomass (AGB) stock and stock change estimates. In the original workflow, the height (H_{POM}) of the measured DPOM is harmonized at breast height (i.e., 1.3 m) and the resulting equivalent diameter at breast height (DBH') is computed with a taper model before estimating tree AGB of the trees with irregular stems in the forest inventory plots. The taper model and the AGB model used in this study are based on three-dimensional (3D) data and destructive data, respectively. In the original workflow, the AGB model has DBH as one of its predictors (i.e., D_{POM} for regular stems and DBH0 for irregular stems). The performances of the AGB model from the original workflow are tested in this study and the plot-level AGB stock and stock change estimates of the two workflows are compared. Other variables: ρ , wood density; TH, total tree height.55

Figure 4.2: Main attributes used in the taper models. The cross-section extracted from the 3D data at the standard breast height (1.3 m) is indicated with all the types of measurements used in the study.57

Figure 4.3: Taper parameter a of each taper model fitted at the tree-level (Eq. 1) and grouped by species. Solid and dotted vertical red lines represent the mean and the mean \pm SD of a across all species, respectively.59

Figure 4.4: Equivalent diameters $D_{area,i}$ along the stem. $D_{area,i}$ is predicted from (i) the taper models fitted on each tree separately (green curves) and (ii) the general model $m1$ fitted on all trees (orange curves). Curves represent $D_{area,i}$ predictions from the two approaches for five individual trees from species showing contrasted stem shapes. Ayous (*Triplochiton scleroxylon*) and Fromager (*Ceiba pentandra*) are species with well-developed buttresses. Sapelli (*Entandrophragma cylindricum*) is known to develop irregularities at the base of the stem with sometimes buttresses. Emien (*Alstonia boonei*) is a fluted species and Iroko (*Milicia excelsa*) has a more circular stem with some irregularities at the base of the stem for the largest individuals. On the right, the cross-sections of the five trees for two reference heights: the breast height (1.3 m) and the height of the point of measurement (H_{POM}) of the reference diameter (D_{POM}) located 50 cm above the irregularities. The sizes of the cross-sections are proportional within trees but not among trees.61

Figure 4.5: The 1ha plot scale relative difference on AGB stock and stock change between the reference approach Loc-DBH and approaches using D_{POM} (Loc- D_{POM} and Pan- D_{POM}) or the pantropical approach with DBH (Pan-DBH). The basal area was computed with DBH. The stock change estimates are based on a 4 years interval re-measurement.62

Figure 5.1: The increasing AGB of two virtual trees with the same D_{POM} according to the increasing size of the tree diameters D_{POM} over time. The first virtual tree has a constant 1.3m H_{POM} , D_{POM} is then equal to the so-called diameter at breast height, DBH (dark blue-green) and, the second virtual tree has its POM raised through the time (light green). For this later virtual tree, the equivalent diameter at breast height (DBH') is 12 % higher than D_{POM} (slope of the linear regression $DBH'-D_{POM}$ without intercept fitted on the trees with $H_{POM}>1.3m$ of the Congolese plots of the study in chapter 4). AGB estimates are based on the same D_{POM} corrected AGB model and with a basic wood density of 0.57 g.m⁻³ for both (Supplementary information of Bauwens et al., 2021).69

Figure 5.2: 3D measurement of stems with a smartphone using sfm process and build-in low-range LiDAR system. Screenshot of three applications built for 3D data acquisition: (a) 3D Scanner App. (b) Polycam. (c) SiteScape (Figure from Gollob et al., 2021).72

Figure 5.3: Tree-centered approaches to manage the issue of irregularly shaped tree stems in aboveground biomass monitoring in tropical forest inventory plots. The approach A is based on conventional tree measurements and, optionally, with an additional measurement: $D_{convhull130}$ (the equivalent diameter of the convex hull at 1.3m height, see text for further details) in the case of A.II and A.III. AGB- D_{POM}

allometric model is the current conventional allometric model requiring the stem diameter D_{POM} as one predictor in the model. AGB-DBH' model is as model calibrated on DBH or equivalent DBH measurement instead of D_{POM} . The approach **B** is based on close-range terrestrial photogrammetry (CRTP) or other scanning methods to extract the DBH' of the focal tree. In **C**, the whole tree is scanned with TLS and the whole aboveground woody volume is modelled and converted into aboveground biomass using conversion factor based on basic wood density. The accuracy of the aboveground biomass estimates increases from the approach *A* to *C*..... **78**

List of tables

Table 2.1: Characteristics of the three validation trees and the 34 additional trees.22

Table 2.2: Results of the regression analysis of the biomass allometric Eqn (4). .27

Table 3.1: Plot description based on field inventory data.38

Table 3.2: Acquisition and processing time for the different scanning setups (SS: FARO1, MS: FARO5, and HMLS: ZEB1).41

Table 3.3: The maximum, mean, and coefficient of variation (standard deviation/mean) of the CHM heights of the different scanning setups.44

Table 3.4: Summary statistics of DBH fitting of all the trees detected by each setup. The root mean square error (RMSE) in percentage is the RMSE divided by the mean DBH.45

Table 4.1: Aboveground biomass (AGB) models retrieved from the literature (m_{PAN}) or fitted in this study ($m_{LOC-DPOM}$ and $m_{LOC-DBH}$).59

Table 4.2: Goodness of fits of the general taper models (Eq. 2) with different fixed covariates used to predict the taper parameter $a_{i,j,k}$. The root mean square error (RMSE), the mean absolute error (MAE) and the mean error were computed over all the cross-sections as well as for cross-sections at a 1.3 m height only. The model m_1 requires $h:d_c$ covariate which is based on $D_{convHull130}$, a variable not routinely measured in forest inventory. For model m_2 , before the selection of the significant covariates in the fitting process, we only selected covariates that are based on conventional measurements in forest inventories.60

Table 4.3: General fixed parameters for the two general taper models of the table 2. The parameters correspond to the equation $a_{ijk} = (\beta_1 + b_{1,i} + b_{1,i,j} + b_{1,i,j,k}) + \beta_2 \cdot DPOM + \beta_3 \cdot h:d_c + \beta_4 \cdot h:d^2$ (Eq. 3).60

Table 4.4: Prediction error of the four approaches tested to tree-level AGB estimates with destructive AGB measurements available for 140 trees. The significance of a bias in the mean error was assessed with t-test (** for $P < 0.01$, ** for $P < 0.01$, * for $P < 0.05$, and ns for not significant). MAE is the mean absolute error.61

Abbreviations

AFOLU: Sector of Agriculture, Forestry, and Other Land Use

AGB: Aboveground biomass

ALS: Aerial Laser Scanning

CHM: Canopy Height Model

CO₂: Carbon dioxide

CRTP: Close range terrestrial photogrammetry

DBH: Diameter at breast height

D_{POM}: Reference diameter measured in the field

DAB: Diameter measured above the buttresses

DTM: Digital Elevation Model

EF: Emission factor

GHA: total tree basal area per hectare of a plot

GHG: Greenhouse gases

GNSS: Global Navigation Satellite System

HMLS: Hand-held mobile laser scanning

H_{POM}: Height of measurement of the diameter D_{POM}

IPCC: Intergovernmental Panel on Climate Change

MLS: Mobile Laser Scanning

MS: Forest inventory plot scanned with Multiple Scans of a Terrestrial Laser Scanning system

NHA: Number of trees (diameter at breast height > 10cm) per hectare of a plot

POM: Point of measurement

PLS: Personal Laser Scanning

PSP: Permanent Sample Plot

QSM: Quantitative Structure Models based on a 3D pointcloud of trees

SLAM: Simultaneous localization and mapping

Sfm: Structure from motion

SS: Forest inventory plot scanned with a single scan

TLS: Terrestrial laser scanning

VLP: Velodyne puck lidar sensor.

ZEB1: the first version of the hand-held scanner of the brand Geoslam.

1

General introduction



1.1 The tropical forests in the global carbon budget

1.1.1 How forests fit into the global carbon budget?

Current human activity profoundly affects the environment, from Earth's major biogeochemical cycles to the evolution of life, leading to a new geological epoch: the Anthropocene (Lewis and Maslin, 2015). The human alteration of biogeochemical cycles has been long recognized (Vitousek, 1992) and specifically that of the carbon cycle (Vitousek et al., 1986). The total net land-atmosphere flux of CO₂ on both managed and unmanaged lands provided a global net removal from 2007 to 2016 according to models: -6.0 ± 3.7 GtCO₂ yr⁻¹ (Jia et al., 2019; yellow rectangle in **Figure 1**). This net removal comes from two main components: (i) The net anthropogenic emissions from the sector of Agriculture, Forestry and Other Land Use (AFOLU) which are 6 ± 3 Gt CO₂ yr⁻¹ and mainly driven by land cover change, including deforestation and afforestation/reforestation, and wood harvesting, and (ii) modelled net removals due to non-anthropogenic processes are 12 ± 3 Gt CO₂ yr⁻¹ on managed and unmanaged lands, driven by environmental changes such as increasing CO₂, nitrogen deposition and climate changes (accounting for the removal of 29% of the CO₂ emitted from all anthropogenic activities: fossil fuel, industry and AFOLU).

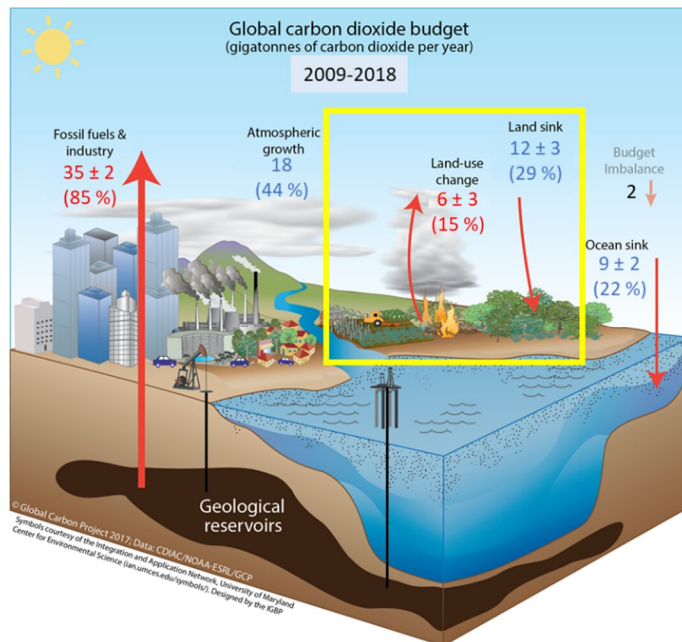


Figure 1.1: Schematic representation of the overall perturbation of the global carbon cycle caused by anthropogenic activities, averaged globally for the decade 2009-2018. The budget imbalance is also shown in grey. This figure is from Le Quéré et al. (2017; 2009) and has been updated with data from Friedlingstein et al. (2019).

1.1.2 How important is the role of tropical forests in the global carbon budget?

The aboveground tropical forest growing stock is around 200 - 250 Gt C (Avitabile et al., 2016; Baccini et al., 2012; Saatchi et al., 2011), about a fifth to a quarter much of the carbon held in the atmosphere or about half of the reserve of coal (Friedlingstein et al., 2019). This pool is however very dynamic through the photosynthesis and the respiration processes leading to large forest-atmosphere fluxes. Given these large fluxes, a small proportional change in either the uptake or the release of CO₂ can result in a large net source or sink (Mitchard, 2018). Many drivers can affect these CO₂ fluxes at different spatial and temporal scales as the air temperature, rainfalls, forest fire, harvest, deforestation, afforestation/reforestation, increase in atmospheric CO₂ concentration (CO₂ fertilisation), and nitrogen deposition (Jia et al., 2019). Depending on the spatial and time scale, anthropogenic activities are directly or indirectly related to these drivers.

The largest potential for reducing AFOLU emissions is through reduced deforestation and forest degradation (0.4–5.8 Gt CO₂-eq yr⁻¹, Jia et al. 2019), activities that are mainly occurring in the tropics (Butsic et al., 2015; Moutinho et al., 2016; Zarin et al., 2016). Besides preserving carbon stocks, the tropical forest has also a second carbon beneficial effect of keeping a land use with a net sink in the case of the remaining structurally intact tropical forests (Lewis et al., 2009; Pan et al., 2011; Phillips and Lewis, 2014; Zarin et al., 2016). This second beneficial effect is nevertheless expected to slow down in the climate-changing future (McDowell et al., 2020; Phillips et al., 2009; Rowland et al., 2015) and seems to be already less important (Brienen et al., 2015; Hubau et al., 2020). Shortly, tropical forests are likely to become a carbon source, owing to continued forest loss and the effect of climate change on the ability of the remaining forests to capture excess atmospheric carbon dioxide (Mitchard, 2018). Note these sink estimates and trends are accompanied by high uncertainties (Jia et al., 2019; Mitchard et al., 2013; Mitchard, 2018; Phillips and Lewis, 2014).

1.1.3 How precise are the carbon stocks and stock change estimates in tropical forests?

Based on IPCC guidelines (2006, 2019), monitoring the forest land annual emissions and removals of greenhouse gases (GHG) requires subdividing this category into managed and unmanaged lands. Managed lands category, defined as “land where human interventions and practices have been applied to perform production, ecological or social functions”, is sub-divided into the forest land remaining forest land (including activities such as logging), deforestation and afforestation/reforestation. The two last sub-categories are land-use changes while no land-use change is occurring in the first category. The emissions and removals of GHG from these lands are estimated following the general equation 1.

$$E = A \times EF$$

Équation 1

Where, E= GHG emissions in tons of CO₂eq; A = activity data relating to the emission source (can be an area, animal numbers or mass unit, depending on the source type) and EF = emission factor for a specific gas and source category, tons per unit of A.

Tropical forest lands are a key category that requires the most accurate estimates of the emissions and removals of GHG. In the case of the subcategory of deforestation, estimating the emissions would be a major challenge without the use of remote sensing data for remote regions as in many parts of the tropics. Spaceborn remote sensing data combined with ground measurements play a key role in determining the loss of forest cover and their fluxes (Achard et al., 2007). The uncertainty on the emissions would then depend on the uncertainty of forest biomass estimates at the pixel level combined with the number of samples, i.e., the number of pixels within the area deforested (EF uncertainty) and the uncertainty related to the detection of the pixel deforested (A uncertainty).

The uncertainty around EF is the result of error propagation from field measurements up to mean aboveground biomass (AGB) density estimates (Mg of aboveground biomass per hectare; **Figure 1.2**). To illustrate the uncertainty related to biomass estimates at a very large scale Mitchard et al. (2013) compared two well known pan-tropical biomass maps based on medium resolution imagery (500 m – 1000 m) and showed substantial differences in pixel AGB values with a little consistency in the direction of the difference. Note that none of the data layers used (imagery and RADAR) to capture the variations of forest biomass are sensitive to the range of biomass values found in tropical forests and often saturate at low biomass values (Mitchard et al., 2013).

The state-of-the-art remote sensing technology for dendrometrics estimates, the Aerial Laser Scanning (ALS, Zolkos et al. 2013) with an area-based approach for modelling plot AGB, could estimate regional/national AGB density with an error of around 5 % (Chen et al., 2016). This is an error similar to the estimates from design-

based approach with conventional forest inventory plot data but with the advantage to be spatially explicit (Chen et al., 2016).

The uncertainties in tropical forest biomass estimates from remote sensing data (medium-resolution imagery, RADAR or ALS) are based on the assumption of no bias throughout the whole workflow from field measurements to biomass maps (Figure 1.2; Chen et al., 2016, 2015). Nevertheless, an important bias might come from the choice of the allometric biomass model used to convert tree field measurement to aboveground biomass (Chave et al., 2004; Chen et al., 2016; Molto et al., 2013; Zhao et al., 2012). Moreover, the absence of bias in the measurement of one of the main features to predict the AGB, the stem diameter, is not guaranteed as we will see in the next section (Clark, 2002; Cushman et al., 2014; Dean et al., 2003; Metcalf et al., 2009; Muller-Landau et al., 2014).

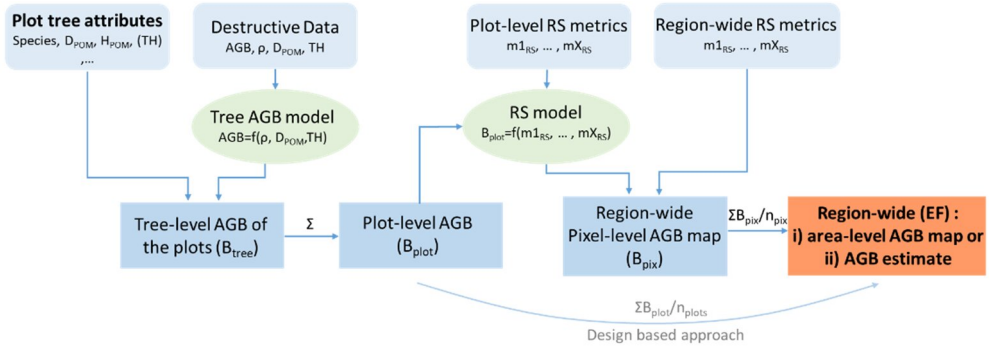


Figure 1.2: Error propagation from the data sources (light blue rectangles) up to the region-wide AGB estimates (light orange rectangle) by using tree aboveground biomass model (Tree AGB model) and remote sensing model (RS model). The region-wide AGB density (Mg/ha) is then used as emission factor (EF) in eq. 1.

1.2. The stem diameter, a key feature in tropical forests monitoring

1.2.1 *Why and how measuring the stem diameter?*

The most important and easiest variable to measure in the field is the stem diameter at the base of the tree. At the tree level, diameter is a proxy of tree size, which is an important life-history trait that determines the probability of regular fruiting (Plumptre, 1995). The diameter is also strongly related to the other descriptors of tree size such as total height (Feldpaush et al. 2011, Banin et al. 2012) and crown dimensions (Antin et al. 2013). Diameter is thus a key predictor to estimate stem and tree volume (Belyea, 1931; Fayolle et al., 2013b; Nogueira et al., 2006) and biomass (Chave et al., 2014, 2005). At the stand level, the distribution of diameters is used to describe stand structure (Rondeux, 1993) and recovery after disturbance. Successive diameter measurements of trees in permanent sample plots (**PSP**) enable the quantification of tree growth (Clark and Clark, 1999; Swaine et al., 1987), wood production (Banin et al., 2014), and forest-level carbon budgets (Clark, 2002; Coomes et al., 2014; Pan et al., 2011).

In PSP, tree diameter is repeatedly measured at the same location on the stem (location defined as the “point of measurement - POM” and its related height: H_{POM}). The international standard for H_{POM} is “at breast height,” and the corresponding diameter is called the diameter at breast height (DBH, Belyea, 1931). This breast height is generally defined as 1.3 m above ground level (Alder and Synnott, 1992; Bruce and Schumacher, 1950), but there are still local variations (e.g. 4.5 ft in the USA and 1.5 m in the South of Belgium). In forest inventories, special recommendations have been made for trees on slopes, leaning trees, forked trees, and trees with local deformation at breast height (Alder and Synnott, 1992; Cailliez and Alder, 1980; Condit et al., 1998; Forbes and Meyer, 1955; Picard and Gourlet-Fleury, 2008; Rondeux, 1993). However, there is no standardized protocol for irregularly shaped stems such as fluted or buttressed trees and trees with stilt roots, even though they are abundant in tropical forests.

1.2.2 *How to measure the diameter on irregular stems?*

Handbooks and technical papers recommend moving the H_{POM} above the buttresses or the stilts to reach a regular part of the stem (**Figure 1.3**). In the case of buttressed trees, Alder and Synnott (1992) recommended using a height of at least 1 m above buttresses so that the POM can remain the same for a decade or more and does not require continual upward adjustment. In some permanent sample plots, diameter measurements have been moved up 30 cm above the buttresses (Cailliez and Alder, 1980), as in Marcá Island, Brazil (Thompson et al., 1992), or 50 cm above the buttresses, as in Barro Colorado Island, Panama (Condit, 1998) and the Amazonian plots of the RAINFOR network (Phillips et al., 2015). Alternatively, focusing on tropical African forests where trees are known to achieve larger diameters (Slik et al.,

2013) and show huge deformations at breast height (Chapman et al., 1998; Letouzey, 1982), Picard and Gourlet-Fleury (2008) recommended fixing the H_{POM} at a standardized height of 4.5 m for all trees belonging to species that develop buttresses. This recommendation was adopted in Mbaïki, Central African Republic (Gourlet-Fleury et al., 2013) and the Central African plots of the DynAffor network (www.dynaffor.org). In the case of fluted trees, two contrasting options have been recommended: either the selection of the POM arbitrarily above the deformation (Alder and Synnott 1992, Condit et al. 1998) or measuring the perimeter of the convex hull of the stem at the standard 1.3 m height (Phillips et al., 2015).

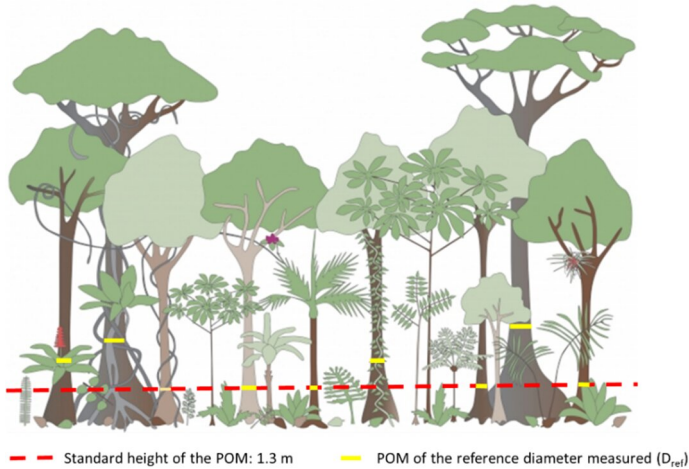


Figure 1.3: The international standard of the point of measurement (POM): the breast height, i.e.: 1.3 m, and the practical diameter POM (D_{ref}) measured in a tropical forest with irregularly shaped tree stems such as buttresses trees. The copyright of the forest drawing belongs to Andreja Brule.

Despite the development of regional and worldwide PSP networks, a standard for measuring the reference diameter for all morphological stem types is still missing. Moreover, the occurrence of irregularities is highly variable in the different forest types and stands, increasing the difficulty of comparing the plots/stands/forest types on the basis of derived diameter metrics as basal area or AGB (Cushman et al., 2021, 2014; Muller-Landau et al., 2014). The information of a higher H_{POM} than the standard height of 1.3 m is an indirect indicator of the presence of irregularities at the breast height in forest inventory plots. **Figure 1.4** shows the importance and the variability of the number of trees with $H_{\text{POM}} > 1.3\text{m}$ in 1 ha plots in Central Africa.

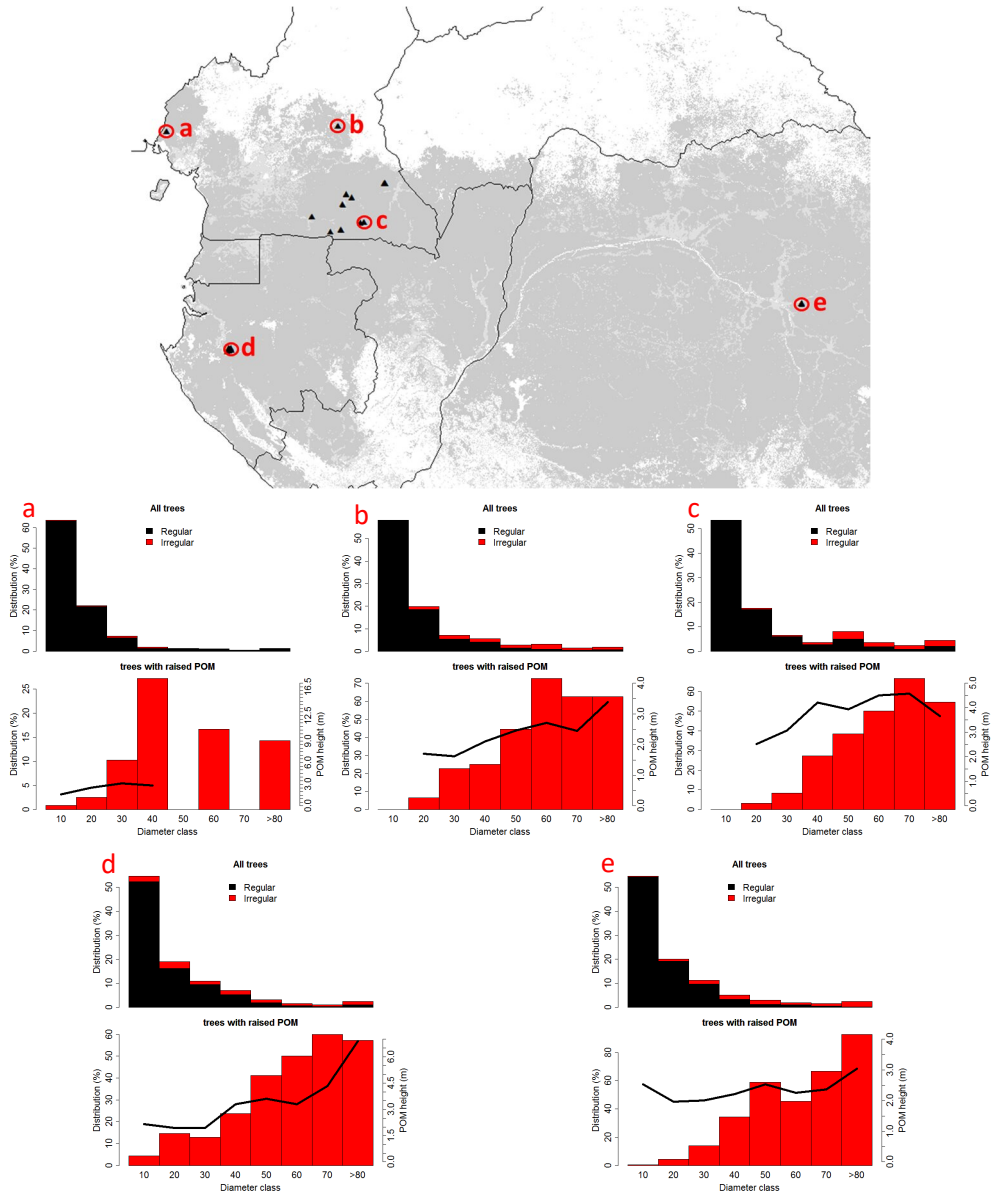


Figure 1.4: The distribution of H_{POM} values higher than 1.3m in 1 ha tropical forest plots of Central Africa (data from Ploton et al., 2020).

1.3. The current methods to measure irregular stem cross-sections

1.3.1 Direct measurements in the field

To accurately measure the basal area and the volume of irregular stems, a variety of methods, including destructive and non-destructive approaches, have been proposed. Destructive methods have been used to develop allometric equations. The irregular parts of stems are logged, and the cross-sections are measured based on georeferenced photographs and digitalization of the outline of the sections (Dean and Roxburgh, 2006; Fayolle et al., 2013a) or drawings on large sheets of paper (Nogueira et al., 2006).



Figure 1.5: Wire method to estimate the basal area of a cross-section (left: shaping the wire, right: counting the number of squares with a reference area).

Non-destructive approaches include the wire method, the convex-concave method and the Terrestrial Laser Scanning (TLS) method. The wire method uses two wires pressed against the irregular stem to shape the cross-section. The shaped wires are then put on a wooden board with a grid and the area of the cross-section is estimated by counting the squares enclosed within the wire (Figure 1.5, Ngomanda et al., 2012). Nevertheless, the flexibility of the wire and the square counting may lead to measurement errors.

The convex-concave method requires various measurements of all convex (spurs) and concave parts (flutes) of the stem to finally model the trunk as an arrangement of a cylindrical element and buttress elements (Figure 1.6; Dean and Roxburgh, 2006; Henry et al., 2010). The simplification of the stem morphology may not be in accordance with the real volume of this irregular part of the stem (Nölke et al., 2015).

The TLS method consists of scanning the tree from different points of view. In tropical forests, this last method is mainly used to model the aboveground volume of the trees. The volume is estimated by fitting geometrical primitives such as cylinders on the resulting 3D point cloud of the scanned trees. The main approach for this fitting process is the so-called quantitative structure models (QSMs; Du et al., 2019; Hackenberg et al., 2015; Raunonen et al., 2013; Trochta et al., 2017). In the case of

irregularly shaped part of the stems, meshing (Nölke et al., 2015; Takoudjou et al., 2018) or fitting free-form curves on the cross-sections (Gollob et al., 2020; Pfeifer and Winterhalder, 2004) are alternatives to the conventional fitting process of cylinders. Nevertheless, only the study of Nölke et al. (2015) used TLS data to address the issue of the buttresses in the context of forest inventory measurements (Figure 1.7).

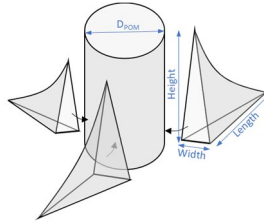


Figure 1.6: Example of a convex-concave method with measurements of the cylindrical and buttresses components (modified figure of Henry et al., 2010).

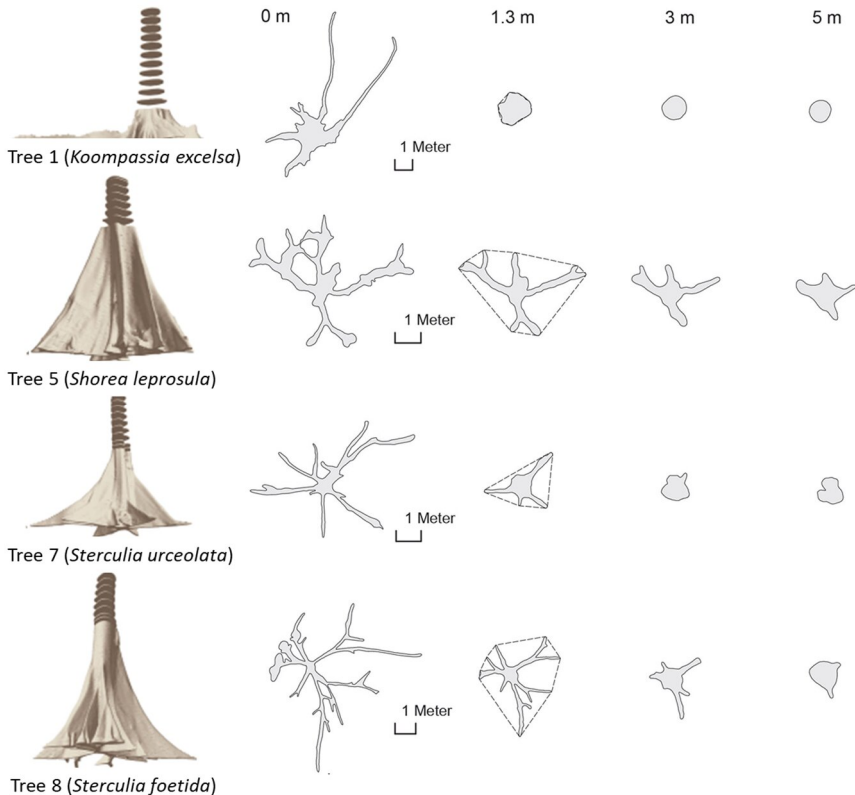


Figure 1.7: The use of Terrestrial Laser Scanning (TLS) to measure irregularly shaped tree stems (modified figure of Nölke et al., 2015).

1.3.2 Model-based approaches

Instead of measuring the basal area at 1.3 m height of the irregular stems, models can be used to estimate this basal area from other stem measurements (covariates) as the diameter above the buttresses (DAB or more general: D_{POM}) and the H_{POM} . These models can be empirical models (Ngomanda et al., 2012) or taper models (Cushman et al., 2021, 2014). The former method will relate the basal area at 1.3m height to covariates without assumptions on the form of the model. The dependency of the model to the calibration data is high and should be only used in the range of the calibration data.

In this latter method, Cushman et al. (2014) suggest measuring diameters of the upper regular part of the stem (i.e. above the buttresses) to calibrate a taper model and project that taper downward up to 1.3 m height (**Figure 1.8**). This approach of the taper model method assumes that the equivalent regular diameter at 1.3m height is highly related to above-ground biomass but this hypothesis was not tested with reference biomass data. Based on 3D data, measuring only the regular part of the stems is not anymore required and taper model could be fitted on cross-sections from the irregular part of the stem as well to increase the consistency of the taper model.

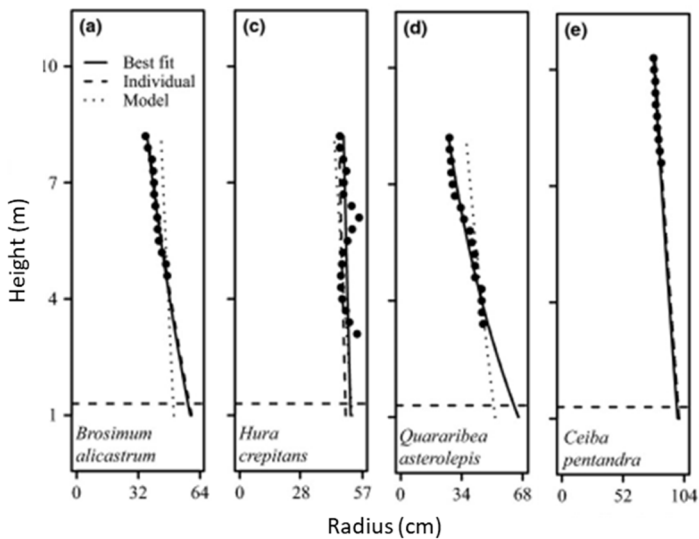


Figure 1.8: Example of a model based approach based on a taper model. Measured taper data of the regular part of the stem with optical denrometer (points) and fitted taper models (lines) for individual trees. Solid lines show the best-fit curves to the measured data for each stem (solid), dashed lines show the taper curves obtained by extrapolating from the 2010 diameter measurement for each tree using the best-fit taper value for the stem, and dotted lines show the extrapolation from the 2010 diameter using the general model applied to that stem. The horizontal dashed line is the standard height at 1.3 m (modified figure of Cushman et al., 2014).

1.4. Research strategy

1.4.1. Research gaps and objectives

Conventional forest inventory measurement tools (graduated tape and caliper) assume circularity in the cross-sections adding many challenges to the monitoring of irregularly shaped tree stems (Clark, 2002; Cushman et al., 2014; Dean et al., 2003; Metcalf et al., 2009; Muller-Landau et al., 2014; Talbot et al., 2014). First studies on the use of 3D measurement tools such as TLS is showing great potential for improving the monitoring of irregularly shaped stems (Nölke et al., 2015) and require further investigations in the context of closed dense tropical forests.

Current tropical tree AGB models do not take into account the bias coming from the calibration data that include irregularly shaped tree stems with nonstandard H_{POM} (Cushman et al., 2014; Muller-Landau et al., 2014; Nölke et al., 2015). While the error due to the AGB model choice is the largest source of error in AGB density estimates (Mg of AGB/ha, Picard et al., 2015), no studies were conducted to assess the magnitude of the ‘allometric’ error coming from nonstandard H_{POM} .

The nonstandard H_{POM} of a large proportion of emergent trees in the upper crown layer leads to a systematic error in AGB stock estimates (Cushman et al., 2014). Indeed, in tropical forests, the largest proportion of irregularly shaped tree stems is usually encountered in these emergent trees (Nölke et al., 2015; Zhiyuan et al., 2013). While these emergent trees account for a large fraction of tropical forest biomass (Bastin et al., 2015; Lutz et al., 2012; Slik et al., 2013), the impact of nonstandard H_{POM} on plot biomass estimates requires further investigations (Cushman et al., 2014; Muller-Landau et al., 2014).

The main bottom approach for investigating forest carbon fluxes is repeated censuses of trees in plots. Current measurement procedures for irregularly shaped tree stems as buttressed trees introduce systematic error in plot-level estimates of biomass change. The H_{POM} of buttressed trees is often moved upwards as buttresses grow. Because of the tree stems taper (diameter decreases with height), biomass growth in buttressed individuals tends to be underestimated. Methods have been introduced to correct biomass growth estimates in individual trees for measurement height increases (Talbot et al., 2014); however, these methods change the distribution of H_{POM} over time, introducing biases in plot-level estimates of biomass change. The magnitude of this error is nevertheless difficult to apprehend since biomass production is not driven by large trees (Ligot et al., 2018). Therefore, it remains unclear how the abundance of trees with irregular stem bases could affect estimates of stand biomass productivity and carbon capture.

The **general objective** of the thesis is to improve the monitoring of large tropical trees with stem irregularities by exploring advanced 3D measuring tools.

The **specific objectives** are i) to identify effective nondestructive measurement tools for measuring irregularly shaped stems at the tree level and the plot level, ii) to propose an effective method to better take into account the singularities generated by the irregularities of some stems in the monitoring of tropical forest biomass and finally, iii) to assess the impact of a better consideration of the irregularly shaped stems in the aboveground biomass stock and stock changes at the plot level.

1.4.2. Structure of the thesis

The conceptual framework of this thesis follows the conventional workflow to estimate the aboveground growing stock volume or biomass of a forest with a special focus, at each step of the workflow, on the issue of nonstandard points of measurement (**Figure 1.9**).

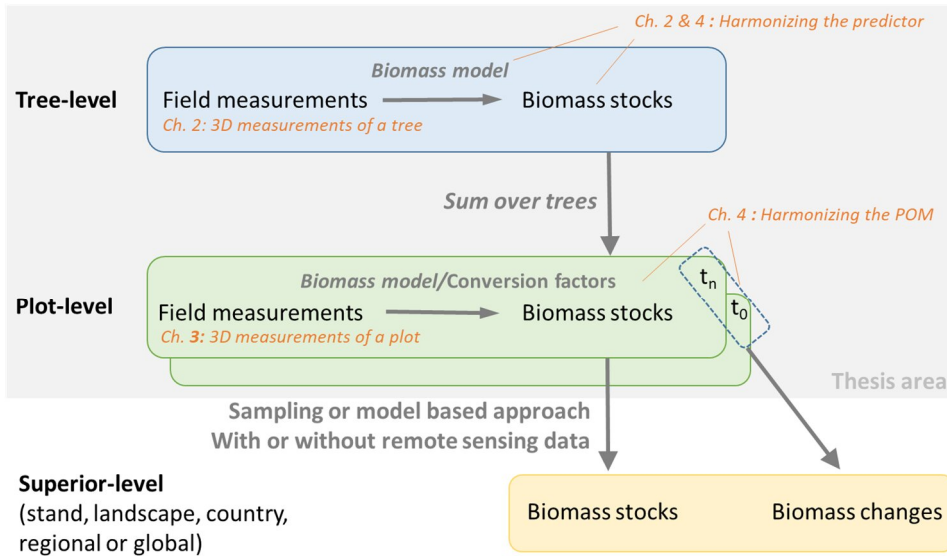


Figure 1.9: Conceptual framework of the thesis. Biomass changes are derived from biomass stocks estimated at two different years ($t_n = n$ years after the year t_0).

In **Chapter 2**, we studied the original close-range terrestrial photogrammetric approach (CRTP or also called structure-from-motion: SfM) to measure the basis of the irregularly shaped stem of some tropical trees and assessed its impact in terms of aboveground biomass estimates. Specifically, we developed the entire workflow to extract cross-sections along the stems from the resulting 3D data of the CRTP approach. We also disentangled the effects of H_{POM} in the development (fitting) of AGB models and its impact on tree AGB estimates.

This study was published in *Methods in Ecology and Evolution*, in an article entitled ‘Terrestrial photogrammetry: a non-destructive method for modelling irregularly shaped tropical tree trunks’ (Bauwens et al., 2017).

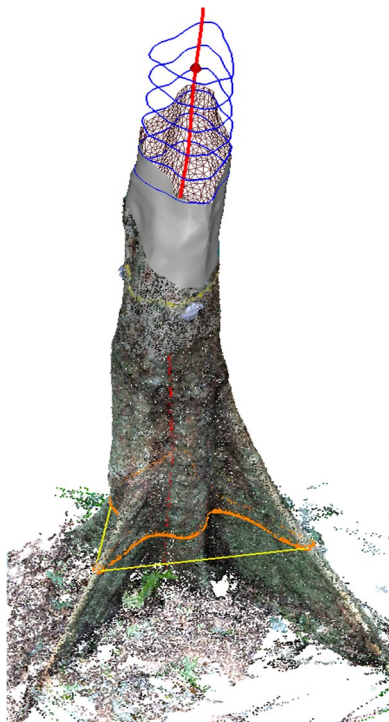
In **Chapter 3**, we explored plot-level 3D measurement methods to have exhaustive 3D measurements of the trees within a focal area. The 3D methods studied are terrestrial laser scanning (TLS) approaches and hand-held mobile laser scanning tool (HMLS) in forests close to our research lab in Belgium. This study was published in *Forests*, in an article entitled ‘Forest Inventory with Terrestrial LiDAR: A Comparison of Static and a Hand-Held Mobile Laser Scanning’ (Bauwens et al., 2016). The forerunner results of this study were the first stage before going further in the use of these technologies to measure in 3D all the stems in tropical forest plots.

In **Chapter 4**, we used the 3D measurement tools identified in **Chapter 2 (CRTP)** and in **Chapter 3 (TLS)** to collect 3D data on 228 trees across 3 sites located respectively in southeastern Cameroon (n=40), in northern Congo Republic (n=102) and northern Democratic Republic of Congo (n=86). We analyzed the taper of these trees with irregularities in the stem to harmonize the H_{POM} at the standard height of 1.3 m. As in Chapter 2, we disentangled the effects of H_{POM} in the development (fitting) of AGB models and its impact on tree AGB estimates. We finally analyzed the effect of this harmonization for AGB stocks and stock change estimates at the plot level. This study was published in *Ecological Applications*, in an article entitled: ‘A 3D approach to model the taper of irregular tree stems: making plots biomass estimates comparable in tropical forests’ (Bauwens et al., 2021).

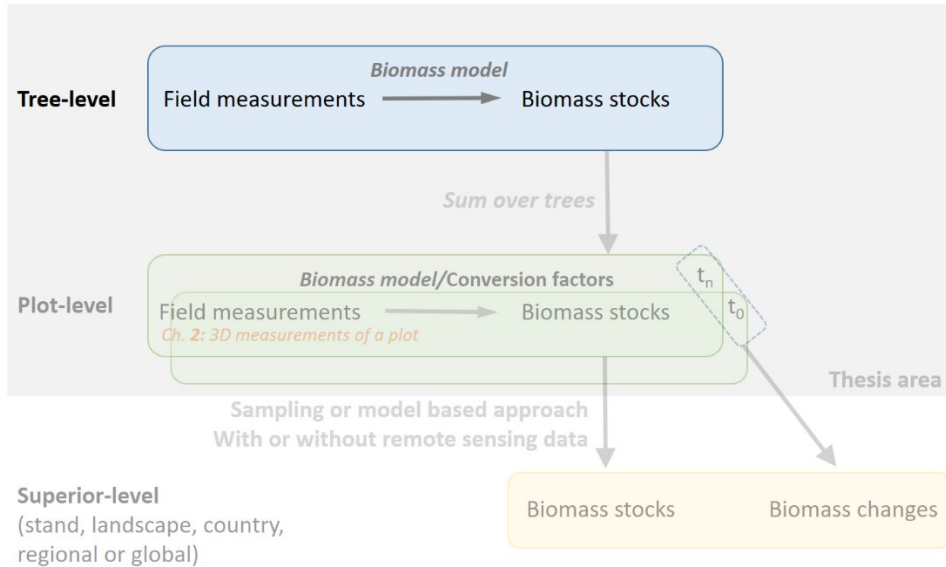
In **Chapter 5**, the main results and achievements of the thesis are summarized and discussed. We discuss the perspective of the 3D measurement tools.

2

3D measurements of irregularly shaped stems



2.1. Preamble



In this chapter, we aimed to develop a new method based on terrestrial close-range photogrammetry for measuring and modeling irregular stems. This approach is cheap and easy to implement in the field as it only requires a camera and a graduated rod. We validated the approach with destructive cross-section measurements along the stem of three buttressed trees. To demonstrate the broader utility of this method, we extended the validated approach to 43 additional trees belonging to two species: *Celtis mildbraedii* (Ulmaceae) and *Entandrophragma cylindricum* (Meliaceae). Based on the 3D models, we computed shape indices for each tree, and we analyzed the stem morphology of the two species. Finally, we analyzed some standardized predictors for the estimation of above-ground biomass.

This chapter is written in the following scientific peer-reviewed paper: Bauwens, S., Fayolle, A., Gourlet-Fleury, S., Ndjele, L. M., Mengal, C., & Lejeune, P. (2017). Terrestrial photogrammetry: a non-destructive method for modelling irregularly shaped tropical tree trunks. *Methods in Ecology and Evolution*, 8(4), 460-471.

2.2. The scientific peer-reviewed paper

Methods in Ecology and Evolution 2017, 8, 460–471

doi: 10.1111/2041-210X.12670

Terrestrial photogrammetry: a non-destructive method for modelling irregularly shaped tropical tree trunks

Sébastien Bauwens^{1*}, Adeline Fayolle¹, Sylvie Gourlet-Fleury², Leopold Mianda Ndjele³, Coralie Mengal⁴ and Philippe Lejeune⁴

¹TERRA Research Centre, Central African Forests, Gembloux Agro-Bio Tech Université de Liège, Passage des déportés 2, 5030 Gembloux, Belgium; ²UPR Bsef, CIRAD, F-34398 Montpellier, France; ³Département d'Ecologie et de Gestion des ressources végétales, University of Kisangani, BP2012 Kisangani, Democratic Republic of Congo; and ⁴BIOSE Research Unit, Gembloux Agro-Bio Tech, University of Liège, Passage des Déportés 2, 5030 Gembloux, Belgium

Summary

1. Irregularly shaped trees including trees with buttresses, flutes or stilt roots are frequent in tropical forests. The lack of an international standard to measure the diameter of such trees leads to high uncertainties in biomass estimation, tree growth and carbon budget monitoring.
2. In this study, we developed a new method based on terrestrial close-range photogrammetry for measuring and modelling irregular stems. This approach is cheap and easy to implement in the field as it only requires a camera and a graduated rod. We validated the approach with destructive cross-section measurements along the stem of three buttressed trees. To demonstrate the broader utility of this method, we extended the validated approach to 43 additional trees belonging to two species: *Celtis mildbraedii* (Ulmaceae) and *Entandophragma cylindricum* (Meliaceae). Based on the three dimensional models, we computed shape indices for each tree, and we analysed the stem morphology of the two species. Finally, we analysed some standardized predictors for the estimation of above-ground biomass.
3. We found a high concordance between diameters derived from the photogrammetric process and destructive diameter measurements along the stem for the three calibration trees. We found that *C. mildbraedii* develop much stronger irregularities than *E. cylindricum*. We also identified a large intraspecific variation in trunk morphology for *E. cylindricum*. The basal area at 1.3 m height ($D_{\text{area}130}$) seems to be a more robust predictor for biomass estimates (lowest Akaike information criterion and relative squared error) than diameter measured above buttresses (DAB) or diameter at breast height estimated from available taper model. Finally, $D_{\text{area}130}$ might be estimated with a good precision [root mean square error (RMSE) < 5%] with linear model based on the field measurements DAB and the perimeter of the convex hull of the buttresses at 1.3 m height ($D_{\text{convhull}130}$).
4. In this study, we showed the high potential of the photogrammetry for measuring and modelling irregular stems. Photogrammetry could then be used as a non-destructive measurement tool to produce correction factors for standardizing the diameter of irregular stems at a reference height which is a key issue in tree growth monitoring and biomass change estimation.

Key-words: above-ground biomass, buttress, diameter above the buttresses, permanent sample plot, point of measurement, shape index, structure from motion, taper model, three dimensional modelling, tropical forest

Introduction

Tropical forests are species-rich and structurally complex ecosystems. Understanding the functioning of these ecosystems and their role in the global carbon cycle requires detailed and repeated tree measurements (Pan *et al.* 2011; Banin *et al.* 2014; Coomes, Burslem & Simonson 2014).

The most important and easiest variable to measure in the field is trunk diameter at the base of the tree. At the tree level, diameter is strongly related to the other descriptors of tree size

such as total height (Feldpausch *et al.* 2011; Banin *et al.* 2012) and crown dimensions (Antin *et al.* 2013). Diameter is thus a key predictor to estimate stem and tree volume (Belyea 1931; Nogueira, Nelson & Fearnside 2006; Fayolle *et al.* 2013b) and biomass (Chave *et al.* 2005, 2014). At the tree level, diameter is a proxy of tree size, which is an important life-history trait that determines the probability of regular fruiting (Plumptre 1995). At the stand level, the distribution of diameters is used to describe stand structure (Rondeux 1993) and recovery after disturbance. Successive diameter measurements of trees in permanent sample plots enable the quantification of tree growth (Swaine, Lieberman & Putz 1987; Clark & Clark 1999), wood production (Banin *et al.* 2014) and forest-level carbon budgets

*Correspondence author. E-mail: bauwens.sebastien@gmail.com

(Clark 2002; Pan *et al.* 2011; Coomes, Burslem & Simonson 2014).

MEASURING TREE DIAMETER

In permanent forest plots, tree diameter is repeatedly measured at the same reference height (defining the 'point of measurement', POM). The international standard for POM is 'at breast height', and the corresponding diameter is called the diameter at breast height (DBH, Belyea 1931). This breast height is generally defined as 1.3 m above ground level (Bruce & Schumacher 1950; Alder & Synnott 1992), but there are still local variations (e.g. 4.5 ft in the USA and 1.5 m in Belgium). In forest inventories, special recommendations have been made for trees on slopes, leaning trees, forked trees and trees with local deformation at breast height (Forbes & Meyer 1955; Cailliez 1980; Alder & Synnott 1992; Rondeux 1993; Condit 1998; Picard & Gourlet-Fleury 2008). However, there is no standardized protocol for irregularly shaped stems such as fluted or buttressed trees and trees with still roots, even though they are abundant in tropical forests.

DEALING WITH TREE IRREGULARITIES

Handbooks and technical papers recommend moving the POM above the buttresses or the stilts to reach a regular part of the stem. In the case of buttressed trees, Alder & Synnott (1992) recommended using a height of at least 1 m above buttresses so that the POM can remain the same for a decade or more and does not require continual upward adjustment. In some permanent sample plots, diameter measurements have been moved up 30 cm above the buttresses (Cailliez 1980), as in Marcá Island, Brazil (Thompson *et al.* 1992), or 50 cm above the buttresses, as in Barro Colorado Island, Panama (Condit 1998), and in the Amazonian plots of the RAINFOR network (Phillips *et al.* 2015). Alternatively, focusing on tropical African forests where trees are known to achieve larger diameters (Slik *et al.* 2013) and show huge deformations at breast height (Letouzey 1982; Chapman, Kaufman & Chapman 1998), Picard & Gourlet-Fleury (2008) recommended fixing the POM at a standardized height of 4.5 m for all trees belonging to species that develop buttresses. This recommendation was adopted in Mbaiki, Central African Republic (Gourlet-Fleury *et al.* 2013), and in the Central African plots of the DynAFor network (www.dynafor.org). In the case of fluted trees, two contrasting options have been recommended: either selection of the POM arbitrarily above the deformation (Alder & Synnott 1992; Condit 1998) or measuring the perimeter of the convex hull of the stem at the standard 1.3 m height (Phillips *et al.* 2015).

THE NEED FOR A STANDARDIZED METHOD

The lack of a worldwide standard for measuring the reference diameter for all morphological stem types may lead to substantial misinterpretations, errors, and biases when estimating the basal area (Clark 2002), above-ground biomass (Dean,

Roxburgh & Mackey 2003; Muller-Landau *et al.* 2014), tree growth (Metcalfe, Clark & Clark 2009) and the carbon budget of tropical forests (Clark 2002; Cushman *et al.* 2014; Muller-Landau *et al.* 2014). Buttressed stems represent up to 80% of trees with a diameter of at least 100 cm in 20 ha in the southwest of China (He *et al.* 2012) and more than 70% of the emergent trees studied in Bangladesh (Mehedi, Kundu & Chowdhury 2012). Irregularly shaped trees account for a large proportion of uncertainty in the carbon budget of tropical forests mainly because large trees contribute significantly to carbon stock (Slik *et al.* 2013; Bastin *et al.* 2015).

MEASURING THE IRREGULAR PART OF THE TREE

To accurately measure the basal area and the volume of irregular stems, a variety of methods, including destructive and non-destructive approaches, have been proposed. Destructive methods have been used to develop allometric equations. The irregular parts of stems are logged, and the cross-sections are measured based on georeferenced photographs and digitalization of the outline of the sections (Dean & Roxburgh 2006; Fayolle *et al.* 2013a) or drawings on large sheets of paper (Nogueira, Nelson & Fearnside 2006).

Non-destructive approaches include the wire method, the convex-concave method and the terrestrial laser scanning (TLS) method. The wire method uses two wires pressed against the irregular stem to shape the cross-section. The shaped wires are then put on a wooden board with a grid, and the area of the cross-section is estimated by counting the squares enclosed within the wire (Ngomanda *et al.* 2012). Nevertheless, the flexibility of the wire and the square counting may lead to measurement errors. The convex-concave method requires various measurements of all convex (spurs) and concave parts (flutes) of the stem to finally model the trunk as an arrangement of a cylindrical element and buttress elements (Dean & Roxburgh 2006; Henry *et al.* 2010). The simplification of the stem morphology may not always be in accordance with the real volume of this irregular part (Nölke *et al.* 2015). The TLS method requires scanning of the tree from different points of view. The resulting three dimensional point cloud is then processed to extract cross-sectional areas (Nölke *et al.* 2015). The TLS method is promising but expensive, and occlusion may hide some parts of the irregularities. Instead of measuring the basal area at 1.3 m height for the irregular trunks, Cushman *et al.* (2014) proposed an alternative method based on the taper of the trees. This taper curve method requires diameter measurements of the regular part of the stem (i.e. above the buttresses) to calibrate a taper model and project that taper downward up to 1.3 m height (Cushman *et al.* 2014). This last method assumes that the equivalent regular diameter at 1.3 m height is highly related to above-ground biomass but this hypothesis has not been validated.

AIMS AND QUESTIONS

In this study, our main objective was to develop a non-destructive method for the three dimensional modelling of tree trunks

suitable for large and irregularly shaped tropical tree trunks. The approach is based on an automated close-range photogrammetric process and was validated on three destructively sampled trees. To demonstrate the broader utility of this method, we extended the validated photogrammetric workflow to 43 additional trees belonging to two species. Thanks to this approach, we achieved three specific objectives which are: (i) to identify the stem morphology variation within a species; (ii) to analyse the ontogenetic variation in stem morphology for the two species; and finally (iii) to identify suitable standardized predictor for biomass estimates of buttressed trees. To reach the last objective, we used biomass data from Fayolle *et al.* (2013a, b). Based on the promising results of the photogrammetric method, we developed practical recommendations at the end of the manuscript.

Materials and methods

THE CLOSE-RANGE PHOTOGRAMMETRIC APPROACH

Field measurements

The photogrammetric process was developed on three buttressed trees: one *Cynometra hankei* (Fabaceae, Nganga) and two *Celtis mildbraedii* (Ulmaceae, Ohia) located at the edge of the Yangambi Reserve, in northern Democratic Republic of Congo (see Kearsley *et al.* 2013 for site description). The approach was then extended to 43 additional trees over a large diameter range to demonstrate the broader utility of this method for tree and forest monitoring. The 43 additional trees include 19 *C. mildbraedii* (Ulmaceae, Ohia) with a diameter between 42 and 98 cm, and 24 *Entandophragma cylindricum* (Meliaceae, Sapelli) with a diameter between 73 and 251 cm (Table 1). All the trees were sampled in the Loundoungou permanent sample plot situated in northern Republic of Congo and part of the DynaFor network (see Appendix S1, Supporting Information, for the site description). These two species are both common in moist Central African forests (Fayolle *et al.* 2014). The only criterion used for the selection of the trees was the DBH class, such that trees with lianas were also retained (Fig. S 2.1).

Before photographing the trees, we cleared small vegetation (stem with DBH < 3 cm and leaves) and small lianas up to 2 m high in a radius <2.5 m around the focal trees (Fig. S 2.2). For the three calibration trees, we used a digital SLR camera Nikon D90 with an 18- to 105-mm lens. We successively fixed the zoom lens with a tape at three different focal lengths (25 mm, 35 mm and 50 mm). We manually adjusted the aperture at $F = 4.5-9$, depending on the focal length, while the other camera settings were kept automatic (focus, ISO and shutter speed). At each focal length, we took a set of photographs all around the tree following a similar image acquisition method as the 'one panorama each step' approach of Wenzel *et al.* (2013). At each footstep around the tree, we took a set of photographs with high overlap (vertical panorama) and cross-convergent images (Fig. SI2.3). The distance from the tree varied between 1 and 3 m. We used two different viewing heights for image acquisition: the head height (1.7 m) and 4 m using a stick. Before taking the photographs, we placed a vertical graduated rod beside the tree to later scale the three dimensional point cloud produced by the photogrammetric process. The same protocol was applied in the field for the 43 additional trees, but a prime lens of 16 mm was used instead of the 18- to 105-mm zoom lens, and panels of coded

targets were used instead of the graduated rod (Fig. S 2.2). The coded targets were used to automate the whole photogrammetric process (more information below).

Motion stereo process

We used the motion stereo process to build the three dimensional structure of the stem. This phase encompasses three steps: the structure-from-motion (SfM) reconstruction process (step 2, Fig. 1), the scaling step (step 3, Fig. 1) and the dense multiview stereo (MVS) matching (step 4, Fig. 1).

In SfM reconstruction, interior (internal geometry of the camera such as the lens distortion model) and exterior (spatial location and direction of images) orientation parameters were computed using a feature-detection-and-description algorithm and Bundle Block Adjustment procedure (Barazzetti, Scaioni & Remondino 2010; Szeliski 2010). The end product is a sparse point cloud of the stem with the location of the cameras (Fig. 1, step 2). The sparse point cloud was then scaled using control points, which were manually placed on the graduated rod in all the images where the rod was visible. For the 43 additional trees, the scaling is based on the reference panel with coded targets which are automatically detected (Fig. S 2.2). Finally, dense MVS matching was performed to produce a three dimensional dense point cloud.

We used PHOTOSCAN Professional v1.0.4 (Agisoft LLC, St. Petersburg, Russia) for the photogrammetric workflow, in a computer with an Intel Core i7-3930K (6 × 2 cores @3.2 Ghz- turbo @3.8 GHz) with an AMD Radeon HD5450 graphics card and 32Go RAM (quad channels PC3-10700 @666 MHz CAS 9-9-9-24).

Post-processing of the three dimensional dense point cloud of the stem

The post-processing phase aims to compute the cross-section of the stem at various heights. Post-processing is divided into two steps: the creation of the stem skeleton (step 5, Fig. 1) and the delineation of the cross-sections (step 6, Fig. 1). The method for the post-processing phase differed between the three calibration trees and the 43 additional trees. A manual procedure was used for the calibration trees to ensure the results were independent of the post-processing procedure, whereas the dense point cloud of the 43 additional trees was post-processed with 3D RESHAPER v10.1.1 scripts. In both case, the methodological steps were the same and are presented below.

To create the stem skeleton, we first defined the stem axis by connecting the centres of 2-cm-thick slices distributed every 20 cm along the z-axis. The contours of the slices were manually digitized using a GIS software for the three calibration trees and automatically delineated for the 43 additional trees (intersection between horizontal planes and a mesh adjusted on the photogrammetric point cloud). The centre of each slice was computed as the farthest location from the edges within the polygon (Fig. S 2.4). This is specifically suited for irregular cross-sections in comparison with other methods (geometrical centre or barycentre) that may define a centre located outside the cross-section.

Based on the skeleton, cross-sections perpendicular to the stem axis were then delineated. For the calibration trees, we digitized another set of 2-cm-thick slices regularly distributed along the stem. For the 43 additional trees, the intersection between the mesh of the trunk and planes perpendicular to the trunk axis was calculated. Finally, we computed the area and perimeter of each cross-section, as well as the perimeter of the convex hull, mimicking tape measurements around the buttresses.

Table 1. Characteristics of the three validation trees and the 34 of the 43 additional trees

No.	Tree no.	Species	DAB (cm)	H_{DAB} (m)	Trunk height (m)	G_{130} (m ²)	$D_{area130}$ (cm)	$D_{ConvHull130}$ (cm)	De_{BA130}	De_v
	Tree C1	OHIA	86	<i>4.6</i>	<i>24</i>	0.75	97.7	158.2	0.74	0.13
	Tree C2	OHIA	52	<i>4</i>	<i>27</i>	0.39	70.9	96.3	0.56	0.33
	Tree C3	NGANGA	71	<i>3.4</i>	<i>17</i>	0.54	83	122.1	0.59	0.19
1	Tree 1	SAPELLI	100.9	<i>5</i>	<i>30</i>	1.09	118.0	0.95	0.17	0.20
2	Tree 2	OHIA	76.3	<i>5.1</i>	<i>29.2</i>	0.61	88.3	0.78	0.77	0.29
3	Tree 3	SAPELLI	124.1	<i>9.7</i>	<i>43</i>	2.13	164.8	1.26	0.67	/
4	Tree 4	OHIA	78.9	<i>5.1</i>	<i>29</i>	0.71	95.2	0.78	0.79	0.29
5	Tree 5	SAPELLI	136.1	<i>7.7</i>	<i>32</i>	2.20	167.3	1.36	0.62	0.25
6	Tree 6	OHIA	82.3	<i>5.5</i>	<i>30</i>	0.76	98.4	0.86	0.77	0.41
7	Tree 7	OHIA	57.1	<i>2.9</i>	<i>18</i>	0.31	62.8	0.68	0.32	0.25
8	Tree 8	SAPELLI	135.2	<i>6.5</i>	<i>45</i>	2.42	175.6	1.28	0.57	0.37
9	Tree 9	SAPELLI	174.9	<i>4</i>	<i>33</i>	3.68	216.4	1.58	0.27	0.28
10	Tree 10	SAPELLI	134.9	<i>4.5</i>	<i>25</i>	2.05	161.7	1.33	0.37	0.27
11	Tree 11	SAPELLI	68.9	<i>2.05</i>	<i>24.5</i>	0.42	73.3	0.59	0.05	0.27
12	Tree 12	SAPELLI	179.9	<i>4.5</i>	<i>34</i>	3.67	216.1	1.69	0.62	0.25
13	Tree 13	SAPELLI	/	<i>5.2</i>	<i>48</i>	2.88	191.6	1.69	0.49	/
14	Tree 14	SAPELLI	/	<i>7.7</i>	<i>27.4</i>	3.38	207.6	2.13	0.33	/
15	Tree 15	OHIA	/	<i>3.8</i>	<i>29.5</i>	0.66	91.6	0.83	0.73	/
16	Tree 16	OHIA	54.0	<i>1.8</i>	<i>19.9</i>	0.25	56.4	0.33	0.10	0.26
17	Tree 17	SAPELLI	113.6	<i>5.8</i>	<i>27</i>	1.51	138.6	1.17	0.52	0.24
18	Tree 18	SAPELLI	127.2	<i>4.6</i>	<i>26.4</i>	1.72	148.1	1.33	0.45	0.24
19	Tree 19	SAPELLI	104.3	<i>3.7</i>	<i>14</i>	1.16	121.3	1.01	0.08	0.24
20	Tree 20	SAPELLI	128.9	<i>4.5</i>	<i>24</i>	1.85	153.4	1.20	0.32	0.26
21	Tree 21	SAPELLI	122.4	<i>7.8</i>	<i>21</i>	2.15	165.6	1.23	0.72	0.31
22	Tree 22	OHIA	54.2	<i>3.3</i>	<i>29.6</i>	0.31	62.8	0.56	0.34	0.36
23	Tree 23	OHIA	39.8	<i>2.15</i>	<i>24</i>	0.14	41.8	0.14	0.14	0.18
24	Tree 24	SAPELLI	202.4	<i>7.7</i>	<i>34.7</i>	4.94	250.8	2.09	0.56	0.22
25	Tree 25	OHIA	74.1	<i>3.5</i>	<i>26.5</i>	0.54	82.7	0.62	0.73	0.34
26	Tree 26	OHIA	78.2	<i>4.5</i>	<i>30</i>	0.74	96.8	0.74	0.74	0.38
27	Tree 28	SAPELLI	126.1	<i>4.5</i>	<i>28.4</i>	1.67	145.9	1.27	0.29	0.20
28	Tree 29	SAPELLI	104.0	<i>1.99</i>	<i>28</i>	0.92	108.5	0.93	0.03	0.15
29	Tree 30	SAPELLI	133.1	<i>4.5</i>	<i>37</i>	1.93	156.9	1.30	0.23	0.28
30	Tree 31	OHIA	78.6	<i>3.8</i>	<i>28</i>	0.41	72.7	0.79	0.69	0.08
31	Tree 32	OHIA	76.2	<i>4.3</i>	<i>30</i>	0.67	92.4	0.80	0.62	0.29
32	Tree 33	OHIA	63.5	<i>4.6</i>	<i>21</i>	0.40	71.6	0.61	0.49	0.23
33	Tree 34	OHIA	43.7	<i>1.6</i>	<i>20</i>	0.15	44.3	0.40	0.05	0.15
34	Tree 35	SAPELLI	114.8	<i>5.8</i>	<i>31.8</i>	1.59	142.1	1.16	0.44	0.21

DAB, diameter above buttresses; H_{DAB} , height where the DAB was measured, that is 50 cm above buttresses; Trunk height, height of the stem up to the first branch; G_{130} , basal area at 1.3 m height; $D_{area130}$, diameter at breast height estimated as the diameter of a circular disc with the same area as G_{130} ; $D_{ConvHull130}$, diameter of a circular disc with the same perimeter as the perimeter measured around buttresses; De_{BA130} , Basal Area Deficit of the cross-section at 1.3 m high; De_v , volume deficit. OHIA, *Celtis mildbraedii* (Ulmaceae); NGANGA, *Cynometra hankei* (Fabaceae); SAPELLI, *Entandophragma cylindricum* (Meliaceae).

Variables measured in the field are italicized while the other variables were computed from the photogrammetric process. Trees in bold are the trees used to validate the method (destructive measurements). The slash, “/”, means “no value”. The absence of value is due to the limitation of the photogrammetric method for these trees. Trees in bold are the trees used to validate the method (destructive measurements). The slash, “/”, means “no value”. The absence of value is due to the limitation of the photogrammetric method for these trees.

DESTRUCTIVE FIELD MEASUREMENTS

Before taking photographs on the three calibration trees, we marked the position of some of the future destructive measurements on the standing stem to further facilitate the validation. These trees were then felled, and the stems were cut into successive 2 m-long logs. The cross-section of each log, including the marked ones, was then estimated with photographs (Dean, Roxburgh & Mackey 2003; Nogueira, Nelson & Fearnside 2006; Fayolle *et al.* 2013a). To scale and rectify those photographs, a 40 cm × 40 cm Plexiglas grid with 5 cm × 5 cm graduations was placed on the cross-section and photographs taken (Fig. S2.4). The first 2 m of the stem were discarded because, for safety reasons, the buttresses were cut prior to felling.

We rectified the photographs of the destructive cross-sections by applying a projective transformation using GIS software prior to manual digitization (see Appendix S2 for method description and quality assessment of this method). The destructive measurements on the marks were used for the validation of the photogrammetric process. Cross-sectional areas calculated from the three dimensional models were thus compared to destructive measurements at the exact same height.

DATA ANALYSIS

To estimate the accuracy of measurements extracted from the three dimensional models (photogrammetric measurements hereafter), the

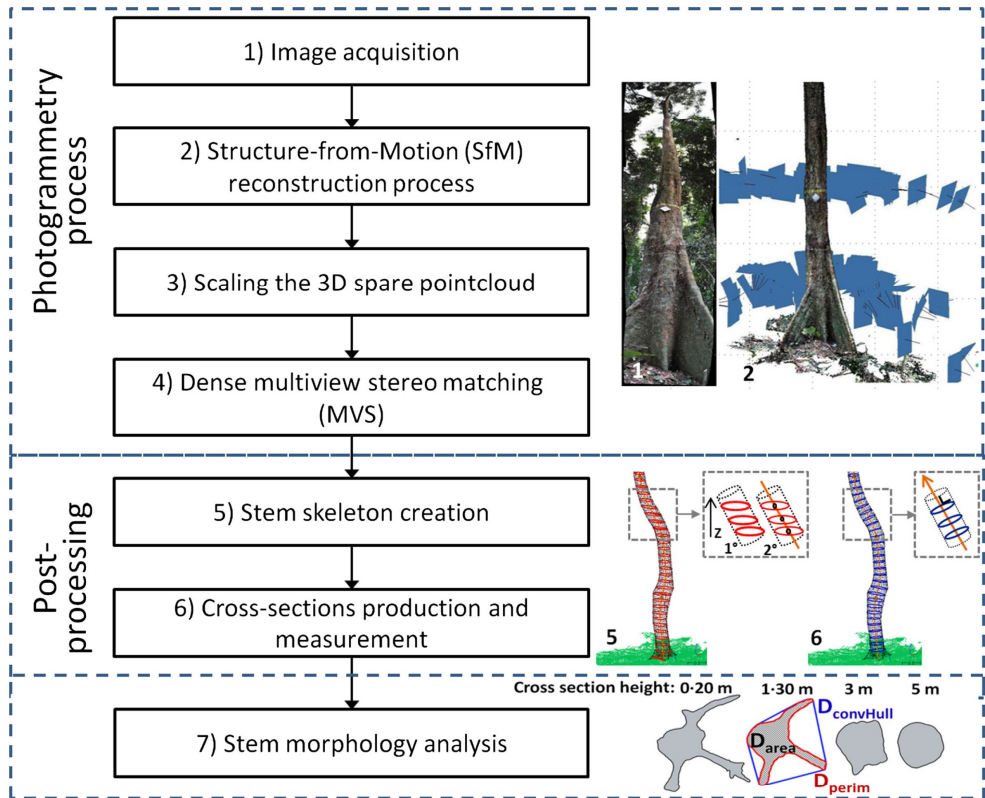


Fig. 1. Workflow of the non-destructive method for the three dimensional tree modelling suitable for large and irregularly shaped tropical trees. The main steps are (1) acquisition of photographs all around the tree, (2) location of the photographs in the three dimensional space based on the structure-from-motion process (the blue squares in sub-Figure 2 corresponds to the photographs), (3) scaling the project with reference points and (4) generating a dense three dimensional point cloud of the stem. In the post-processing phase, the tree skeleton is computed (step 5) by slicing the point cloud along the z-axis and estimating the centre of each cross-section. Then, measurements of cross-sections are carried out perpendicular to the skeleton (step 6). Finally, in step 7, based on the cross-sectional measurements, the stem morphology is analysed by computing shape indices and fitting taper curves. [Colour figure can be viewed at wileyonlinelibrary.com]

bias and the root means square error were first computed for the three validation trees.

Description of the stem shape

For the stem morphology analysis of the 43 additional trees, we converted our photogrammetric measurements into diameters, since diameter is more frequently used than basal area to quantify tree size in forest sciences. The area and the perimeter of the cross-sections were converted into diameter by computing the diameter of a disc with the same area (D_{area}) and the same perimeter (D_{perim}), respectively. The diameter of a disc with the same perimeter as the convex hull was also computed (D_{convHull}).

Shape indices. To better quantify the buttressed part of the 43 additional trees and to analyse ontogenetic variations, we focused on two common shape indices among the large number of indices

available (Pulkkinen 2012). The Basal Area Deficit index (D_{cBA} , previously used for buttressed tropical trees in Dean 2003; Ngomanda *et al.* 2012; and Nölke *et al.* 2015) is defined as one minus the ratio of the basal area of the cross-section over the area of a circular disc with the same perimeter as the cross-section (eqn 1):

$$D_{\text{cBA}} = \frac{\text{BA}_{\text{perim}} - \text{BA}_{\text{area}}}{\text{BA}_{\text{perim}}} = 1 - \left(\frac{D_{\text{area}}}{D_{\text{perim}}} \right)^2, \quad \text{eqn 1}$$

with BA_{perim} the area of a disc with the same perimeter as the perimeter of the cross-section (in m^2), BA_{area} the area of the cross-section (in m^2), and D_{area} and D_{perim} as defined above (in cm). As a result, D_{cBA} is equal to zero for a circular disc and tends to one as the cross-section becomes more irregular (Ngomanda *et al.* 2012). According to Nölke *et al.* (2015), a cross-section with a $D_{\text{cBA}} < 0.05$ can be considered circular.

The Volume Deficit (D_{v}) is defined as the proportion of the volume of the buttressed part of the stem that is not considered when this part

is assumed to be a cylinder with a diameter equal to the diameter above the buttresses (DAB):

$$D_{\text{cv}} = \frac{V_b - V_{\text{cyl}}}{V_b} = 1 - \frac{(\pi/4) DAB^2 H_{\text{DAB}}}{V_b}, \quad \text{eqn 2}$$

with V_b , the volume of the buttressed part of the stem (in m^3), V_{cyl} the volume of a cylinder with diameter equal to DAB (in m^3), that is the diameter at 50 cm above the buttresses (in m), and H_{DAB} the measurement height of DAB (in m). As a result, D_{cv} is equal to zero for a cylindrical stem and D_{cv} tends to one as the taper of the buttressed part increases. We used the same DAB definition as Nölke *et al.* (2015) to ease comparison with their form index $f_b = V_b/V_{\text{cyl}}$.

Based on the photogrammetric data, we finally studied an objective method to determine the height of the highest buttress and the height of DAB by defining a threshold based on the difference between D_{area} and D_{ConvHull} .

Biomass predictors

To identify the most robust standardized predictor for biomass estimates of buttressed trees, we studied the quality of the allometric relationship between the total above-ground biomass and the following individual predictors: diameter at the standard height of 1.3 m based on the basal area measurement ($D_{\text{area}130}$) and based on the perimeter of the convex hull around the buttresses ($D_{\text{ConvHull}130}$) and the equivalent regular DBH deduced from taper model (DBH_{eq}).

We used Metcalfe, Clark & Clark (2009)'s taper model to estimate the equivalent regular DBH (DBH_{eq}) as this model showed the best results compared to four other taper models on 190 buttressed stems at Barro Colorado Island, Panama (Cushman *et al.* 2014). The model is:

$$D_i = \text{DBH}_{\text{eq}} \cdot e^{-b_1(h_i-1.3)}, \quad \text{eqn 3}$$

with D_i the diameter (in cm) at height h_i (in m), DBH_{eq} the equivalent regular diameter at 1.3 m (in cm), and b_1 is a parameter. We fitted the taper model with diameters measured above buttresses to deduce the DBH_{eq} . Two equivalent regular diameters at 1.3 m were deduced: $\text{DBH}_{\text{eqAll}}$ and $\text{DBH}_{\text{eqSub}}$. $\text{DBH}_{\text{eqAll}}$ is estimated by including all the diameters measured above the buttresses, whereas $\text{DBH}_{\text{eqSub}}$ is estimated with a subset of the diameters between H_{DAB} and 10 m high as in the field protocol of Cushman *et al.* (2014).

As no destructive measurements of biomass were done in the Loundoungou permanent sample plot, the biomass data used to analyse the predictors are a subset ($n = 15$) of Fayolle *et al.* (2013a, b) data from south-east of Cameroon. We only selected the *E. cylindricum* trees as this is the only species for which photogrammetric data were available. We fitted the following allometric model to the biomass data:

$$\text{Ln}(\text{AGB}) = a \text{Ln}(D) + b \text{Ln}(D^2), \quad \text{eqn 4}$$

where AGB is the tree above-ground biomass (in Mg), D is one of the size predictors mentioned in the previous section (in cm), and a and b are the model parameters. In order to correct for the systematic bias induced by the log-transformation, when back-transforming the data, we applied a first-order correction factor (CF), which was calculated as follows (Baskerville 1972; Sprugel 1983).

$$\text{CF} = e^{(\text{RSE}^2/2)}, \quad \text{eqn 5}$$

Afterwards, we compared the biomass prediction of our species-specific models with the multispecies models of Fayolle *et al.* (2013a, b) and Chave *et al.* (2005, 2014).

Finally, we studied the relationship between $D_{\text{area}130}$ and alternative field measurements: DAB, H_{DAB} and $D_{\text{ConvHull}130}$ in order to estimate $D_{\text{area}130}$ indirectly. We fitted all possible combinations of the linear model based on these three predictors and their interactions. We also fitted power models (i.e. linear models on log-transformed data) with the most relevant combination of the predictors, but these last fits did not maintain normality in the residuals. The selection of the models was performed with the leaps routine in the R software, and the final model fitting was achieved with the package nlme. We applied a flexible weight of the variance on the models in order to avoid heteroscedasticity, and we added species effect on the residuals. The relative Root mean square error (RMSE) was computed as the RMSE divided by the mean diameter of the data set.

Results

THE PHOTOGAMMETRIC PROCESS

We took an average of 188 photographs and spent *c.* 20 min for each calibration tree and per focal length. During the SfM step (Fig. 1, step 2), we were able to orientate and locate the photographs taken with the focal length of 25 mm, but the reconstruction process failed for the set of photographs taken with focal lengths 35 and 50 mm. The time needed for processing was around 3 h and 30 min for each tree, with 2 h spent for SfM, 20 min spent for pointing markers and other manual interventions, and 1 h spent for MVS matching. The 20 min of manual intervention was not necessary for the 43 additional trees as they were photographed with coded targets. The resulting three dimensional point cloud was composed, for each tree, of ~525 000 points at the 'medium'-quality parameter setting in the dense matching step. From the 43 trees photographed for the morphological analysis 79% were successfully oriented in the SfM step (i.e. 34 trees). The success rate might be improved by restarting the SfM process on the first poor results, but we wanted to limit manual intervention during the photogrammetric process. The main factor that could explain this first unsuccessful SfM process for some trees is the low distance between the operator and the tree during the images acquisition (distance < 1.5 m to avoid clearing small to medium vegetation). The overlap between the images is then insufficient to match them.

No significant bias in diameter estimation was noticed when comparing cross-section measurements manually delineated from the three dimensional point cloud and destructive reference measurements at the exact same height (rectified photograph of the marked cross-section; bias = 0.66 cm, $P = 0.073$, d.f. = 6). A slight bias is noticed between measurements deduced from mesh and the destructives references (bias = 0.86 cm, $P = 0.02$, d.f. = 6). Nevertheless, the reference measurements based on the rectified photograph have also a limited precision and accuracy that might influence the bias reported (Appendix S2).

STEM MORPHOLOGY VARIATION

To better quantify the buttressed part of the 34 remaining trees and to analyse ontogenetic variations, we used two shape

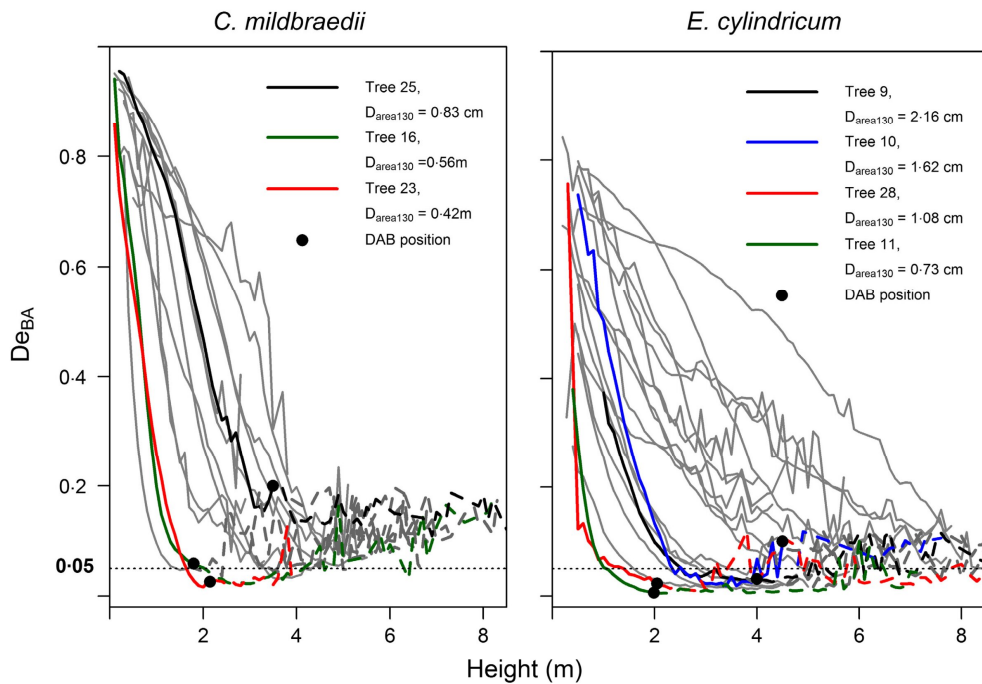


Fig. 2. Variation of the shape index De_{BA} (Basal Area Deficit) along the stem for 14 *C. mildbraedii* and 20 *E. cylindricum*. The coloured lines correspond to trees with contrasted diameters, and the black dots, as well as the intersection between the solid and dashed lines, indicate the position of the diameter above buttresses (DAB). Cross-sections with a De_{BA} below the 0.05 reference value are considered circular. [Colour figure can be viewed at wileyonlinelibrary.com]

indices. The first shape index (the Basal Area Deficit: De_{BA}) strongly decreased along the stem in the first metres (i.e. the buttressed part of the stem) in both species, but tended to stabilize at 4.5 m height for *C. mildbraedii* and not before 8 m for *E. cylindricum* (Fig. 2). The trunk appeared to be much more regular above 4.5 m for most *C. mildbraedii* trees though not circular ($De_{BA} > 0.05$, the reference value for circular cross-section).

There was extensive intraspecific variation in the development of irregularities along the stem. The intraspecific variation tended to be greater for *E. cylindricum* since some trees could be considered circular ($De_{BA} \leq 0.05$) from 1 m height (trees 11 and 28, in red and green, respectively, in Fig. 2) while others were greatly irregular up to 8 m height. This variation was not fully attributable to tree size since the largest trees were not necessarily the most irregular ones along the stem. For instance, the large *E. cylindricum* tree 9 (in black, with a diameter of 219 cm) was circular from 2.5 m height whereas some smaller trees have strong irregularities up to 8 m.

The average De_{BA} at the DAB height is 0.08, showing that determining height of the DAB in the field is in accordance with the height where the stems turn out to be more regular. The choice of 3% threshold for the relative difference between

$D_{ConvHull}$ and D_{area} seems to be a good reference value to objectively define the height of the highest buttress and increased to 5% if the tree did not reach this threshold within the 10 first metres of the stem (Table S 3.1). Finally, within the 34 trees with three dimensional data, four trees were left without information on the DAB height due to obstruction by surrounding vegetation.

When comparing tree size at 1.3 m ($D_{area130}$) to stem irregularities at 1.3 m (De_{BA130}), we found that irregularities increased with the diameter of the trees (Fig. 3). *Celtis mildbraedii* trees tended to develop much stronger irregularities than *E. cylindricum* trees for the same diameter at 1.3 m. The development rate of irregularities (slope of the relationship between De_{BA130} and $D_{area130}$) was almost six times larger for *C. mildbraedii* than for *E. cylindricum*, showing the ontogenetic difference between these two irregularly shaped tree species. The relationship between tree size and tree irregularities at 1.3 m was weaker for *E. cylindricum* ($R^2 = 0.34$) than for *C. mildbraedii* ($R^2 = 0.88$). This might be due to the great intraspecific variation in tree irregularities within this species as already identified along the stem (Fig. 2).

The second shape index, the Volume Deficit Index (De_v), varied between 0.08 and 0.41 among the 31 additional trees for

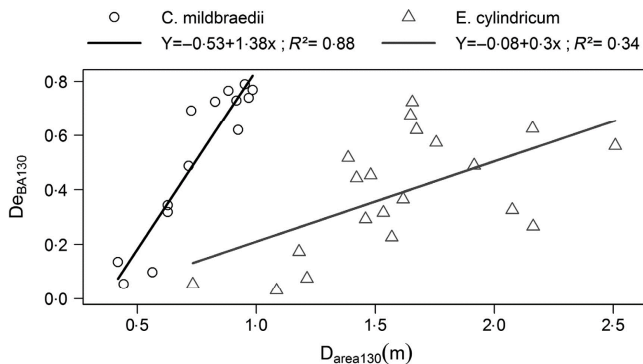


Fig. 3. Relationship between the shape index De_{BA} (Basal Area Deficit) at 1.3 m height and the diameter of a disc with the same area as the basal area at 1.3 m height ($D_{area130}$).

which the above buttress height (H_{DAB}) was attained by the three dimensional model (Table 1). We did not find any significant difference in mean De_V between the two species ($P = 0.43$, $t = -0.80$). The mean De_V value across all trees was $0.26 (\pm 27\%)$, which means that on average 26% of the volume of the buttresses is not considered when the volume is estimated as a cylinder with the diameter above buttresses (DAB). The De_V increased with DAB, indicating that the taper of the basal area of the buttressed part of the trunk increased with tree size, and this was stronger for *C. mildbraedii* than for *E. cylindricum*. The highest De_V value was observed for the largest *C. mildbraedii* (Table 1).

STANDARDIZING THE HEIGHT OF DIAMETER MEASUREMENTS

Among the biomass allometric models fitted on the 15 *E. cylindricum* from Cameroon (Fayolle *et al.* 2013a, b; Appendix S3), the model providing the best fit on biomass data was the m2 model with the predictor variable $D_{area130}$ (lowest Akaike information criterion (AIC) and relative squared error (RSE), Table 2). The m1 model based on the predictor variable DAB lost a high proportion of information compared to m2 (lowest AICw). Models using estimated DBH_{eq} from Metcalf, Clark & Clark (2009) taper model (m4 and m5) improved slightly the prediction of biomass compared to m1 as well as the model m3 which required the measurement of the perimeter around the buttresses ($D_{ConvHull130}$). These results based on a low number of samples ($n = 15$) tend to show that building biomass allometric equation with the variable $D_{area130}$ might reduce substantially the root mean square error of biomass allometric model. Moreover, using this standardized variable on existing allometric equation which were fitted with a mixed of DBH and DAB seems to reduce the important bias encountered on biomass estimates of large trees (diameter > 100 cm, Fig. 4).

The relationships between the $D_{area130}$ derived from the three dimensional models and several field measurements are shown in the Fig. 5. We found that $D_{area130}$ was best explained (lowest BIC) with the following variables: the combination of $D_{ConvHull130}$ and H_{DAB} ($D_{ConvHull130} : H_{DAB}$), the

combination of DAB and H_{DAB} (DAB : H_{DAB}) and DAB (model md1 of the Table S3.3). The best model with only two variables was the model md5 with $D_{ConvHull130}$ and DAB as explanatory variables. No residual effect of species was found for these two models. The relative RMSE of the models md1 and md5 are, respectively, 4.5% (absolute RMSE of 5.8 cm) and 4.6% (absolute RMSE of 5.9 cm), and the exponents of the power model used for the residual variance are, respectively, 0.793 and 0.719.

Discussion

In this study, we found a good agreement between diameters derived from the three dimensional models and the destructive measurements along the stem for the three validation trees. Our results (RMSE < 1 cm on tree diameter) were better than the ones reported in a study on small trees in boreal forests (RMSE = 2.39 cm, Liang *et al.* 2014). We therefore believe that the non-destructive approach based on close-range terrestrial photogrammetry developed in this study is an objective and accurate method that can be used to measure large and irregularly shaped tropical trees.

To illustrate the broader utility of our method, we applied the whole photogrammetric process to 43 additional trees belonging to two species. According to expectations, we found that tree irregularities decreased along the stem; and that tree irregularities at 1.3 m height increased with tree size with greater irregularities for *C. mildbraedii* than for *E. cylindricum*. The Basal Area Deficit in *E. cylindricum* trees was similar to the 0.39 mean value of 102 buttressed trees measured in Gabon (Ngomanda *et al.* 2012), while in *C. mildbraedii*, De_{BA} was far greater (0.52). We also identified a large intraspecific variation in trunk morphology for *E. cylindricum* which can, for similar diameters, be almost regular or show fully developed buttresses (Letouzey 1982; Meunier, Mombogou & Doucet 2015).

Since the research of Chave *et al.* (2005, 2014) on biomass allometry, different studies aimed to improve the precision of allometric equations by adding information on crowns (e.g. mean radius of the crown or height of the crown) in their equation to reduce the high bias encountered on biomass estimates of large trees (diameter > 100 cm, Antin *et al.* 2013;

Table 2. Results of the regression analysis of the biomass allometric eqn (4)

Model	Predictor D	D	D^2	Intercept	AIC	AIC _w	RSE	d.f.
m1	DAB	*			-0.8	0.0008	0.202	12
m2	D_{area130}	***	.	*	-15.1	1.0000	0.125	12
m3	$D_{\text{ConvHull130}}$	***	**	**	-9.9	0.07	0.149	12
m4	$\text{DBH}_{\text{eqAll}}$	*	.	*	-3.6	0.003	0.184	12
m5	$\text{DBH}_{\text{eqSub}}$	***	*	**	-5.7	0.009	0.171	12

AIC, Akaike information criterion; RSE, relative squared error.

AIC_w is the relative likelihood of the models.

The asterisks refer to the significance of the parameter: ., $0.1 < P \text{ value} < 0.05$; *, $0.05 < P \text{ value} < 0.01$; **, $0.01 < P \text{ value} < 0.001$; *** $P \text{ value} < 0.001$.

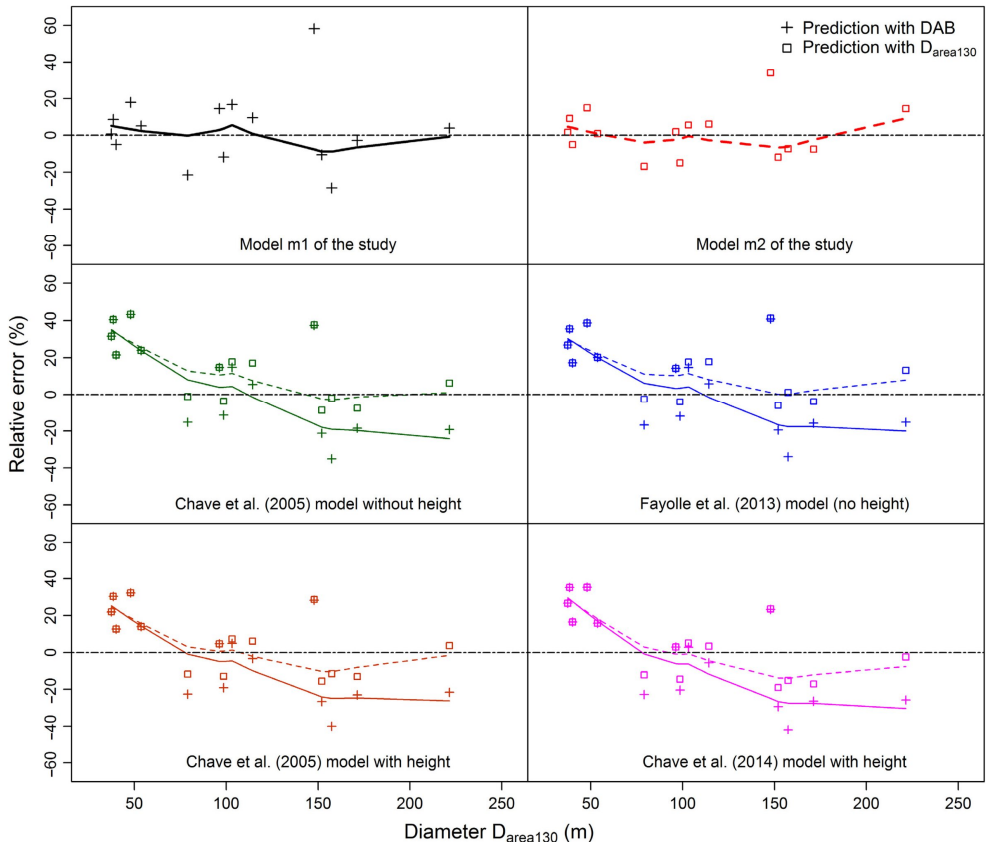


Fig. 4. Biomass error of different allometric models according to the diameter used. The model m1 is the model fitted with DAB, the model m2 is the model fitted with D_{area130} , the Chave et al. (2005, 2014) model without height is the model for moist forest which is fitted with a mixed of DBH and DAB data, the Fayolle et al. (2013a, b) model is a local multispecies model which is fitted with a mixed of DBH and DAB data, the Chave et al. (2005, 2014) model with height is the model for moist forest requiring the height in addition to diameter and basal wood density (also fitted with a mixed of DBH and DAB data) and the Chave et al. (2014) model with height is a model requiring the height in addition to diameter and basal wood density (also fitted with a mixed of DBH and DAB data). The solid and dashed lines are local fitted lines (loess fitting with a span of 2/3), the solid line is fitted on biomass data predicted with DAB (cross symbols) and the dashed line on biomass data predicted with D_{area130} (square symbols). DAB, diameter above buttresses. [Colour figure can be viewed at wileyonlinelibrary.com]

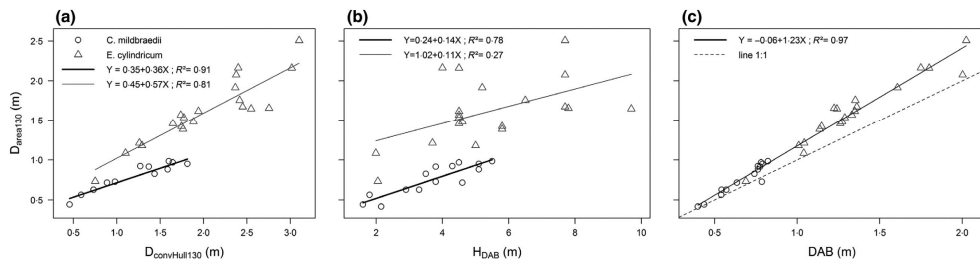


Fig. 5. Relationships between the diameter of a disc with the same area as the basal area at 1.3 m height ($D_{\text{area}130}$) and field measurements including the diameter of the convex hull measured at 1.3 m height ($D_{\text{ConvexHull}130}$) around the buttresses (a); the height of the diameter above buttresses (H_{DAB}) (b); and the diameter above buttresses (DAB) at a variable height (c).

Goodman, Phillips & Baker 2014; Ploton *et al.* 2016). This study shows that a higher accuracy on biomass estimates might also be achieved by standardizing the diameter to $D_{\text{area}130}$ on the existing biomass allometric equations.

In addition, $D_{\text{area}130}$ standard might be predicted with a good precision (RMSE < 5%) by using statistical relationships related to easily measurable variables such as DAB and the perimeter of the convex hull of the buttresses at 1.3 m height, regardless of the species (this study, Ngomanda *et al.* 2012; Nölke *et al.* 2015). These are promising results for the standardization of diameter measurement height in permanent sample plot which is a key issue for tree growth monitoring (Metcalf, Clark & Clark 2009) and biomass estimation (Muller-Landau *et al.* 2014). The systematic use of terrestrial photogrammetry and/or terrestrial LiDAR scanning (Nölke *et al.* 2015) in tree and forest monitoring offers new opportunities to directly measure irregularly shaped trees as well as to develop correction methods to extract diameter measurements at any measurement height (e.g. taper model in Appendix S3 and models relating $D_{\text{area}130}$ with easily measurable variables). These correction methods are needed for growth comparisons between trees, within and between sites.

In comparison with terrestrial LiDAR scanning, close-range photogrammetry combines a high mobility that reduces the occlusion generated by stem irregularities and surrounding vegetation, a low cost, a high portability, and a low acquisition time, that places this approach as a new competitive tool for measuring the base of the trunks. Nevertheless, as other terrestrial remote sensing tools, low vegetation and lianas limit measurements possibilities in dense forest as in the study site. In this study, the photogrammetric process failed for 21% of the photographed trees due to non optimal acquisition, as we wanted to limit our impact on the vegetation surrounding the focal trees. Moreover, measurements up to the top of the buttresses were not possible for four of the 34 remaining trees due to the same problem. The actual technical limits of the tool are the non 100% success of the SfM process, the high computer processing time and the manual cleaning of the dense point cloud. To ensure a high rate of success of the SfM reconstruction process, some recommendations are proposed in the next section.

Recommendations

On the basis of our own experience as well as on a literature review, we make the following additional suggestions to ensure the success and quality of the photogrammetric process in tropical forests. The automatic SfM process is the most critical step in the overall photogrammetric process, and its correct achievement is not guaranteed. The success of SfM is highly related to (i) the quality of the camera gear and its lens distortion model, (ii) the image acquisition protocol (angle view and overlapping of the images), and (iii) the quality of the images acquired which should not be blurred, under/overexposed or backlit.

CAMERA GEAR QUALITY

Low-cost uncalibrated consumer-grade digital cameras are now commonly used to build three dimensional models of well illuminated objects as buildings or statues. The most obvious examples are popular projects made and shared with the browser-based SfM software PHOTOSYNTH[®] (Microsoft, photosynth.net). However, it must be kept in mind that successful photogrammetric process and accurate results depend on the image quality, consistency, and uniformity. The camera should therefore have high-quality optics, a large sensor size and a high autofocus speed in low-light environment.

We succeeded in the SfM step for the three calibration trees with only the widest focal length (25 mm) because of the higher overlap between images compared to longer focal lens. In addition to a wide focal lens, a fixed lens is also recommended because of the better geometric stability than zoom lens (Shortis *et al.* 2006). We thus recommend using a prime wide angle lens (focal inferior to 35 mm). Otherwise, in compact cameras with an optical zoom, no zooming (zoom of 1×) is recommended as it is the widest angle and leads to a more stable principal distance than other zooms (Läbe & Förstner 2004).

IMAGE ACQUISITION PROTOCOL AND LENS DISTORTION MODEL

The first step of the photogrammetric process is the image acquisition. The protocol to acquire images should follow the suggestions of Wenzel *et al.* (2013) to take a panorama of the

object of interest at each step, but cross-convergent images should also be taken at each step (Fig. S2.3). Several angles of view are also recommended (e.g. one set of images taken at head height and another set taken above with a monopod for instance). Adding reference points around the tree will also increase the success of the automatic SfM process. We then suggest using a coded target around the tree which will be automatically detected and used as reference points for the SfM process (Fig. S2.2).

As the forest is an extreme environment for the photogrammetric process (low luminosity, backlight, movement of the leaves and changing depth), any extra information that can help the SfM step are important. We observed in several photogrammetric projects that adding a precise lens distortion model as an input to the SfM step leads to successful results, though the SfM failed without lens distortion model. In order to build the lens distortion model, self-calibration of the camera is thus recommended: (i) before each image acquisition with a certain focal length, if the focal length is modified during the image acquisition campaign, or (ii) before an image acquisition campaign when using a single prime lens. The self-calibration of the camera means that we estimate intrinsic parameters of the camera based on a set of images. The estimation of these geometric characteristics, that is, the focal length (f) of the lens, the coordinates of the centre of projection of the image (x_p , y_p) and the radial lens distortion coefficients, is performed automatically using a photogrammetric software applications. The set of images should be capture in an illuminated scene with textured and non-flat objects (e.g. a corner of a messy desk) or on dedicated contrasted panel proposed by the photogrammetric software such as a chess board. The parameters of the camera should be the same as the parameters used in the field, more specifically the zoom and focus of the camera.

In this study, we were able to model the three dimensional structure of the stem of tropical trees up to 12 m height. The height limitation is due to the backlight of some images, and the lower resolution and higher inclination of the images of the upper part of the tree. Oblique images are not recommended in the photogrammetric process because of the shift in depth between two neighbouring pixels, which leads to a disparity gradient (Wenzel *et al.* 2013). To model the upper part of the trunk for volume or biomass estimations, the use of a large telescopic pole to raise the camera up to the top of the trunk would be needed or the use of a drone with protections around the propellers to avoid contact with the branches.

IMAGE QUALITY

In photogrammetry, a good image is an image that is not blurred, that is well exposed, and sharp. The use of automatic settings (specifically, automatic aperture, shutter speed and ISO) and automatic focus guarantees, on average, a good image quality. The various settings of each photograph are now well managed by the latest photogrammetric software.

Using autofocus during image acquisition results in a change in the optical and geometrical property of the lens

between each image. According to Fraser & Al-Ajlouni (2006), changing the focus does not have a significant effect on distortion parameters. Läbe & Förstner (2004) reported a significant effect on camera calibration when changing focus in photographs closer than 0.5 m from the object. As photographs of the trunk are taken at a distance further than 0.5 m in our protocol, we would recommend focusing each picture to ensure sharpness. Finally, the diffuse light of an overcast day is recommended compared to the direct light of a sunny day.

Authors' contributions

S.B., A.D., S.G.-F. and P.L. designed the study; S.B. and C.M. conducted the fieldwork; S.B. and C.M. did most of the data analysis; S.B., A.D. and S.G.-F. wrote the manuscript and L.M.N. and P.L. supervised the research and reviewed the manuscript.

Acknowledgements

We thank the Center for International Forestry Research (CIFOR), Resources and Synergies Development (RSD) and the University of Kisangani, through the REFORCO project funded by the European Union, for their financial and logistic support. We thank also the INERA Yangambi, who hosted this study in their research area, and more specifically Henri Badjoko, for his assistance in the fieldwork. We thank the DynAlFor team for their logistic support and their assistance in the fieldwork in Congo and the CIB-Olam company, partner of the DynAlFor project, who hosts the PSP of Loumdougou. Part of S. Bauwens time was supported with funds from Fonds Français pour l'Environnement Mondial through the DynAlFor Project and also with the fund from the World Bank throughout the PreREDD+ Project. We also thank the ngo Nature + for their administrative support.

Data accessibility

The original photogrammetric point clouds and the destructive sampling data are available through ORBI (<http://hdl.handle.net/2268/202113>).

References

- Alder, D. & Synnott, T.J. (1992) *Permanent Sample Plot Techniques for Mixed Tropical Forest*. Tropical forestry papers, Oxford Forestry Institute, Oxford, UK, No. 25, 124 p.
- Antun, C., Péissier, R., Vincent, G. & Couteron, P. (2013) Crown allometries are less responsive than stem allometry to tree size and habitat variations in an Indian monsoon forest. *Trees*, **27**, 1485–1495.
- Banin, I., Feldpausch, T.R., Phillips, O.I. *et al.* (2012) What controls tropical forest architecture? Testing environmental, structural and floristic drivers. *Global Ecology and Biogeography*, **21**, 1179–1190.
- Banin, L., Leis, S.L., Lopez-Gonzalez, G. *et al.* (2014) Tropical forest wood production: a cross-continental comparison. *Journal of Ecology*, **102**, 1025–1037.
- Barazzetti, L., Scaioni, M. & Remondino, F. (2010) Orientation and 3D modelling from markerless terrestrial images: combining accuracy with automation. *The Photogrammetric Record*, **25**, 356–381.
- Baskerville, G.L. (1972) Use of logarithmic regression in the estimation of plant biomass. *Canadian Journal of Forest Research*, **2**, 49–53.
- Bastin, J.F., Barbier, N., Réjou-Méchain, M. *et al.* (2015) Seeing Central African forests through their largest trees. *Scientific Reports*, **5**, 13156.
- Belyea, H.C. (1931) *Forest Measurement*. Wiley & Sons, New York, NY, USA; Chapman & Hall, London, UK.
- Bruce, D. & Schumacher, F.X. (1950) *Forest Mensuration*. McGraw-Hill Book Co., New York, NY, USA.
- Cailliez, F. (1980) *Forest Volume Estimation and Yield Prediction – Volume Estimation*. F.A.O. Forestry Paper 22/1, Rome, Italy, 98p.
- Chapman, C.A., Kaufman, L. & Chapman, L.J. (1998) Buttress formation and directional stress experienced during critical phases of tree development. *Journal of Tropical Ecology*, **14**, 341–349.
- Chave, J., Andalo, C., Brown, S. *et al.* (2005) Tree allometry and improved estimation of carbon stocks and balance in tropical forests. *Oecologia*, **145**, 87–99.

- Chave, J., Rejou-Mechain, M., Burquez, A. *et al.* (2014) Improved allometric models to estimate the aboveground biomass of tropical trees. *Global Change Biology*, **20**, 3177–3190.
- Clark, D.A. (2002) Are tropical forests an important carbon sink? Reanalysis of the long-term plot data. *Ecological Applications*, **12**, 3–7.
- Clark, D.A. & Clark, D.B. (1999) Assessing the growth of tropical rain forest trees: issues for forest modeling and management. *Ecological Applications*, **9**, 981–997.
- Condit, R. (1998) *Tropical Forest Census Plots: Methods and Results From Barro Colorado Island, Panama and a Comparison With Other Plots*. Springer-Verlag, Berlin, Germany.
- Coomes, D.A., Burslem, D.F. & Simonson, W.D. (2014) *Forests and Global Change*. Cambridge University Press, Cambridge, UK.
- Cushman, K.C., Muller-Landau, H.C., Condit, R.S. & Hubbell, S.P. (2014) Improving estimates of biomass change in buttressed trees using tree taper models. *Methods in Ecology and Evolution*, **5**, 573–582.
- Dean, C. (2003) Calculation of wood volume and stem taper using terrestrial single image close-range photogrammetry and contemporary software tools. *Silva Fennica*, **37**, 359–380.
- Dean, C. & Roxburgh, S. (2006) Improving visualisation of mature, high-carbon sequestering forests. *Forest Biometry, Modelling and Information Sciences*, **1**, 48–69.
- Dean, C., Roxburgh, S. & Mackey, B.G. (2003) Growth modelling of *Eucalyptus regnans* for carbon accounting at the landscape scale. *Modelling Forest Systems* (eds A. Amaro, D. Reed & P. Soares), pp. 27–39. CABI, Cambridge, UK.
- Fayolle, A., Doucet, J.-L., Gillet, J.-F., Bourland, N. & Lejeune, P. (2013a) Tree allometry in Central Africa: testing the validity of pantropical multi-species allometric equations for estimating biomass and carbon stocks. *Forest Ecology and Management*, **305**, 29–37.
- Fayolle, A., Rondeux, J., Doucet, J.-L., Ernst, G., Bouissou, C., Quevauxvillers, S., Bourland, N., Feteke, F. & Lejeune, P. (2013b) Réviser les tarifs de cubage pour mieux gérer les forêts du Cameroun. *Bois et Forêts des Tropiques*, **317**, 35–49.
- Fayolle, A., Picard, N., Doucet, J.-L., Swaine, M., Bayol, N., Bénédet, F. & Gourlet-Fleury, S. (2014) A new insight in the structure, composition and functioning of central African moist forests. *Forest Ecology and Management*, **329**, 195–205.
- Feldpausch, T.R., Banin, L., Phillips, *et al.* (2011) Height-diameter allometry of tropical forest trees. *Biogeosciences*, **8**, 1081–1106.
- Forbes, R.D. & Meyer, A.B. (1955) *Forestry Handbook*. Ronald Press Company, New York, NY, USA.
- Fraser, C.S. & Al-Ajlouni, S. (2006) Zoom-dependent camera calibration in digital close-range photogrammetry. *Photogrammetric Engineering & Remote Sensing*, **72**, 1017–1026.
- Goodman, R.C., Phillips, O.L. & Baker, T.R. (2014) The importance of crown dimensions to improve tropical tree biomass estimates. *Ecological Applications*, **24**, 680–698.
- Gourlet-Fleury, S., Mortier, F., Fayolle, A., Baya, F., Ouedraogo, D., Benedet, F. & Picard, N. (2013) Tropical forest recovery from logging: a 24 year silvicultural experiment from Central Africa. *Philosophical Transactions of the Royal Society of London B: Biological Sciences*, **368**, 20120302.
- He, Z., Tang, Y., Deng, X. & Cao, M. (2012) Buttress trees in a 20-hectare tropical dipterocarp rainforest in Xishuangbanna, SW China. *Journal of Plant Ecology*, **6**, 187–192.
- Henry, M., Besnard, A., Asante, W.A., Eshun, J., Adu-Bredu, S., Valentini, R., Bernoux, M. & Saint-Andre, L. (2010) Wood density, phytomass variations within and among trees, and allometric equations in a tropical rainforest of Africa. *Forest Ecology and Management*, **260**, 1375–1388.
- Kearsley, E., de Haulleville, T., Hufkens, *et al.* (2013) Conventional tree height-diameter relationships significantly overestimate aboveground carbon stocks in the Central Congo Basin. *Nature communications*, **4**, 2269.
- Läbe, T. & Förstner, W. (2004) Geometric stability of low-cost digital consumer cameras. *Proceedings of the 20th ISPRS Congress*, Istanbul, Turkey, pp. 528–535.
- Letouzey, R. (1982) *Manuel de Botanique Tropicale – Afrique Tropicale: Tome 1*. Centre Technique Forestier Tropical, Nogent sur Marne, France.
- Liang, X., Jaakkola, A., Wang, Y., Hyypää, J., Honkavaara, E., Liu, J. & Kaartinen, H. (2014) The use of a hand-held camera for individual tree 3D Mapping in forest sample plots. *Remote Sensing*, **6**, 6587–6603.
- Mehedi, M.A.H., Kundu, C. & Chowdhury, M.Q. (2012) Patterns of tree buttressing at Lawachara National Park, Bangladesh. *Journal of Forestry Research*, **23**, 461–466.
- Metcalf, C.J.E., Clark, J.S. & Clark, D.A. (2009) Tree growth inference and prediction when the point of measurement changes: modelling around buttresses in tropical forests. *Journal of Tropical Ecology*, **25**, 1–12.
- Meunier, Q., Moubogou, C. & Doucet, J.-L. (2015) *Les Arbres Utiles du Gabon*. Presses Agronomiques de Gembloux, Gembloux, Belgium.
- Muller-Landau, H.C., Detto, M., Chisholm, R.A., Hubbell, S.P. & Condit, R. (2014) Detecting and projecting changes in forest biomass from plot data. *Forests and Global Change* (eds D.A. Coomes, D.F.R.P. Burslem & W.D. Simonson), pp. 381–416. Cambridge University Press, Cambridge, UK.
- Ngomanda, A., Mavouroulou, Q.M., Obiang, N.L.E., Iponga, D.M., Mavougou, J.-F., Lepengue, N., Picard, N. & Mbatchesi, B. (2012) Derivation of diameter measurements for buttressed trees, an example from Gabon. *Journal of Tropical Ecology*, **28**, 299–302.
- Nogueira, E.M., Nelson, B.W. & Fearnside, P.M. (2006) Volume and biomass of trees in central Amazonia: influence of irregularly shaped and hollow trunks. *Forest Ecology and Management*, **227**, 14–21.
- Nölke, N., Fehrmann, L., I Nengah, S.J., Tiryan, T., Seidel, D. & Kleinn, C. (2015) On the geometry and allometry of big-buttressed trees – a challenge for forest monitoring: new insights from 3D-modeling with terrestrial laser scanning. *iForest-Biogeosciences and Forestry*, **8**, 574–581.
- Pan, Y., Birdsey, R.A., Fang, J. *et al.* (2011) A large and persistent carbon sink in the world's forests. *Science*, **333**, 988–993.
- Phillips, O.L., Baker, T.R., Brienen, R. & Feldpausch, T.R. (2015) *Field manual for plot establishment and remeasurement*. <http://www.rainfor.org/en/manuals>.
- Picard, N. & Gourlet-Fleury, S. (2008) *Manuel de Référence Pour L'installation de Dispositifs Permanents en Forêt de Production Dans le Bassin du Congo*. COMIFAC, Yaounde, Cameroon.
- Ploton, P., Barbier, N., Takoudjou Momo, S. *et al.* (2016) Closing a gap in tropical forest biomass estimation: taking crown mass variation into account in pantropical allometries. *Biogeosciences*, **13**, 1571–1585.
- Plumptre, A.J. (1995) The importance of “seed trees” for the natural regeneration of selectively logged tropical forest. *The Commonwealth Forestry Review*, **25**, 3–258.
- Pulkkinen, M. (2012) On non-circularity of tree stem cross-sections: effect of diameter selection on cross-section area estimation, Bitterlich sampling and stem volume estimation in Scots pine. *Silva Fennica*, **46**, 747–986.
- Rondeux, J. (1993) *La Mesure des Arbres et des Peuplements Forestiers*. Les presses agronomiques de Gembloux, Gembloux, Belgium.
- Shortis, M.R., Bellman, C.J., Robson, S., Johnston, G.J. & Johnson, G.W. (2006) Stability of zoom and fixed lenses used with digital SLR cameras. *Proceedings of the ISPRS Commission V Symposium of Image Engineering and Vision Metrology*, Citeseer, pp. 285–290.
- Slik, J.W., Paoli, G., McGuire, K. *et al.* (2013) Large trees drive forest above-ground biomass variation in moist lowland forests across the tropics. *Global Ecology and Biogeography*, **22**, 1261–1271.
- Sprugel, D.G. (1983) Correcting for bias in log-transformed allometric equations. *Ecology*, **64**, 209–210.
- Swaine, M.D., Lieberman, D. & Putz, F.E. (1987) The dynamics of tree populations in tropical forest: a review. *Journal of Tropical Ecology*, **3**, 359–366.
- Szeleski, R. (2010) *Computer Vision: Algorithms and Applications*. Springer-Verlag, London Limited, London, UK.
- Thompson, J., Proctor, J., Viana, V., Milliken, W., Ratter, J.A. & Scott, D.A. (1992) Ecological studies on a lowland evergreen rain forest on Maracá Island, Roraima, Brazil. I. Physical environment, forest structure and leaf chemistry. *Journal of Ecology*, **80**, 689–703.
- Wenzel, K., Rothermel, M., Fritsch, D. & Haala, N. (2013) Image acquisition and model selection for multi-view stereo. *ISPRS-International Archives of the Photogrammetry, Remote Sensing and Spatial Information Sciences*, **1**, 251–258.

Received 31 May 2016; accepted 12 September 2016

Handling Editor: Sean McMahon

Supporting Information

Additional Supporting Information may be found online in the supporting information tab for this article:

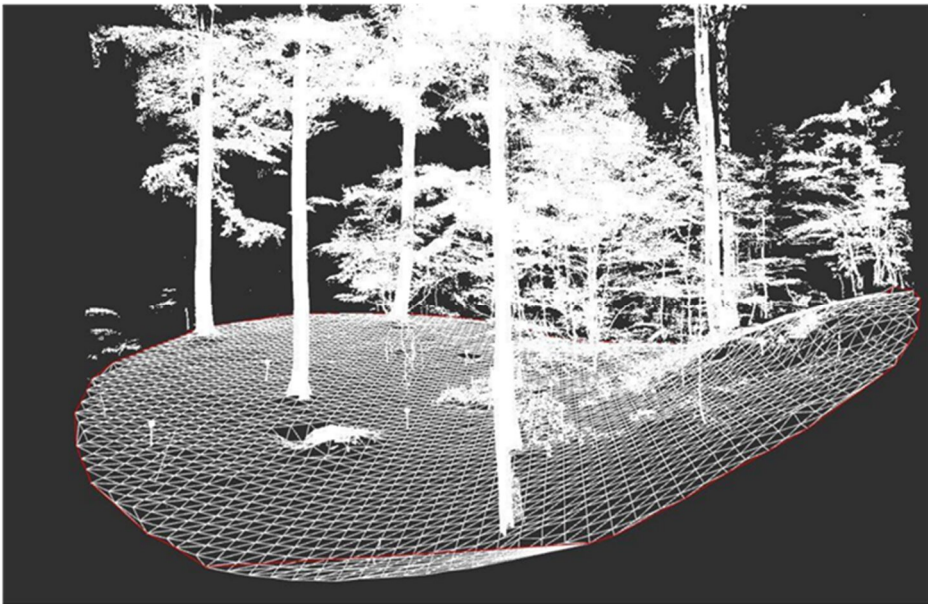
Appendix S1. Description of the Loudoungou site (Republic of Congo).

Appendix S2. Methodology and validation of the photogrammetric process.

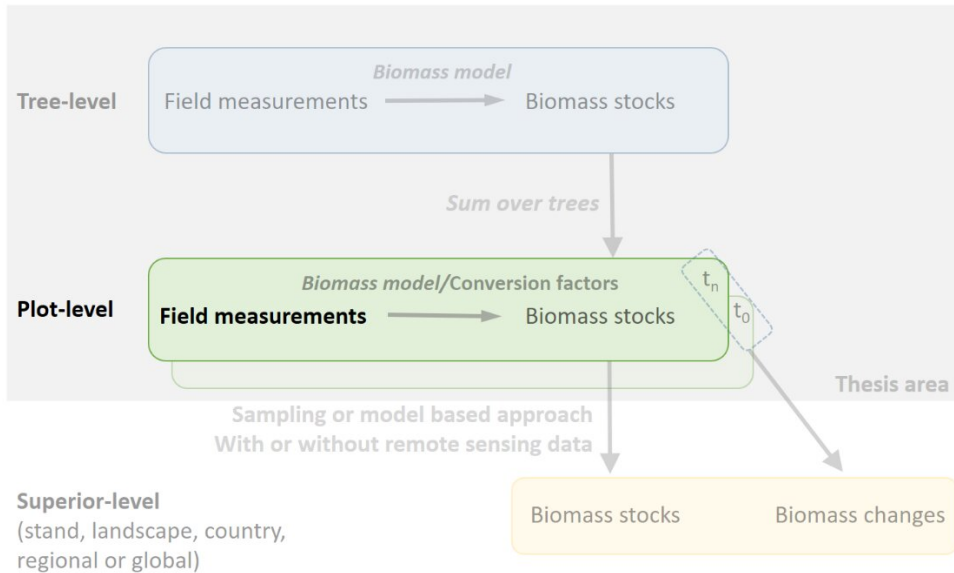
Appendix S3. POM definition, formatting biomass data and $D_{\text{area}130^\circ}$ field variable relationships.

3

3D stem measurements at the plot-level



3.1. Preamble



In this chapter, we assessed the potential of the 3D measurement tools that are terrestrial laser scanning (TLS) and hand-held mobile laser scanning (HMLS) to scan all the trees within an area at once. The research was led in forests close to our research lab in Belgium. Having all the trees 3D scanned in the plot allows the use of other allometries and conversion factors than conventional tree-level AGB models. We focused the study on the first step of the workflow starting at the plot level. The forerunner results of this study were the first stage before going further in the use of these technologies to measure in 3D all the stems in tropical forest plots.

This chapter is written in the following scientific peer-reviewed paper: Bauwens, S., Bartholomeus, H., Calders, K., & Lejeune, P. (2016). Forest inventory with terrestrial LiDAR: A comparison of static and hand-held mobile laser scanning. *Forests*, 7(6), 127.

3.2. The scientific peer-reviewed paper



Article

Forest Inventory with Terrestrial LiDAR: A Comparison of Static and Hand-Held Mobile Laser Scanning

Sébastien Bauwens^{1,†,*}, Harm Bartholomeus^{2,†,*}, Kim Calders^{3,4} and Philippe Lejeune⁵

¹ TERRA Research Unit, Gembloux Agro-Bio Tech, University of Liège, Passage des Déportés 2, Gembloux 5030, Belgium

² Laboratory of Geo-information Science and Remote Sensing, Wageningen University, Droevendaalsesteeg 3, Wageningen 6708 PB, The Netherlands

³ Earth Observations, Climate and Optical Group, National Physical Laboratory, Hampton Road, Teddington, Middlesex TW11 0LW, UK; kim.calders@npl.co.uk

⁴ Department of Geography, University College London, Gower Street, London WC1E 6BT, UK

⁵ BIOSE Research Unit, Gembloux Agro-Bio Tech, University of Liège, Passage des Déportés 2, Gembloux 5030, Belgium; p.lejeune@ulg.ac.be

* Correspondence: sebastien.bauwens@ulg.ac.be (S.B.); harm.bartholomeus@wur.nl (H.B.); Tel.: + 32-81-62-26-42 (S.B.); +31-317-48-17-92 (H.B.)

† These authors contributed equally to this work.

Academic Editors: Juha Hyypä, Xinlian Liang and Eetu Puttonen

Received: 16 April 2016; Accepted: 6 June 2016; Published: 21 June 2016

Abstract: The application of static terrestrial laser scanning (TLS) in forest inventories is becoming more effective. Nevertheless, the occlusion effect is still limiting the processing efficiency to extract forest attributes. The use of a mobile laser scanner (MLS) would reduce this occlusion. In this study, we assessed and compared a hand-held mobile laser scanner (HMLS) with two TLS approaches (single scan: SS, and multi scan: MS) for the estimation of several forest parameters in a wide range of forest types and structures. We found that SS is competitive to extract the ground surface of forest plots, while MS gives the best result to describe the upper part of the canopy. The whole cross-section at 1.3 m height is scanned for 91% of the trees (DBH > 10 cm) with the HMLS leading to the best results for DBH estimates (bias of -0.08 cm and RMSE of 1.11 cm), compared to no fully-scanned trees for SS and 42% fully-scanned trees for MS. Irregularities, such as bark roughness and non-circular cross-section may explain the negative bias encountered for all of the scanning approaches. The success of using MLS in forests will allow for 3D structure acquisition on a larger scale and in a time-efficient manner.

Keywords: forestry; terrestrial laser scanning; hand-held mobile laser scanning; HMLS; TLS; SIAM; digital elevation model; stem mapping

1. Introduction

Forests provide various ecosystem services, such as carbon storage, maintaining biodiversity, and wood production. Information on the current state and recent changes of forests are important basics for forest managers, policy-makers, conservation planners, and forest scientists. Forest inventories are the main tool used to describe the structure and quantify the forest resources. For large areas, the traditional approach is a statistical inventory of the forest, which results in the establishment of sample plots. Forest information deduced from parameters collected in the plots is then summarized for each stratum of the area inventoried.

Field parameters in sample plots are traditionally limited to the measurement methods available or the efficiency and the accuracy with which the measurement can be taken [1]. The tree parameters most frequently measured and used are diameter at breast height (DBH) of all trees and a sample of heights as they are strongly related to stem volume and above-ground biomass of the tree. Other tree attributes, such as the location, tree height, and height of the first living branch may also be recorded but are often not measured for every tree on sample plots because these measurements are labor-intensive [2]. An automated, instrument-based technique having the potential to augment conventional manual techniques would be of great interest, particularly in terms of objectivity and repeatability of results and time saving [3].

In remote sensing, the emergence of Light Detection and Ranging (LiDAR) in the late 1990s provided new insights to assess forest structure and the three-dimensional distribution of plant canopies at the plot level and regional scales. LiDAR is an active remote sensing method that can accurately measure distances by transmitting laser energy and analyzing the returned energy. LiDAR can be operated from spaceborne, airborne, or terrestrial platforms, with each platform serving specific forest inventory needs. Static terrestrial laser scanning (TLS), also known as ground-based LiDAR, offers the capacity to retrieve the 3D vegetation structure with millimeter accuracy [4].

The interest on TLS as a tool for forest plot measurement started in the past decade. The first reports based on this technique were published in 2003 [5–7] and 2004 [8–11]. The objective of these early studies was to explore the TLS potential for basic field measurements, such as measuring DBH and tree height [2]. Other variables of tree structure (e.g., crown, stem, or whole tree dimensions) can be observed and measured in the TLS data by time-consuming manual interpretation [10,12,13], although semiautomatic algorithms have been developed with various degrees of success [14–19]. Recently, a promising fully-automatic processing for volume estimates at the plot level has been proposed by Raunonen [20]. Data describing specific characteristics of individual trees can also be summarized to describe characteristics at the plot level, as stem density [10], the overall volume of biomass [18–21], or the fuel capacity in a forest [22]. Stand parameters can also be directly computed from TLS data as basal area [23], gap fraction [24,25], and Leaf Area Index (LAI) [26]. In addition to algorithms improvements for extracting forest attributes of TLS data, the acquisition protocol should also be optimized in the plot.

The occlusion effect occurring in TLS data is one of the main limitations of the use of this tool in forestry. Occlusion is the fact that some stems, branches, twigs, and leaves, or parts of it, may not be scanned as they are hidden by elements closer to the scanner. This is inherent to the static nature of TLS. To tackle the occlusion effect, the plot can be scanned with multiple scans (MS) instead of one single scan (SS) in the center of the plot or a statistical methods can be used [23–27]. The former solution, the MS approach, requires pre-scan preparations (setting up the plot and target placement). The targets are then used as tie-points between the single scan data during the co-registration process. The pre-scan preparations in the field for the multi-scan approach reduce the cost-effectiveness of this technology, whereas the statistical approach is limited to a few stand parameters, such as basal area estimations.

Laser scanners have recently been placed on moving ground platforms and designated as mobile laser scanners (MLS). MLS systems typically combine a laser scanner with an inertial measurement unit (IMU) and Global Navigation Satellite System (GNSS), making it analogous to airborne laser scanning (ALS). The quality of the final data (registered point cloud) is then related to the precision and accuracy of the three components, as well as the synchronization of these components. The accuracy of the MLS data are usually inferior to registered multi-scan TLS data [28]. For instance, MLS mounted on a car was reported to have an elevation accuracy of around 3.5 cm and a planimetric accuracy of 2.5 cm [29]. The advantage of MLS is the reduction of the occlusion effects, as well as increasing the areas scanned. The introduction of MLS in tree measurement started in early 2010 [30,31]. These first studies focused on sparse urban trees scanned from a MLS mounted on car. To our knowledge, no MLS study were conducted in forest environment before 2013 [32]. The limitation of the use of MLS in

forest areas is probably due to the low GNSS signal detection under forest cover leading to too low accuracy. Moreover, the use of a moving platform limits the use in forest ecosystems, since mounting the devices on a car, quad, or all-terrain vehicle may still not allow spatially-continuous mapping, nor does it correspond well with the non-destructive nature of LiDAR data acquisition. To encompass the moving limitation of MLS, the Finnish Geodetic Institute created a backpack mounted laser scanner [33] leading to the concept of personal laser scanning (PLS). An updated version of their PLS was tested in a forest environment, but the lack of proper satellite visibility during the field measurements led to less accurate platform positions, which also undermined the heading angle estimates [28].

Recently, a hand-held mobile laser scanning (HMLS) system was introduced by Bosse *et al.* [34], using the movement of the operator as a platform. This system (further described in the materials section) tackles some drawbacks of the traditional TLS setup, since the movement through the plot results in a theoretically unlimited number of scan-positions, which minimizes occlusion effects. Unlike MLS, forest cover is no longer a limitation, as HMLS does not need satellite positioning (GNSS). To assure good portability of the instruments concessions are made on the quality of the LiDAR module, resulting in a limited range (20–30 m) and lower accuracy (3 cm). A first study was carried out by Ryding *et al.* [35] to study the potential of HMLS for forest surveys. Their study, which is conducted in a restricted forest area dominated by hash and with small trees (DBH mean < 10 cm), showed first promising results in using this technology.

In this study, our main objective was to assess and compare the HMLS and TLS approaches for the estimation of several forest parameters in a wide range of forest types and structures. The influence of topography and forest structure was also analyzed. The same LiDAR scanning protocols were applied in all the plots, one protocol for the HMLS and two protocols for the TLS (the single or the multi-scan approach).

2. Materials and Methods

2.1. Instrumentation

For the static TLS data acquisition a FARO Focus 3D 120 (FARO, 250 Technology Park Lake Mary, FL 32746, United States) is used. This scanner uses phase-shift-based LIDAR technology to measure the XYZ locations of objects and further returns the intensity of the returned LIDAR beam (905 nm wavelength and a beam divergence of 0.19 mrad). The FARO scanner has a maximum range of 120 m and can collect 9.76×10^5 points per second with an accuracy of 2 mm at 10 m. Its lightweight (5.2 kg) construction, small size (24 cm × 20 cm × 10 cm) and short scanning time (e.g., 3 min without photograph with 1/5th of the full resolution) make it very appropriate for forest studies. The mixed pixels and range/intensity cross-talk effects, which limit the accuracy of phased-shifted based LiDAR at the edge of objects, were limited by enabling the “Clear Sky” and “Clear Contour” FARO filters in the hardware, as well as using the “ghost points” filter in the FARO Scene software. For each plot several FARO scans are done (see description further on), which are co-registered using 12 white spheres with a diameter of 19.5 cm that are placed within the plot.

As HMLS, we used the ZEB1, which consists of a 2D laser scanner (905 nm wavelength and a beam divergence of approximately 7 mrad), combined with an inertial measurement unit (IMU). These are both mounted on top of a spring, itself mounted on a hand grip [34]. The laser specifications cite a 30 m measurement range, but this is unlikely to be achieved outdoors (due to ambient solar radiation), and a survey swath of up to 15–20 m around the instrument is more realistic [36]. The hand-held part of the scanner (0.7 kg) is linked to a data logger carried in a backpack (3.6 kg). As the user carries the ZEB1 and walks through the environment, the scanner head swings back and forth creating a 3D scanning field with data being captured at the speed of movement. The scanner is a time-of-flight laser with a rate of 43,200 points/s (40 lines/s with a laser pulse interval of 0.25°) and a field of view of 270° horizontally and approximately 120° vertically. No additional information about the intensity of the returned signal is collected.

ZEB1 uses the Simultaneous Localization and Mapping (SLAM) algorithm to locate the scanner in an unknown environment and to register the whole 3D point clouds, relying on both the IMU data and feature detection algorithms. Optimal functioning of the alignment algorithm occurs in environments with well-distributed static unique surface features all around the sensor, providing consistent laser returns to facilitate convergence in the processing algorithms [36].

Processing of the raw ZEB1 data to a consistent 3D point cloud has to be done through an online processing service offered by GeoSLAM, for which processing charges need to be paid. The total processing cost depends on the length of the walked track. Following the manufacturer, the final 3D point cloud product has a scan range noise (accuracy) at 10 m of 30 mm in an indoor environment and 50 mm in bright light environments.

2.2. Study Area

The study area is located in the south of Belgium, close to the town of Vencimont, which is part of the Ardenne natural region. In the surroundings a large variety of forest types occur, ranging from young production forests to old growth forest. The area has an average elevation of approximately 200 meters and is characterized by gentle hills, with elevation differences of approximately 100 meters. The climate is temperate maritime, with cool summers and moderate winters, and precipitation in all seasons (Köppen: Cfb). Ten plots were laid out during the leaf-on period in varying forest types, forest structure, and covering different slope classes (Figure 1, Table 1 and Figure S1). The plots were selected in such a way that the maximum variation in forest types (broadleaved, coniferous, and mixed), tree density (NHA from 113 to 1344 trees/ha), and terrain properties (flat to steep) was achieved.

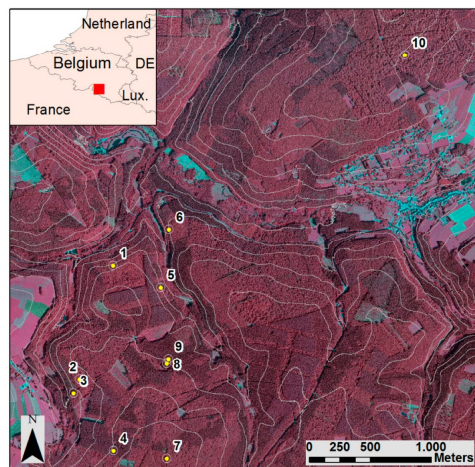


Figure 1. Overview of the study area, with the locations of the plots (IR orthoimage with contour interval of 20 m of elevation).

Table 1. Plot description based on field inventory data.

Plot	Forest Type	Slope (%)	Stand Structure	Main Species	Under-story	NHA (N) (trees ha ⁻¹)	GHA (m ² ·ha ⁻¹)	D _{min} -D _{max} (cm)
1	B	32.5	Coppice	<i>Carpinus betulus</i> and <i>Betula</i> spp.	1	835 (59)	46.2	10–135
2	B	11	Even-aged	<i>Fagus sylvatica</i>	0	113 (8)	29.8	44–68
3	B	11.2	Uneven-aged	<i>Fagus sylvatica</i>	1	127 (9)	28.6	14–80
4	C	16.9	Even-aged	<i>Pseudotsuga menziesii</i>	1	113 (8)	32.9	51–68
5	C	28.7	Even-aged	<i>Picea abies</i>	0	410 (29)	26.3	23–36
6	M	24.9	Even-aged	<i>Quercus</i> spp. and <i>Pinus sylvestris</i>	2	439 (31)	20.0	11–40
7	B	5.1	Uneven-aged	<i>Fagus sylvatica</i>	1	283 (20)	33.5	10–82
8	C	6.2	Even-aged	<i>Picea abies</i>	0	1344 (95)	75.5	10–44
9	C	6.0	Even-aged	<i>Picea abies</i>	0	594 (42)	45.8	21–46
10	B	10.5	Uneven-aged	<i>Fagus sylvatica</i>	1	424 (30)	30.0	10–79

Forest type, B: broadleaves, C: Coniferous, M: mixed. Understory, 0: no understory, 1: light understory, 2: dense understory; NHA is the number of trees (DBH > 10 cm) per hectare and N is the number of trees in the plot. GHA is the basal area per hectare. D_{min}-D_{max} shows the diameter of the thickest and smallest tree in the plot with a minimum DBH threshold of 10 cm.

2.3. Data Collection

According to the results of Trochta *et al.* [37] in mixed natural forests dominated by beech, with MS (using two to four scan positions) 90% of the trees are detected (*i.e.*, 50% of the cross-section at 1.3 m of height is visible) at a distance of 10–15 m of the scanners. This rate decrease to 80% when the SS setup is used. National forest inventory concentric plots have a maximum radius of less than 20 m and usually around 15 m for diameter at breast height (DBH) measurements. Following this information, and according to the objectives of the study, the plots were laid out with a radius of 15 m. From the center points, poles were placed in the cardinal directions to indicate the locations for the FARO scanner. The directions were measured using a compass and the distance to the center of the plot is determined with the ultrasound instrument VERTEX IV. Locations in between the cardinal points were indicated with secondary poles, to simplify the ZEBI data acquisition.

The TLS scanner was placed at the center of each plot and at the four cardinal points (Figure 2). If the cardinal point was too close to a tree included in the plot (distance less than 1 meter for instance) or just behind a tree, the scanner was slightly moved to a position where occlusion was less an issue. Full hemispherical scans with a point spacing of 0.045 degrees were done (1/5th of the full resolution) for a total of 28.4 million points per scan. Twelve spheres were set up within the plot as targets for co-registering the five scans.

A fixed pattern was followed for the HMLS data acquisition, which is shown in Figure 2. Scanning started in the south location. The scanning path is designed to have (1) a good distribution of the scanning positions (the plot is crossed four times and the path assures that the plot border is scanned at least once); (2) a pattern which reduces scanner range noise; and (3) avoids problems associated with drift, which can occur if the SLAM algorithm does not result in a good alignment. To prevent this, the path ends at the starting point (closing the loop), crosses the path several times (local loops) and some border sections are covered twice. For both scanning methods the time of data acquisition is recorded.

The reference field measurement was conducted at the same moment as the LiDAR scanning. The data collected were species, DBH, and tree position (azimuth and distance from the plot center) of all the trees with a diameter >10 cm which are inside the 15 m radius plot.

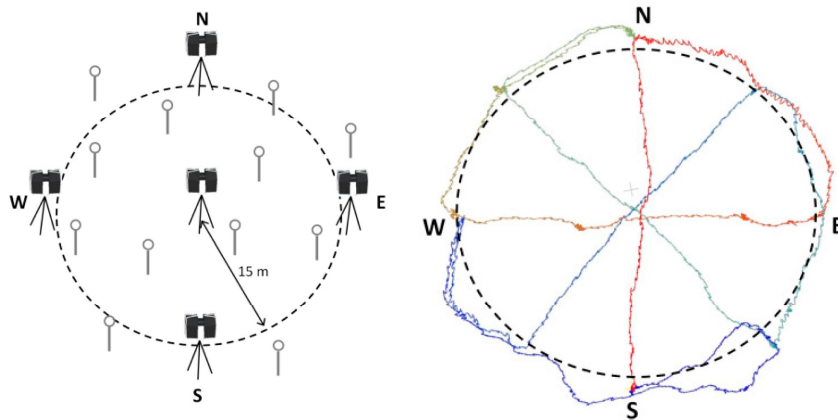


Figure 2. Locations of the TLS and the spheres (left) and walking pattern for the HMLS data acquisitions (starting in red and ending in dark blue) (right).

2.4. LiDAR Data Pre-Processing

The raw LiDAR data from the two scanners are processed to three point cloud datasets, which are used for further analysis and the extraction of forest parameters. The first dataset consists of the single TLS scan at the central position only. This implies that trees are, per definition, only observed from one direction and that occlusion will have a large influence on the derived forest parameters. This SS dataset will further be referred to as “FARO1”. For the second dataset, the five TLS scans are co-registered using the white spheres within the Scene software [38]. This dataset will further be referred to as “FARO5”. Resulting point clouds are used as the basis for the alignment of the FARO and ZEB1 data. ZEB1 raw data were uploaded to the GeoSLAM server, where the processing to a registered point cloud is done.

In order to ease the comparison of the registered point clouds and allow analysis at tree level, the ZEB1 point cloud is rotated and translated to the FARO5 data. First, a rough alignment was done by selecting corresponding points and using the align function in CloudCompare [39]. If no corresponding point were found, the ZEB1 was manually moved and rotated to match the FARO point cloud. These steps resulted in a rough alignment with an accuracy of approximately 5–20 cm. To improve the alignment, the Hybrid Multi-Station Adjustment (HMSA) in RiScan Pro 2.0 [40], was used. The HMSA algorithm modifies the orientation and position of each dataset in several iterations to calculate the best overall fit, for which point cloud features like planes and meshes are used. First, digital terrain models (DTMs) with different resolutions (FARO5: 50 cm; ZEB1: 50 cm and 10 cm) are computed. The FARO and ZEB1 DTMs are then aligned automatically in the HMSA process, thus aligning the point clouds as well. The final alignment was visually checked by making cross-sections of the point cloud data. For satisfactory results multiple (3 to 7) subsequent MSA runs were needed. This procedure is not required if the ZEB1 is used in an operational setting, as long as data only have to be collected at the plot level. Since the ZEB1 is not equipped with an internal GPS system, geo-rectification of the data would require additional processing steps, like placing artificial targets of which the location is known.

2.5. Scanning Completeness of the Trees

First, the completeness of the stem point cloud is compared between the three scanning methods: FARO1, FARO5, and ZEB1. The analysis is carried out on the top plan view with a sliced point cloud at a height of 125–135 cm above the terrain. Thus, cross-sections of the stems appear as a partial or full ring. Depending on the degree of ring closure, cross sections are classified into five quality

classes: (1) <25%; (2) 25%–50%; (3) 50%–75%; (4) >75%; and (5) whole cross-section. A sixth class, “Not detected”, is used for trees located on the stem map from field measurements and which does not have a cross-section in the LiDAR slice. In addition to the comparison of the quality of the stem point cloud between the scanning methods, we analyzed the influence of the stand characteristics and the terrain on the completeness of the point clouds. To test the significant effect of these environmental variables, we studied the relationship between the completeness of the cross-sections (proportion of closure) and the plots and terrain variables reported in the Table 1. The significance of the factors was determined by using linear mixed-effects models with, as a random factor, the plot ID (function `lme` from the library `nlme` of the R software). As the dependent variable corresponds to a proportion of closure class, we first converted it to a quantitative variable by replacing the class by the mid-class proportion value. Then, we applied an angular transformation (Equation (1)) in order to guarantee appropriate application conditions in the case of linear regressions [41]:

$$Y' = 2\arcsin\sqrt{Y} \quad (1)$$

where Y' represents the transformed variable, and Y , the original one (*i.e.*, the closure proportion of the cross section).

2.6. Extraction of Forest Parameters from the Point Clouds

The extraction of forest parameters was done with the open source software Computree using the algorithms from the ONF-ENSAM plugin [19]. The main steps used from this plugin are (1) terrain extraction and generation of rasters (a DTM and canopy height model: CHM) with a resolution which depends of the topography: 50 cm for flat plots and 10 cm for plots on slopes; (2) clustering of points; (3) creation of virtual logs; (4) skeletonization; and (5) stem mapping and DBH computation. The outputs of this process are a DTM, CHM, stem map, and DBH estimates. An interpolation and smoothing process was applied to the DTM to fill the pixels with missing values.

2.7. Analysis

Next, the comparison of the stem maps computed with Computree and the outcomes of the field inventory were compared in terms of the number of trees correctly detected (producer’s accuracy) and falsely detected trees (commission error), as well as differences in tree location between scanning methods.

The DTM and CHM outputs were analyzed and the derived DBH values for the FARO1, FARO5, and ZEB1 datasets were compared to field measurements. The root mean square error (RMSE) and bias between the LiDAR DBH and the field DBH were calculated.

The significance of plot level factors (stand structure, understory, number of trees per hectare (NHA), and basal area per hectare (GHA)), the slope and tree level factors (species, DBH, and bark roughness class of the species) on the quality of DBH estimates (difference between LiDAR DBH and field DBH) was tested by using a linear mixed-effects models with, as a random factor, the plot ID.

3. Results

3.1. Data Collection

The different scanning setups show large differences in the time which is needed to acquire and process the point cloud data. Positioning the spheres in the plot for registering the scans of the MS method is time consuming compared to the other measurements methods (40 min compared to 6 min for the FARO scanner and 11 min for ZEB1 (Table 2)). Setting up the plot and scanning from five locations with the TLS (FARO5) takes three times longer than scanning with ZEB1. The SS method and scanning with ZEB1 take less time than field measurements.

Table 2. Acquisition and processing time for the different scanning setups (SS: FARO1, MS: FARO5, and HMLS: ZEB1).

		FARO1	FARO5	ZEB1	Field Measurements
Fieldwork					
	Setting up	6 min	40 min	11 min	20–45 min
	Scan(s)	4–6 min	35 min	13 min	
Total		10 min	1 h 15 min	24 min	32 min
Processing data *					
	Registering	5 min	37 min	20 min	10 min
	Computree	4 min	47 min	1 h 26 min	
Total		9 min	1 h 24 min	1 h 46 min	

The setting up line in the table refers to the preparation of the scanner for FARO1, to the installation of the spheres and the preparation of the scanner for the FARO5 and to the preparation of the scanner and the initialization of the IMU for the ZEB1. Field measurements were measurement of the DBH with tape and determining the position of the trees (azimuth and distance). *the processing of the data is done by an experienced person. The registration time of the ZEB1 scans only includes the processing at the GeoSLAM server.

3.2. TLS Pre-Processing

The registration of the five scans (FARO5) was done with a minimum precision of 4 mm for the ten plots (*i.e.*, the average difference of the spheres positions between the scans in the final point cloud is less than 4 mm). The automatic co-registration of the ZEB1 scans gave satisfactory results for eight of the ten plots, although the exact precision cannot be determined. From the ZEB1 point cloud alone it could be determined that the automatic co-registration did not succeed for plot 2 and the quality of the registration of the plot 6 was not good enough for stem measurements. Plot 2 has a low number of trees, which hinders the object recognition in the SLAM algorithm, leading to a “slip” of the object recognition algorithm which results in a clearly different pattern than we walked. Plot 6 has a higher stem density, but also a dense understory with moving leaves. This understory might affect the co-registration of the ZEB1 scan too, which resulted in slight offsets of the points at the stems and presence of many double stems in the point cloud. Therefore, further analysis does not include plots 2 and 6.

3.3. Visual Comparison

Due to the limited range of the ZEB1, the laser does not reach most of the treetops and the point density in the upper canopy is rather low. A higher proportion of the points are located to the lower height level in the ZEB1 point clouds compare the TLS one. This higher proportion of points in the lower part of the plots with ZEB1 is due to the higher beam divergence of the ZEB1 and to the oscillating movement of the 2D scanner, which is in favor of horizontal scanning.

A comparison between the FARO5 and ZEB1 setup shows that the point clouds acquired with the ZEB1 is much noisier. Nevertheless, the points of the ZEB1 slice appear to be within and outside the stem and the density of points around the trunk follows a Gaussian shape with a mode located in the outline of the cross section (Figure 3). Indeed, the point density modes of the ZEB1 chart bar (5 mm in width) in transects of the transversal slice of the trunk match with the modes of FARO5 (red and yellow dashed lines). Fitting cylinders to the trunk should, therefore, result in the same diameters using the two technologies.

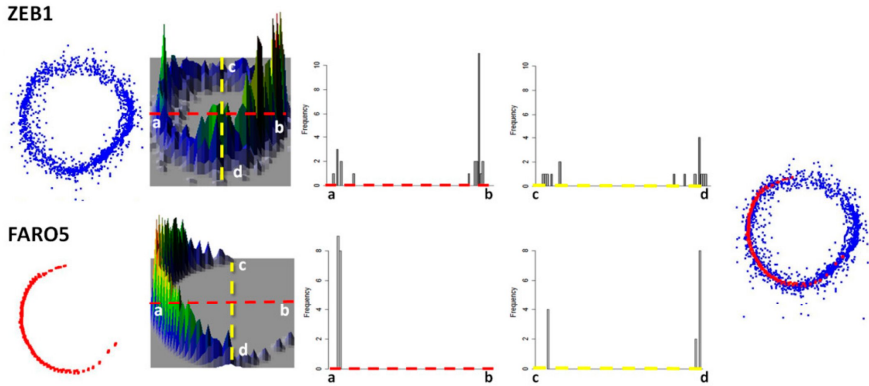


Figure 3. Comparison of a 1.3 m height slice of the point cloud (thickness of 10 cm) of one *Picea abies* stem scanned with the hand-held mobile laser scanning ZEB1 and with the multiscan method (FARO5). From the left, we have the top view of the slices, the 3D density graph of the slices, histograms of transects within the slices with bins of 5 mm (red dotted line are transects following the x axis and the yellow dotted line are transects following the y axis) and, finally, on the right, we have an overlay of the ZEB1 slice and the FARO5 slice.

3.4. The Success of Scanning Trees

In the eight plots studied, the number of trees detected from the LiDAR scans compared to the field inventory data shows that all the trees (DBH > 10 cm) were detected with the FARO5 and ZEB1 scanning method, whereas 17% of the trees are not detected when using a single scan (FARO1) (Figure 4). Due to the high number of scan positions with the ZEB1, this method results in the best spatial cover throughout the plot. As a result, the percentage of trees for which more than half of the cross-section is scanned is 1%, 79%, and 93% respectively for FARO1, FARO5, and ZEB1 setups (Figure 4). The whole cross-section is scanned for no trees with FARO1, for 42% of the trees with FARO5, and for 91% of the trees with ZEB1. The observations of the cross-section at 1.3 m height further showed that two trees were measured twice during the field survey in the dense plot 8, indicating that errors may also occur in field inventories.

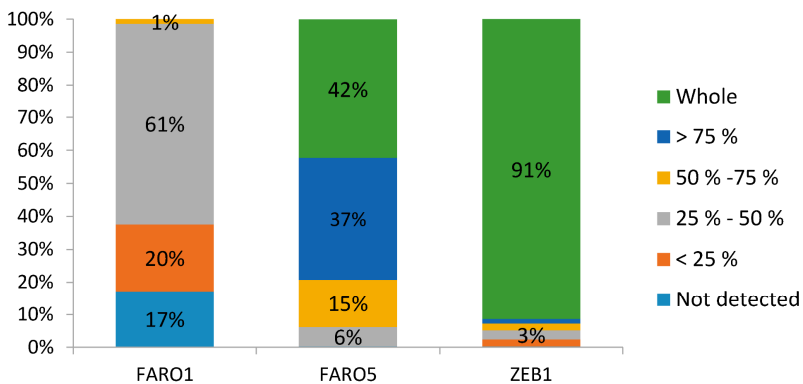


Figure 4. Percentage of the cross-section closure between the three different scanning methods according to the visual interpretation of the point cloud slices at 1.3 m height (thickness of 10 cm) of the eight plots.

The influence of stand factors and the slope for scanning trees are different for the scanning methods. The main significant factor affecting the proportion of the trees scanned for FARO1 is the slope. For FARO5, the only significant factor is the combination of NHA and GHA ($NHA \times GHA$) whereas for ZEB1, the understory is the only significant factor (the coefficient of the random effect of the plots is limited and the p -values are, respectively, 0.00, 0.01, and 0.01 for FARO1, FARO5, and ZEB1 models).

3.5. Extraction of Forest Parameters

3.5.1. DTM and CHM Comparison

By subtracting the DTM rasters between the different scanning methods, no observable bias is noticed, but for plots on a slope (plots 1 and 4), there are local pixel differences when comparing the FARO1 DTM with the FARO5 DTM (Figure 5). These differences are mainly between -1 m and 1 m, with some deviations up to -3.6 m and 3.5 m and outliers up to 12 m (plot 1) or 18 m (plot 4). The DTM differences between FARO1 and FARO5 have much larger variation for the sloping plots (plots 1–5), compared to the flat plots (plots 7–10) (Figure 5). As we do not have the same difference between the DTM of FARO5 and ZEB1, the local DTM divergence of FARO1 would mainly be the result of the scanning setup which engenders large occluded area. Refining parameters (e.g., reducing the resolution from 10 cm to 50 cm) for the DTM generation may reduce these local differences. DTMs generated from FARO5 and ZEB1 are similar with only a slight bias (less than 20 cm) for the DTM difference of plot 4 (Figure 5). The high herbaceous strata in plot 4 may explain this higher variation between FARO5 and ZEB1 DTMs.

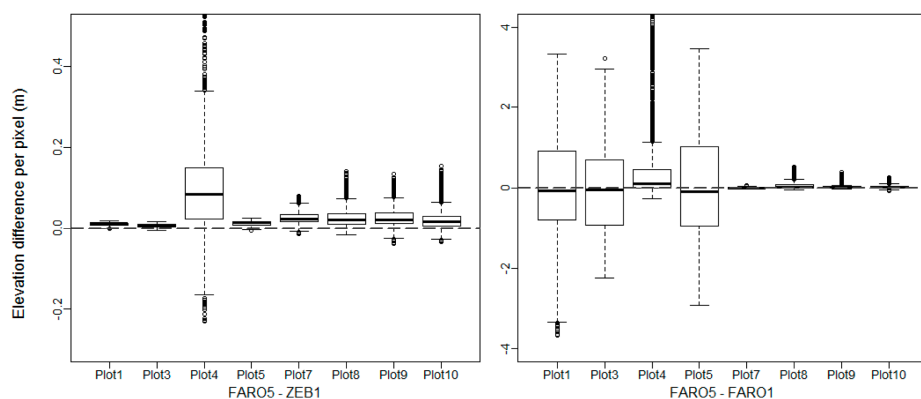


Figure 5. DTM differences comparing different scan setups. The bias is generally low, but slope and understory leads to variation in the generated DTMs (note that the y -axis scale is different for the two graphs).

The CHM differences between the setups are shown for each plot in Figure 6. The FARO1 setup is not suitable for studying the canopy top for plots of 15 m radius. Based on Figure 7, with FARO1 a reliable canopy height analysis might be done for a plot of maximum 5 m radius. For FARO1, the mean canopy height is on average underestimated by 3.1 m (Figure 6 and Table 3) and the CHM is highly variable compared to the other setups (high coefficient of variation: CV in Table 3). The CHM derived from ZEB1 data never reaches a height of 25 m, which is the range limit of the ZEB1 LiDAR scanner (Table 3). Moreover, an important part of the lasers does not overpass 15 to 20 m (Table 3 and Figure 7c,d). This range limitation explains the important differences noticed for the plots 3, 4, 8, and 9 (Figure 6 and Table 3). In plot 4, the stand is a mature even-aged stand of Douglas (*Pseudotsuga*

menziesii) with crowns starting at a height of 20–25 m and total heights reaching 40–45 m, which explain the high CHM difference (up to 40 m) noticed in the Figure 6.

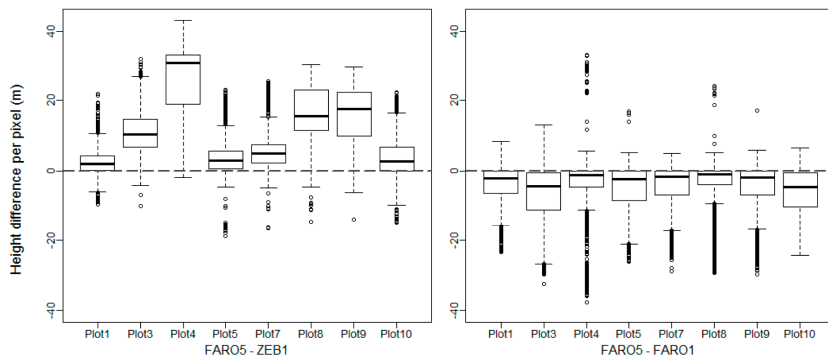


Figure 6. CHM differences comparing different scan setups.

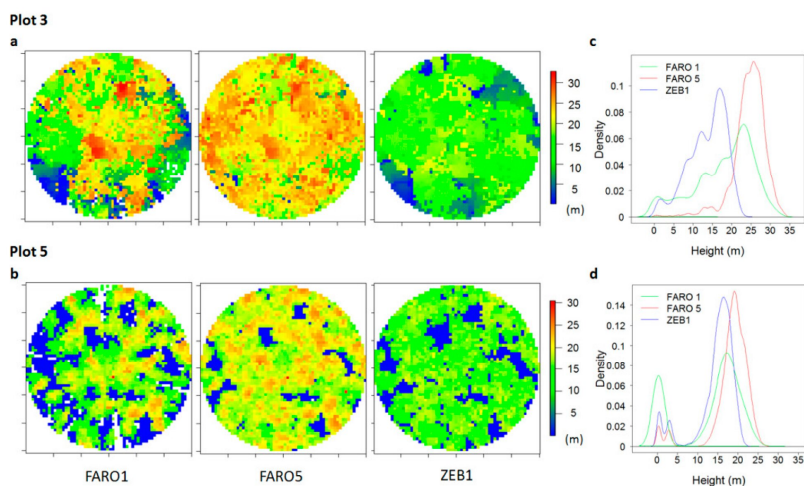


Figure 7. CHM illustration of two plots with the three different scanning methods.

Table 3. The maximum, mean, and coefficient of variation (standard deviation/mean) of the CHM heights of the different scanning setups.

Plot	FARO1			FARO5			ZEB1		
	Max (m)	Mean (m)	CV (%)	Max (m)	Mean (m)	CV (%)	Max (m)	Mean (m)	CV (%)
1	22.6	14.1	34	29.5	17.4	17	22.1	14.9	17
3	32.8	19.0	40	33.5	24.5	17	24.0	14.0	34
4	40.4	29.9	38	45.9	33.0	39	24.6	15.8	29
5	30.6	17.5	46	30.4	18.9	26	21.9	15.3	32
7	26.1	17.5	43	29.0	20.1	21	21.3	15.2	29
8	33.3	23.5	31	33.3	25.3	15	21.0	12.6	50
9	32.0	21.0	43	30.7	22.9	23	22.3	12.7	52
10	25.7	10.4	46	28.6	15.9	38	21.7	12.2	32

Only pixels with a height of more than 2 m were used to compute the mean and the standard deviation.

3.5.2. Stem Mapping and DBH Estimation

Processing the point clouds of FARO1, FARO5 and ZEB1 with Computree results in an average true tree detection rate (producer's accuracy for trees with DBH > 10 cm) of, respectively, $78\% \pm 18\%$, $93\% \pm 8\%$, and $90\% \pm 12\%$, and an average percentage of false trees (commission error) of $21\% \pm 18\%$, $22\% \pm 21\%$, and $31\% \pm 24\%$. The average difference between stem locations of FARO5-FARO1, FARO5-ZEB1 is, respectively, 2.8 ± 14 cm and 4.2 ± 7.5 cm. So, deformations, from drift or bad registration of the ZEB1 point clouds, are not observed in the eight plots.

In comparison to field DBH measurements, the FARO5 and ZEB1 setups show similar reliable DBH estimates, with a bias lower than -0.2 cm and a RMSE lower than 1.5 cm (Figure 8, Table 4). DBH of almost all correctly-detected trees is determined with an accuracy of <3 cm (respectively 96% and 98% of the trees scanned for FARO5 and ZEB1). These rates decrease to, respectively, 78% and 73% for an accuracy <1 cm. The bias and the RMSE of FARO1 is much higher compared to the two other setups with a relative RMSE of 13.4%, while it is less than 5% for the others setups. The FARO1 setup results in a clearly worse performance of the DBH determination showing that the circle-fitting used in our method is not able to deal with incomplete scanning of tree stems, where the algorithm has no problem estimating DBH with the "noisy" data from ZEB1.

Table 4. Summary statistics of DBH fitting of all the trees detected by each setup. The root mean square error (RMSE) in percentage is the RMSE divided by the mean DBH.

Setup	Bias	RMSE (cm)	RMSE (%)
FARO1	-1.17	3.73	13.4
FARO5	-0.17	1.3	4.7
ZEB1	-0.08	1.11	4.1

Depending of the scanning method, one or two factors at the tree level have a significant effect on DBH estimates: the bark-roughness of the species (smooth or rough) and the size of the tree (DBH). For FARO1, only the bark-roughness has a highly significant effect on the accuracy of DBH estimates, with a higher negative bias for species with rough bark ($p = 0.00016$). For FARO5, the size of the tree and the bark roughness with the mean slope of the plot have a significant effect on the accuracy of DBH estimates ($p = 0.0001$). Finally, with ZEB1, both tree level factors have a significant effect on the accuracy of DBH estimates ($p = 2.2 \times 10^{-16}$), but the random factor plot is also significant ($p = 2.7 \times 10^{-5}$). The significance of the factor plot may hide the influence of another variable as the registration quality with the SLAM algorithm. Nevertheless, the Figure 8 shows the high relationship between DBH accuracy and size of the trees for ZEB1.

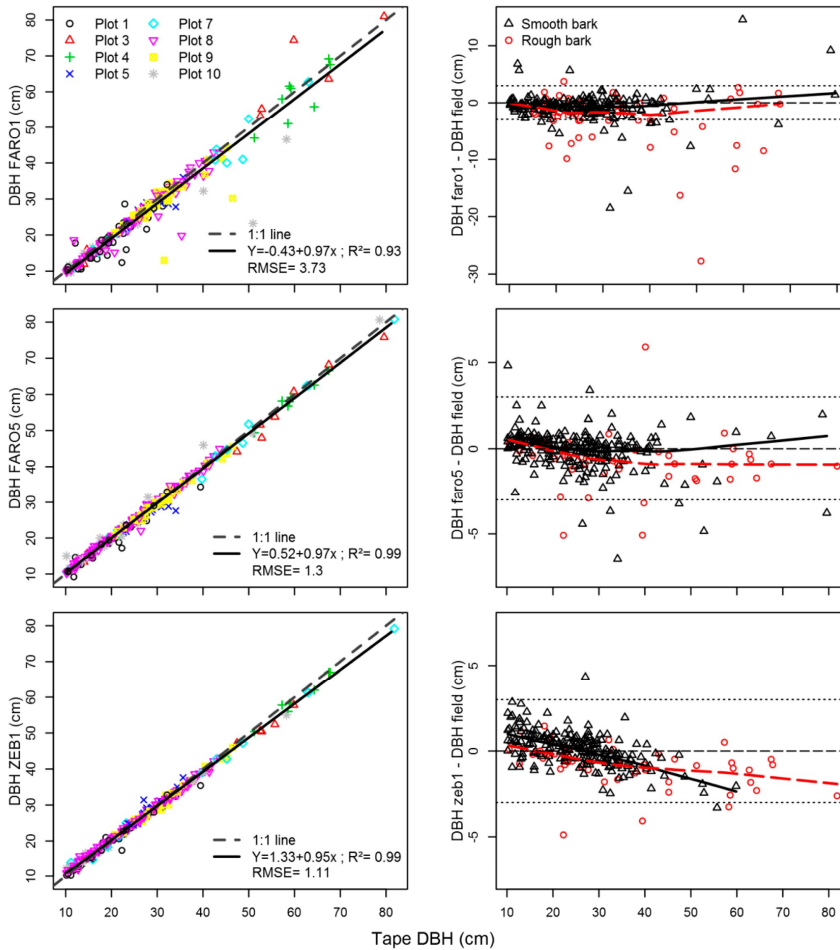


Figure 8. On the **left**, scatterplots of the DBH measured with the tape versus the DBH derived from the different LiDAR data of all the trees detected. The dashed line shows the 1:1 line and the solid line the trend-line. On the **right**, the diameter difference between DBH estimates from LiDAR and DBH measured in the field with a tape (the y scale of the residual plot of FARO 1 is different to the other residual plots). The solid grey curve is composed of local fitted lines (LOESS fitting with a span of $2/3$) for the species classified as smooth bark species and the long dashed red curve shows local fitted lines for the rough bark species. The y values of the horizontal dotted lines are, respectively, 3 cm and -3 cm, which are threshold values discussed in the results.

4. Discussion

The SS method has on average a tree detection rate of 80% in all boreal and temperate forest types (Table S1). With SS, scanning trees at 1.3 m height in sloping terrain is more difficult as branches above 1.3 m height of the surrounding trees occlude the stems of the trees of the lower part of the plot and low vegetation (under 1.3 m height) occlude the stems of the upper part of the plot. The MS method increases the tree detection rate to more than 95% for plots with an area of less than 0.15 ha. The use of a HMLS allows a better tree detection rate than MS TLS and with a very competitive acquisition time.

The HMLS combined with SLAM algorithms have a better registration accuracy in forest environments compared to the traditional MLS registering process, which uses GNSS data. Nevertheless, the high beam divergence of the HMLS reduces the penetration of the laser through the understory compared to the scanner used in TLS.

For plots with an area of less than 0.10 ha, SS and MS TLS methods, as well as HMLS using SLAM algorithms, produce suitable DTMs. The SS approach can then be used for DTM production in traditional forest inventory plots in order to combine it with ALS data. The ability of TLS to directly measure the height of the canopy top is limited because of occlusion. Due to the limited range and the high beam divergence of the HMLS it is also not possible to get reliable information of the canopy top. HMLS with a higher range and a lower beam divergence still needs to be tested for canopy top description. Otherwise, the combination of TLS data with aerial information as ALS or photogrammetric point cloud will offer a unique complete 3D description of the forest structure.

Comparing SS and MS DBH estimates with the same scanner show that partial information of the cross section of the trees limits the accuracy and the precision of the DBH estimates (Table S1). Moreover, the roughness of the bark seems to have influence in the accuracy of TLS DBH estimates based on circle fitting, as Brolly and Kiraly [42] noticed. The low precision of the HMLS scanner and the use of the SLAM algorithm for the registration do not impact the global accuracy and precision of DBH estimates. Nevertheless, with the HMLS, the DBH accuracy may be significantly influenced by the quality of the SLAM registration in the plot and the size of the tree. The influence of this last factor is also noticed by Ryding *et al.* [35]. The roughness of the bark also seems to have an influence. The high completeness of the cross-section scanned with HMLS could also reintroduce other methods for estimating the basal area of the cross-section, such as polygons [43], free-form curves [44], or mesh adjustment.

The high influence of the size of the tree for DBH estimates of completely-scanned trunks (which is the case for trees scanned with MS TLS and HMLS) might be explained by two factors. First, the larger the tree, the more irregular the shape of the base of the trunk is and the rougher the bark is. The irregularities at the base of the trunk might induce an overestimation of the diameter measured with the tape as the tape measures the convex hull of the cross-section. On the other hand, least square circle fitting on irregular cross-sections, as well as on a tree with rough bark, will induce lower diameter estimation than tape measurement as the concave parts of the irregular cross section and of the bark weight in the circle fitting. Secondly, the smaller the tree, the higher the chances that the tree will have low branches and having other small trees with low branches surrounding it. These low branches will have an influence in the least square circle fitting by inducing an overestimation of the diameter. Due to its high beam divergence, the HMLS is more sensitive to these small branches than the MS TLS approach.

The algorithms used to extract DBH still need improvements at two levels: the estimation of the breast height (1.3 m) and filtering the false trees detected. The challenging issues of these two points are not often discussed in the forestry TLS literature, whereas some other studies also show a high proportion of false trees (11% in [14], 12% in [45], 0%–1.4% in [42], 1%–2% in [46], 6% in [47], and 14.4% in [28]). Results which are influenced by the DBH threshold chosen in their studies. In forestry, the ground level (height = 0 m) is defined as the highest point of the ground around the tree. The algorithms used to extract the DBH do not always use this definition. The comparison with field measurement could then be more difficult if the breast height is not marked on the trunk for comparing the point of measurement prior to the analysis of the DBH estimates. In this study we adjusted the theoretical height of the algorithm to be, on average, in accordance with the point measurement used in the field.

The use of PLS, such as HMLS, for scanning the forest is promising for the description of the 3D structure of the forest. These scanners will be able to scan larger areas than TLS. The registering success is still a challenging issue when the SLAM algorithm is used with the HMLS data as 20% of the plots were not registered properly and DBH estimates of the remaining plots were also influenced by the

quality of the registration (significance of the random effect of the plots). In addition to improvements in the registering process, a scanner with a higher range and a lower beam divergence will increase the quality of scanning forest with HMLS. With the current equipment it is not possible to scan the top of canopy and determine tree height, which would be important to estimate, e.g., timber volume and biomass accurately.

5. Conclusions

The use of a human operator as a mobile platform for laser scanning will significantly reduce the actual limitation for acquisition of 3D laser data in forests. The recent progress in automatic registration of scans and the reduction of the weight of the scanners has taken laser scanning to an operational level to retrieve the 3D structure of the forest and for forest monitoring. When acquisition speed is most important, Single Scan TLS is fastest, but the analysis of these data shows that a large number of trees remains undetected and the partial scanning of the trees results in low usability. HMLS is faster than Multi Scan TLS and yields better results for a number of tree parameters (DBH and tree detection). However, due to the limited range of the ZEB1 used in this study, the canopy is poorly described, resulting in a low usability of HMLS for heights above 15–20 m. With HMLS, almost the entire section at breast height of all of the trees is scanned, which will reintroduce other methods than circle or cylinder fitting to estimate basal area and volumes at the stand level. The actual challenging issue are processing scanner data at the plot or stand level. Automatic tree detection still needs to be improved and the volume estimates of the trees processed at the stand level need to be validated. Relating these data to other remote sensing data will offer new, accurate field data to upscale forest parameters, such as basal area or stand volume.

Supplementary Materials: The following are available online at <http://www.mdpi.com/1999-4907/7/6/127>, Figure S1: Images of the 10 forest plots studied, Table S1: Summary of experimental design, scanner settings, and methodologies of previous studies on automatic stem detection and DBH extraction from TLS data for forest inventory.

Acknowledgments: We thank Fond Français pour l'Environnement through the DynAfFor project and the World Bank through the PreREDD+ project who financially supported the time spent by S.B. for this research. We also thank the technical team of the Forest Resources Management unit of Gembloux Agro Bio Tech (University of Liège) who assisted us for field work and Nature + for their administrative support.

Author Contributions: S.B., H.B. and K.C. designed the study, S.B. and H.B. conducted the fieldwork; S.B. did most of the data-analysis; H.B., S.B. and K.C. wrote the manuscript and P.L. supervised the research and reviewed the manuscript.

Conflicts of Interest: The authors declare no conflict of interest. The founding sponsors had no role in the design of the study; in the collection, analyses, or interpretation of data and in the writing of the manuscript.

References

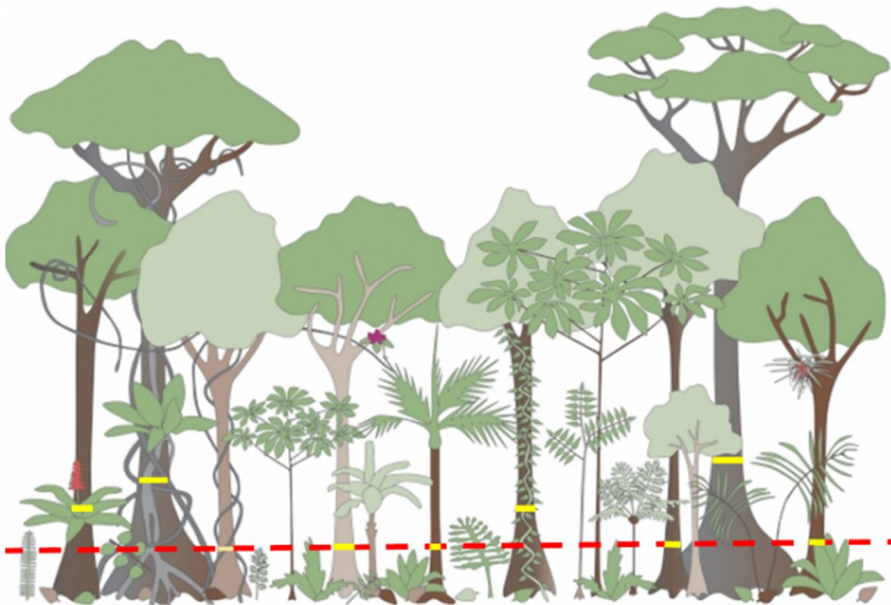
1. Newnham, G.J.; Armston, J.D.; Calders, K.; Disney, M.I.; Lovell, J.L.; Schaaf, C.B.; Strahler, A.H.; Danson, F.M. Terrestrial laser scanning for plot-scale forest measurement. *Curr. For. Rep.* **2015**, *1*, 239–251. [CrossRef]
2. Liang, X. Feasibility of Terrestrial Laser Scanning for Plotwise Forest Inventories. Available online: <http://lib.tkk.fi/Diss/2013/isbn9789517112994/isbn9789517112994.pdf> (accessed on 15 June 2016).
3. Lovell, J.L.; Jupp, D.L.B.; Newnham, G.J.; Culvenor, D.S. Measuring tree stem diameters using intensity profiles from ground-based scanning lidar from a fixed viewpoint. *ISPRS J. Photogramm. Remote Sens.* **2011**, *66*, 46–55. [CrossRef]
4. Van Leeuwen, M.; Nieuwenhuis, M. Retrieval of forest structural parameters using LiDAR remote sensing. *Eur. J. For. Res.* **2010**, *129*, 749–770. [CrossRef]
5. Erikson, M.; Karin, V. Finding tree-stems in laser range images of young mixed stands to perform selective cleaning. In Proceedings of the ScandLaser Scientific Workshop on Airborne Laser Scanning of Forest, Umea, Sweden, 3–4 September 2003.

6. Simonse, M.; Aschoff, T.; Spiecker, H.; Thies, M. Automatic determination of forest inventory parameters using terrestrial laserscanning. In Proceedings of the ScandLaser Scientific Workshop on Airborne Laser Scanning of Forest, Umea, Sweden, 3–4 September 2003; Volume 2003, pp. 252–258.
7. Watt, P.J.; Donoghue, D.N.M.; Dunford, R.W. Forest Parameter Extraction Using Terrestrial Laser Scanning. Available online: http://www.natscan.uni-freiburg.de/suite/pdf/030916_1642_1.pdf (accessed on 15 June 2016).
8. Aschoff, T.; Thies, M.; Spiecker, H. Describing forest stands using terrestrial laser-scanning. *Int. Arch. Photogramm. Remote Sens. Spat. Inf. Sci.* **2004**, *35*, 237–241.
9. Haala, N.; Reulke, R.; Thies, M.; Aschoff, T. Combination of Terrestrial Laser Scanning with High Resolution Panoramic Images for Investigations in Forest Applications and Tree Species Recognition. Available online: http://www.isprs.org/proceedings/XXXIV/5-W16/papers/PanoWS_Dresden2004_Haala.pdf (accessed on 15 June 2016).
10. Hopkinson, C.; Chasmer, L.; Young-Pow, C.; Treitz, P. Assessing forest metrics with a ground-based scanning lidar. *Can. J. For. Res.* **2004**, *34*, 573–583. [[CrossRef](#)]
11. Thies, M.; Spiecker, H. Evaluation and future prospects of terrestrial laser scanning for standardized forest inventories. *Forest* **2004**, *2*, 1.
12. Côté, J.-F.; Widłowski, J.-L.; Fournier, R.A.; Verstraete, M.M. The structural and radiative consistency of three-dimensional tree reconstructions from terrestrial lidar. *Remote Sens. Environ.* **2009**, *113*, 1067–1081. [[CrossRef](#)]
13. Fleck, S.; Mölder, I.; Jacob, M.; Gebauer, T.; Jungkunst, H.F.; Leuschner, C. Comparison of conventional eight-point crown projections with LIDAR-based virtual crown projections in a temperate old-growth forest. *Ann. For. Sci.* **2011**, *68*, 1173–1185. [[CrossRef](#)]
14. Bienert, A.; Scheller, S.; Keane, E.; Mohan, F.; Nugent, C. Tree Detection and Diameter Estimations by Analysis of Forest Terrestrial Laserscanner Point Clouds. Available online: http://www.isprs.org/proceedings/XXXVI/3-W52/final_papers/Bienert_2007.pdf (accessed on 15 June 2016).
15. Calders, K.; Newnham, G.; Burt, A.; Murphy, S.; Raunonen, P.; Herold, M.; Culvenor, D.; Avitabile, V.; Disney, M.; Armston, J.; et al. Nondestructive estimates of above-ground biomass using terrestrial laser scanning. *Methods Ecol. Evol.* **2015**, *6*, 198–208. [[CrossRef](#)]
16. Côté, J.-F.; Fournier, R.A.; Egli, R. An architectural model of trees to estimate forest structural attributes using terrestrial LiDAR. *Environ. Model. Softw.* **2011**, *26*, 761–777. [[CrossRef](#)]
17. Dassot, M.; Colin, A.; Santenoise, P.; Fournier, M.; Constant, T. Terrestrial laser scanning for measuring the solid wood volume, including branches, of adult standing trees in the forest environment. *Comput. Electron. Agric.* **2012**, *89*, 86–93. [[CrossRef](#)]
18. Lefsky, M.; McHale, M.R. Volume estimates of trees with complex architecture from terrestrial laser scanning. *J. Appl. Remote Sens.* **2008**, *2*, 023521.
19. Othmani, A.; Piboule, A.; Krebs, M.; Stolz, C.; Voon, L.L.Y. Towards Automated and Operational Forest Inventories with T-Lidar. Available online: <https://hal.archives-ouvertes.fr/hal-00646403/document> (accessed on 15 June 2016).
20. Raunonen, P.; Casella, E.; Calders, K.; Murphy, S.; Akerblom, M.; Kaasalainen, M. Massive-scale tree modelling from TLS data. *ISPRS Ann. Photogramm. Remote Sens. Spat. Inf. Sci.* **2015**, *2*, 189–196. [[CrossRef](#)]
21. Huang, H.; Li, Z.; Gong, P.; Cheng, X.; Clinton, N.; Cao, C.; Ni, W.; Wang, L. Automated methods for measuring DBH and tree heights with a commercial scanning lidar. *Photogramm. Eng. Remote Sens.* **2011**, *77*, 219–227. [[CrossRef](#)]
22. García, M.; Danson, F.M.; Riano, D.; Chuvieco, E.; Ramirez, F.A.; Bandugula, V. Terrestrial laser scanning to estimate plot-level forest canopy fuel properties. *Int. J. Appl. Earth Obs. Geoinform.* **2011**, *13*, 636–645. [[CrossRef](#)]
23. Strahler, A.H.; Jupp, D.L.; Woodcock, C.E.; Schaaf, C.B.; Yao, T.; Zhao, F.; Yang, X.; Lovell, J.; Culvenor, D.; Newnham, G.; et al. Retrieval of forest structural parameters using a ground-based lidar instrument (Echidna®). *Can. J. Remote Sens.* **2008**, *34*, S426–S440. [[CrossRef](#)]
24. Danson, F.M.; Hetherington, D.; Morsdorf, F.; Koetz, B.; Allgöwer, B. Forest canopy gap fraction from terrestrial laser scanning. *IEEE Geosci. Remote Sens. Lett.* **2007**, *4*, 157–160. [[CrossRef](#)]
25. Lovell, J.L.; Haverd, V.; Jupp, D.L.B.; Newnham, G.J. The Canopy Semi-analytic P gap and Radiative Transfer (CSART) Model: A Novel Approach to Estimating Forest Canopy Gap Fraction from Terrestrial Laser Scanning Data. *Remote Sens.* **2015**, *7*, 1111–1127. [[CrossRef](#)]

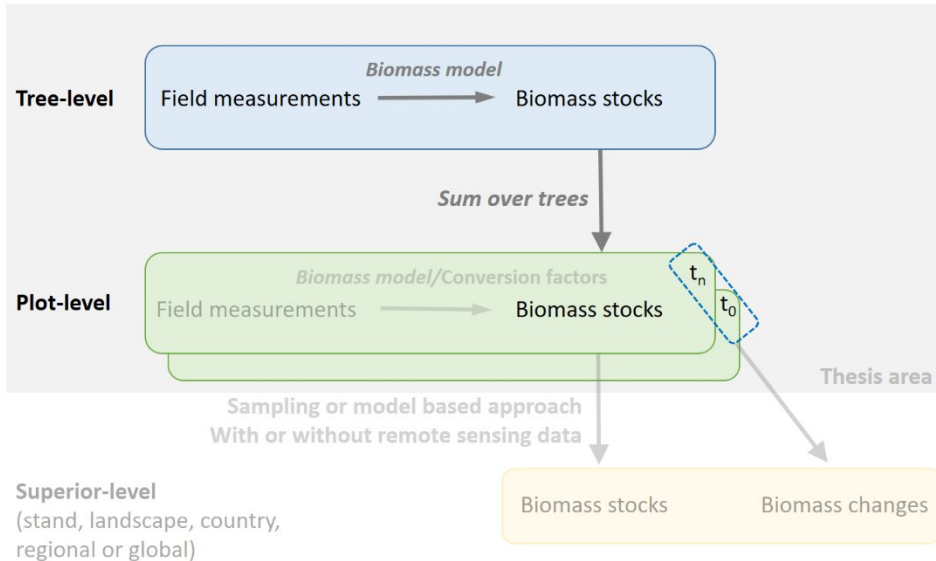
26. Hosoi, F.; Omasa, K. Factors contributing to accuracy in the estimation of the woody canopy leaf area density profile using 3D portable lidar imaging. *J. Exp. Bot.* **2007**, *58*, 3463–3473. [[CrossRef](#)] [[PubMed](#)]
27. Jupp, D.L.; Culvenor, D.S.; Lovell, J.L.; Newnham, G.J. Evaluation and validation of canopy laser radar (LIDAR) systems for native and plantation forest inventory. *Final Report to the Forest and Wood Products Research & Development Corporation(FWPRDC: PN 02.2902) CSIRO* **2005**, *20*, 192–197.
28. Liang, X.; Kukko, A.; Kaartinen, H.; Hyypä, J.; Yu, X.; Jaakkola, A.; Wang, Y. Possibilities of a Personal Laser Scanning System for Forest Mapping and Ecosystem Services. *Sensors* **2014**, *14*, 1228–1248. [[CrossRef](#)] [[PubMed](#)]
29. Kaartinen, H.; Hyypä, J.; Kukko, A.; Jaakkola, A.; Hyypä, H. Benchmarking the performance of mobile laser scanning systems using a permanent test field. *Sensors* **2012**, *12*, 12814–12835. [[CrossRef](#)]
30. Jaakkola, A.; Hyypä, J.; Kukko, A.; Yu, X.; Kaartinen, H.; Lehtomäki, M.; Lin, Y. A low-cost multi-sensoral mobile mapping system and its feasibility for tree measurements. *ISPRS J. Photogramm. Remote Sens.* **2010**, *65*, 514–522. [[CrossRef](#)]
31. Rutzinger, M.; Pratihast, A.K.; Oude Elberink, S.; Vosselman, G. Detection and modelling of 3D trees from mobile laser scanning data. *Int. Arch. Photogramm. Remote Sens. Spat. Inf. Sci.* **2010**, *38*, 520–525.
32. Holopainen, M.; Kankare, V.; Vastaranta, M.; Liang, X.; Lin, Y.; Vaaja, M.; Yu, X.; Hyypä, J.; Hyypä, H.; Kaartinen, H.; et al. Tree mapping using airborne, terrestrial and mobile laser scanning—A case study in a heterogeneous urban forest. *Urban For. Urban Green.* **2013**, *12*, 546–553. [[CrossRef](#)]
33. Kukko, A.; Kaartinen, H.; Hyypä, J.; Chen, Y. Multiplatform mobile laser scanning: Usability and performance. *Sensors* **2012**, *12*, 11712–11733. [[CrossRef](#)]
34. Bosse, M.; Zlot, R.; Flick, P. Zebedee: Design of a spring-mounted 3-d range sensor with application to mobile mapping. *IEEE Trans. Robot.* **2012**, *28*, 1104–1119. [[CrossRef](#)]
35. Ryding, J.; Williams, E.; Smith, M.J.; Eichhorn, M.P. Assessing Handheld Mobile Laser Scanners for Forest Surveys. *Remote Sens.* **2015**, *7*, 1095–1111. [[CrossRef](#)]
36. James, M.R.; Quinton, J.N. Ultra-rapid topographic surveying for complex environments: The hand-held mobile laser scanner (HMLS). *Earth Surf. Process. Landf.* **2014**, *39*, 138–142. [[CrossRef](#)]
37. Trochta, J.; Král, K.; Janik, D.; Adam, D. Arrangement of terrestrial laser scanner positions for area-wide stem mapping of natural forests. *Can. J. For. Res.* **2013**, *43*, 355–363. [[CrossRef](#)]
38. FARO Scene—version 5.4. FARO Verwaltungs GmbH. 2015. Available online: <http://www.faro.com/> (accessed on 15 June 2016).
39. CloudCompare—version 2.6. Available online: <http://www.cloudcompare.org/> (accessed on 15 June 2016).
40. RIEGL LMS, RiSCAN PRO Version 2.0. Software Description and User's Instructions. 2016. Available online: <http://www.riegl.com/> (accessed on 15 June 2016).
41. Dagnélie, P. *Statistique Théorique et Appliquée, Tome 2: Inférences à une et à Deux Dimensions*; Bruxelles-Université, Ed.; De Boeck & Larcier: Bruxelles, Belgium, 2006.
42. Brolly, G.; Kiraly, G. Algorithms for stem mapping by means of terrestrial laser scanning. *Acta Silv. Lignaria Hung.* **2009**, *5*, 119–130.
43. Wezyk, P.; Koziol, K.; Glista, M.; Pierzchalski, M. Terrestrial Laser Scanning versus Traditional Forest Inventory. First Results from the Polish Forests. Available online: http://www.isprs.org/proceedings/XXXVI/3-W52/final_papers/Wezyk_2007.pdf (accessed on 15 June 2016).
44. Pfeifer, N.; Winterhalder, D. Modelling of tree cross sections from terrestrial laser scanning data with free-form curves. *Int. Arch. Photogramm. Remote Sens. Spat. Inf. Sci.* **2004**, *36*, 76–81.
45. Murphy, G. Determining stand value and log product yields using terrestrial lidar and optimal bucking: A case study. *J. For.* **2008**, *106*, 317–324.
46. Poeschel, P.; Newnham, G.; Rock, G.; Udelhoven, T.; Werner, W.; Hill, J. The influence of scan mode and circle fitting on tree stem detection, stem diameter and volume extraction from terrestrial laser scans. *ISPRS J. Photogramm. Remote Sens.* **2013**, *77*, 44–56. [[CrossRef](#)]
47. Schilling, A.; Maas, H.-G.; Lingnau, C. Tree detection by row recovery on *Eucalyptus* spp. Plantations from TLS data. In Proceedings of the EARSeL 34th Symposium, Warsaw, Poland, 16–20 June 2014.



Making tropical forest plots comparable



4.1. Preamble




In this chapter, we aimed to better include the specificities of the irregularly shaped stems into the entire workflow for estimating the aboveground biomass and biomass change in tropical forests. We used the technologies tested in the previous chapters to measure and model irregularly shaped stems.

This chapter is written in the following scientific peer-reviewed paper: Bauwens, S., Ploton, P., Fayolle, A., Ligtot, G., Loumeto, J. J., Lejeune, P., & Gourlet-Fleury, S. (2021). A 3D approach to model the taper of irregular tree stems: making plots biomass estimates comparable in tropical forests. *Ecological Applications*, 31(8), e02451.

4.2. The scientific peer-reviewed paper

Ecological Applications, 31(8), 2021, e02451
© 2021 by the Ecological Society of America.

A 3D approach to model the taper of irregular tree stems: making plots biomass estimates comparable in tropical forests

S. BAUWENS,^{1,6} P. PLOTON,² A. FAYOLLE,¹ G. LIGOT ,¹ J. J. LOUMETO,³ P. LEJEUNE,¹ AND S. GOURLET-FLEURY^{4,5}

¹TERRA Teaching and Research Centre - Forest is Life, Gembloux Agro-Bio Tech, University of Liege, 5030 Gembloux, Belgium

²AMAP, IRD, CNRS, INRAE, CIRAD, Université Montpellier, Montpellier, France

³Faculté des Sciences et Techniques, Laboratoire de Botanique et Écologie, Université Marien NGOUABI, B.P. 69, Brazzaville, Republic of Congo

⁴CIRAD, Forêts et Sociétés, F-34398 Montpellier, France

⁵Forêts et Sociétés, CIRAD, Université Montpellier, Montpellier, France

Citation: Bauwens, S., P. Ploton, A. Fayolle, G. Ligot, J. J. Loumeto, P. Lejeune, and S. Gourlet-Fleury. 2021. A 3D approach to model the taper of irregular tree stems: making plots biomass estimates comparable in tropical forests. *Ecological Applications* 31(8):e02451. 10.1002/eap.2451

Abstract. In tropical forests, the high proportion of trees showing irregularities at the stem base complicates forest monitoring. For example, in the presence of buttresses, the height of the point of measurement (H_{POM}) of the stem diameter (D_{POM}) is raised from 1.3 m, the standard breast height, up to a regular part of the stem. While D_{POM} is the most important predictor for tree aboveground biomass (AGB) estimates, the lack of harmonized H_{POM} for irregular trees in forest inventory increases the uncertainty in plot-level AGB stock and stock change estimates. In this study, we gathered an original non-destructive three-dimensional (3D) data set collected with terrestrial laser scanning and close range terrestrial photogrammetry tools in three sites in central Africa. For the 228 irregularly shaped stems sampled, we developed a set of taper models to harmonize H_{POM} by predicting the equivalent diameter at breast height (DBH') from a D_{POM} measured at any height. We analyzed the effect of using DBH' on tree-level and plot-level AGB estimates. To do so, we used destructive AGB data for 140 trees and forest inventory data from eight 1-ha plots in the Republic of Congo. Our results showed that our best simple taper model predicts DBH' with a relative mean absolute error of 3.7% ($R^2 = 0.98$) over a wide D_{POM} range of 17–249 cm. Based on destructive AGB data, we found that the AGB allometric model calibrated with harmonized H_{POM} data was more accurate than the conventional local and pantropical models. At the plot level, the comparison of AGB stock estimates with and without H_{POM} harmonization showed an increasing divergence with the increasing share of irregular stems (up to –15%). The harmonization procedure developed in this study could be implemented as a standard practice for AGB monitoring in tropical forests as no additional forest inventory measurements is required. This would probably lead to important revisions of the AGB stock estimates in regions having a large number of irregular tree stems and increase their carbon sink estimates. The growing use of three-dimensional (3D) data offers new opportunities to extend our approach and further develop general taper models in other tropical regions.

Key words: allometric aboveground biomass model; biomass changes; buttresses; close-range terrestrial photogrammetry; point of measurement of stem diameter; stem profile; structure from motion; taper; terrestrial laser scanning

INTRODUCTION

Tropical forests play a key role in the terrestrial global carbon cycle (Pan et al. 2011), but their estimated contribution and response to global environmental changes are still subject to a high degree of uncertainty (Mitchard et al. 2013, 2014, Phillips and Lewis 2014).

Estimates of forest carbon stocks are mainly based on indirect tree-level biomass estimates, using allometric models to convert forest inventory data into

aboveground biomass (AGB, Fig. 1). Tree biomass estimates are then summed at the plot scale and the resulting plots biomass estimates are then upscaled to larger areas (e.g., a landscape, a region, a country) using design- or model-based inference approaches, with or without ancillary data (Gibbs et al. 2007, McRoberts 2010, McRoberts et al. 2010, Clark and Kellner 2012).

It has been demonstrated that the propagation of errors from tree measurements to large-scale carbon stock estimates largely depends on the choice of the AGB allometric model (Chave et al. 2004, Zhao et al. 2012, Molto et al. 2013, Chen et al. 2016). In the tropics, general (multispecies) AGB models are most commonly used to predict tree AGB (Brown et al. 1989, Overman

Manuscript received 11 December 2020; revised 11 March 2021; accepted 6 April 2021; final version received 31 August 2021. Corresponding Editor: Yude J. Pan.

⁶E-mail: Bauwens.sebastien@gmail.com

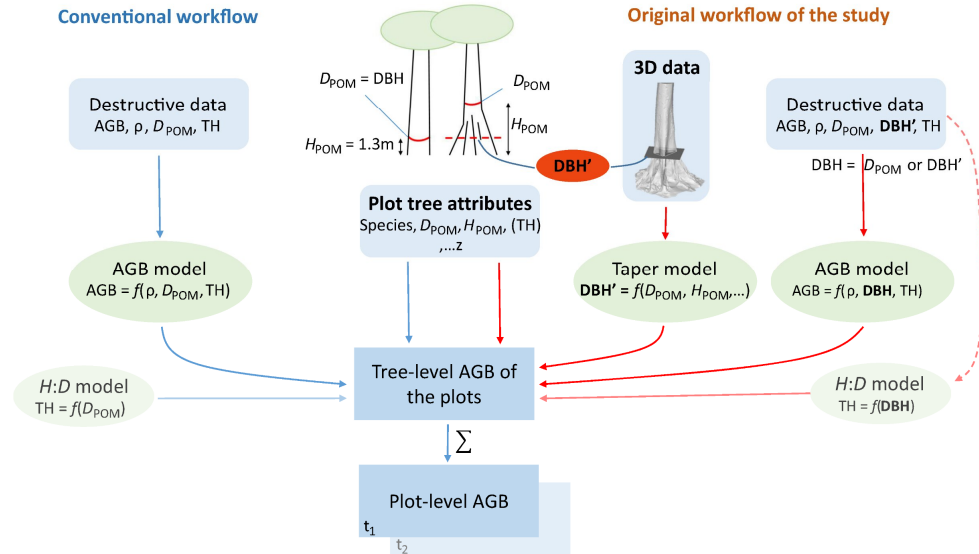


FIG. 1. Conventional (left) and original (right) workflows for plot-level aboveground biomass (AGB) stock and stock change estimates. In the original workflow, the height (H_{POM}) of the measured D_{POM} is harmonized at breast height (i.e., 1.3 m) and the resulting equivalent diameter at breast height (DBH') is computed with a taper model before estimating tree AGB of the trees with irregular stems in the forest inventory plots. The taper model and the AGB model used in this study are based on three-dimensional (3D) data and destructive data, respectively. In the original workflow, the AGB model has DBH' as one of its predictors (i.e., D_{POM} for regular stems and DBH' for irregular stems). The performances of the AGB model from the original workflow are tested in this study and the plot-level AGB stock and stock change estimates of the two workflows are compared. Other variables: ρ , wood density; TH, total tree height.

et al. 1994, Higuchi et al. 1998, Chave et al. 2005, 2014, Nogueira et al. 2008, Fayolle et al. 2013, 2018). General allometric models typically use tree diameter (D_{POM}) measured at the point of measurement (POM), which is either the 1.3-m reference height or above any deformation, total tree height (TH), and species average wood basic density (ρ) as predictors.

When developing AGB models, an important step of model diagnosis consists of assessing how model error varies with change in fitted or predictor values. The pantropical AGB model of Chave et al. (2014), which is the most widely used model, shows a clear error pattern with tree biomass, with a large AGB overestimation for small trees and an underestimation for large trees (>20 Mg, Fig. 2 in Chave et al. 2014). Using the publicly available data set of Chave et al. (2014), it can be shown that the error shows a similar structure with tree diameter, with a positive mean relative error for trees with diameter ≤ 140 cm (mean = 14%, median = 7%, and $n = 3,988$) and, a negative mean relative error for the trees larger than 140 cm (mean = -14%, median = -16%, $n = 16$ and a maximum diameter of 212 cm). This systematic underestimation of AGB for large trees has been found in independent studies using this pantropical model or a similar AGB model functional form (i.e., a power model based on the compound

variable $\rho \times D_{POM}^2 \times TH$) in Amazonia (Goodman et al. 2014, Gonzalez de Tanago et al. 2018, Lau et al. 2019) and central Africa (Ploton et al. 2016, Bauwens et al. 2017). A hypothesis to explain this bias is that variation in crown-diameter allometry, either across sampling sites (Goodman et al. 2014) or during tree ontogeny (Ploton et al. 2016), is not fully captured by the model's predictors (i.e., D_{POM} , TH, and ρ) while it influences tree allometry. Another hypothesis for the underestimation of large tree AGB is that such trees often present deformations (e.g., buttresses) at the standard breast height (i.e., 1.3 m) so that the measured diameter (D_{POM}) is taken higher and is systematically lower than the equivalent diameter at breast height because of stem taper. Bauwens et al. (2017) developed a method based on 3D data to harmonize the height (H_{POM}) of the measured D_{POM} by computing the equivalent diameter at breast height (DBH'), which is defined as the diameter of a circle having the same area as the measured basal area at 1.3 m height. Using destructive biomass data from Cameroon, the authors demonstrated that using DBH' instead of D_{POM} in a published AGB model reduced the AGB underestimation for large trees with an irregular stem (Fig. 4 in Bauwens et al. 2017). This last method has operational perspectives as DBH' could be estimated from correction models previously fitted on 3D data

without requiring additional measurements in forest inventories.

Across 97 1-ha forest inventory plots in central Africa (from a subsample of Ploton et al. 2020), H_{POM} values greater than 1.3 m represent $9\% \pm 9\%$ (mean \pm standard deviation) of the trees with $D_{\text{POM}} \leq 70$ cm and this proportion rises to $55\% \pm 31\%$ for trees with $D_{\text{POM}} > 70$ cm, suggesting that trees with irregular stem base dominate among large tropical trees in this region. Since large trees disproportionately contribute to AGB stocks (Lutz et al. 2012, Slik et al. 2013, Bastin et al. 2015), any systematic errors in AGB prediction induced by the use of non-standard H_{POM} would have an important influence on plot AGB estimates and associated uncertainties (Cushman et al. 2014, Muller-Landau et al. 2014). The influence of this error pattern on the changes of the biomass stock over time is less easy to apprehend since biomass production is not driven by large trees (Ligot et al. 2018). Therefore, it remains unclear how the abundance of trees with irregular stem bases could affect estimates of stand biomass productivity and carbon capture. In all cases, the conversion of D_{POM} to DBH' , whether using taper models (Cushman et al. 2014, Bauwens et al. 2017) or empirical statistical models (Ngomanda et al. 2012, Bauwens et al. 2017), has the potential to improve plot AGB estimates and their comparison (among plots and over time). The use of a taper model compared to empirical statistical models has the advantage to be less sensitive to field protocol for measuring the diameter of trees with irregularities at the standard height (e.g. of field protocols: D_{POM} measured 30 or 50 cm, 1 m, or even more above the buttresses).

In this study, we developed a correction procedure aiming to harmonize the H_{POM} by estimating DBH' , the equivalent diameter at the standard breast height (1.3 m), for irregular tree stems and assess its effect on biomass estimates at the tree and plot level. Specifically, we (1) used 3D tree data to develop a general taper model that predicts DBH' from information available in conventional forest inventories. Then we (2) used destructive AGB data to assess the potential fit improvement in allometric models by using DBH' in the AGB predictors instead of D_{POM} . We also assessed the prediction error of the pantropical AGB model when using DBH' instead of D_{POM} in the model. Last, we (3) used forest inventory data to evaluate the effect of the H_{POM} harmonization on biomass stocks and stock changes at the plot level, considering our local AGB model fitted with DBH' as the reference.

MATERIAL AND METHODS

The taper study sites

We collected 3D data on 228 trees, distributed in three sites in central Africa. A total of 40 trees were sampled in the first site in Cameroon ($14^{\circ}6.867' \text{ N}$, $14^{\circ}33.133' \text{ E}$) using terrestrial laser scanning (TLS), 102 trees were

sampled in the second site in the Republic of Congo ($2^{\circ}22.520' \text{ N}$, $17^{\circ}4.771' \text{ E}$) using close-range terrestrial photogrammetry (CRTP), and 86 trees were sampled in the third site in the Democratic Republic of Congo ($0^{\circ}12.057' \text{ N}$, $25^{\circ}20.580' \text{ E}$) using TLS (Appendix S1: Table S1). We recorded the tree species, the H_{POM} , and the D_{POM} of each sampled tree. H_{POM} was measured using a laser rangefinder device (VERTEX IV) and D_{POM} was measured with a tape or, if the height of measurement was too high ($H_{\text{POM}} > 4.5$ m), in the lab by automatically extracting D_{POM} at the required measured H_{POM} with the 3D data from TLS or CRTP. Before collecting 3D data of the trees, we cleared the small vegetation (stem with diameter < 5 cm and leaves) and small lianas up to 2 m high in a radius < 2.5 m around the focal trees.

We selected 11 abundant focal species with potential stem irregularities and for each of them, we sampled at least five trees spanning a diameter range as wide as possible. To expand our analysis to a large variety of stem shapes, we also selected less abundant species with contrasted stem irregularities and species with more regular stems. For the analyses, we defined a categorical variable called “species” that separately includes the focal species, two other species with more than five trees measured and having contrasted shapes (Emien, *Alstonia boonei* De Wild with its potential fluted trunk and Iroko, *Milicia excelsa* (Welw.) C.C. Berg with its more regular shape), and a group containing the species with fewer than five trees (totaling 32 trees). The variable species thus contains 14 categories (11 focal species, two other species with more than five trees, and one group of other species with 31 trees, Appendix S1: Table S1).

Post-processing of 3D point clouds

We extracted trunk metrics of the 3D point clouds obtained from TLS and CRTP by following the workflow detailed in Bauwens et al. (2017). The outputs are cross-sections realized every 10 cm along the stem axis up to 1 m above the H_{POM} of each tree. For each cross-section (Fig. 2), we extracted (1) diameter of a theoretical circle with area equal to the real area of the cross-section at that height l ($D_{\text{area},l}$ in m), (2) the convex hull length that imitates a tape tight around the stem, express in equivalent diameter ($D_{\text{convHull},l}$ in m), and (3) the perimeter expressed in equivalent diameter of a circle with the same perimeter ($D_{\text{perim},l}$ in m).

Taper profiles of irregularly shaped tree stems

Most taper models require total tree height to express height in relative terms. Tree height is, however, difficult to measure in tropical forests and subject to large measurement uncertainties due to a frequently high, dense, and multi-layered canopy. This variable, hence, is not systematically available in forest inventory data sets. We therefore tested a variety of taper models (Appendix S1:

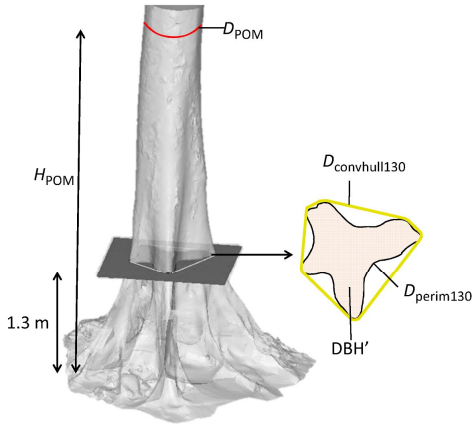


FIG. 2. Main attributes used in the taper models. The cross section extracted from the 3D data at the standard breast height (1.3 m) is indicated with all the types of measurements used in the study.

Table S2) that do not require total tree height as an explicative variable and that rely on few parameters to ease further analyses. Based on the best Akaike Information Criterion ($AIC = 2k - 2\ln(L)$), the Root Mean Square Error ($RMSE = \sqrt{1/n \cdot \sum_1^n (\hat{D}_{\text{areal},k} - D_{\text{areal},k})^2}$) and the simplicity of the model, we finally selected the following model:

$$D_{\text{area},l} = \frac{D_{\text{POM}} h_l^a}{H_{\text{POM}}^a} + \varepsilon_l \quad (1)$$

with $D_{\text{area},l}$ the equivalent diameter of the cross-section area l at the height h_l (in m); D_{POM} , the diameter measured in the field (50 cm above the buttresses or above other local deformations; in m); h_l , the height l above the ground and along the stem at which $D_{\text{area},l}$ is predicted (in m); H_{POM} , the height of measurement of D_{POM} (in m); and a , the taper parameter.

Prediction of the taper parameter

After identifying the taper model that fits the best at the tree level, we generalized Eq. 1 to predict the most reliable equivalent diameter (DBH') for any tree measured in forest inventories (Eq. 2). We used different covariates that would potentially explain individual variations of the taper parameter $a_{i,j,k}$. These covariates are the species and the site (both categorical covariates) and quantitative trunk metrics based on measured (or easily measurable) variables in forest inventories: D_{POM} , H_{POM} , $D_{\text{convhull130}}$, buttresses convex taper (bct), slenderness coefficients ($h:d$, $h:d^2$, $h:d_c$, $h:d_c^2$), hardness

coefficient (hdn), and the deficit basal area index (DeBA) (definitions in Appendix S1: Table S3).

When fitting the general taper model, we took into account the hierarchical structure of the data, which relies on the multiple stem measurements realized along each sample tree. We grouped these within-tree observations (l) into upper hierarchy levels: tree (k), species (j), and site (i) (several trees per species and per site). Within-tree observations are likely to be correlated with the correlation as a function of distances between measurements (Tasissa and Burkhardt 1998). This violates the assumption of independence required to apply the nonlinear least squares method, resulting in unbiased parameter estimates but biased and inconsistent estimates of their variance (West et al. 1984). Mixed-effects models allow autocorrelation to be at least partly accounted for by including random effects (Burkhardt and Tomé 2012). The random effects are assumed to follow a multivariate normal distribution with a mean of zero and a positive-definite variance-covariance matrix. In addition to the mixed-effect approach, the reduction of the correlations among within-tree observations was taken into account with the first-order continuous autoregressive structure. Eq. 1 thus became

$$D_{\text{area}} \text{ijkl} = \frac{D_{\text{POM}i,j,k} H_{i,j,k,l}^{a_{i,j,k}}}{H_{\text{POM}i,j,k}^{a_{i,j,k}}} + \varepsilon_{ijkl} \quad (2)$$

with

$$a_{i,j,k} = (\beta_1 + b_{1i} + b_{1i,j} + b_{1i,j,k}) + \beta_2 D_{\text{POM}i,j,k} + \beta_3 h : dc_{i,j,k} + \beta_4 h : d_{i,j,k}^2 + \beta_5 \text{Sp}_{i-X} + \beta_6 D_{\text{convHull130}i,j,k} + \beta_7 \text{Site}_X + \dots + \beta_n X_n. \quad (3)$$

$D_{\text{area}} \text{ijkl}$ is the equivalent diameter of the cross-section area at height l for tree k belonging to species j in site i , $a_{i,j,k}$ is the taper model parameter for tree k belonging to species j in site i . $\beta = (\beta_1, \dots, \beta_n)$ are the fixed effects (general parameters), b_{1i} is the site-level random effect, $b_{1i,j}$ is the species within site-level random effect and $b_{1i,j,k}$ is the tree within the species and site and ε_{ijkl} is the within-group residual error. Sp_{i-X} and Site_X are dummy covariates. The random effect b_{1i} is assumed to be independent for different i , $b_{1i,j}$ is assumed to be independent for different i, j and independent of b_{1i} , $b_{1i,j,k}$ is assumed to be independent for different i, j, k and independent of $b_{1i,j}$ as well as independent of b_{1i} . The ε_{ijkl} are assumed to be independent for different i, j, k, l and independent of the random effects. The vector of tree random effects and the vector of within-tree residual error terms (ε_l) are both assumed to be multivariate normally distributed (Lejeune et al. 2009). The variance-covariance matrix of the within-tree error terms (R_l) was modeled through a first-order autoregressive correlation structure (Eq. 4) and an exponential function of the

variance covariate (Eq. 5), which provided the best fit

$$\text{corr}(\varepsilon_{ijkl}, \varepsilon_{ijkl'}) = \rho_{ijkl'} = \rho^{|h_{ijkl} - h_{ijkl'}|} \quad (4)$$

$$\text{Var}(\varepsilon_{ijkl}) = \sigma^2 \exp(2\delta_{S_{ij}} v_{ijkl}) \quad (5)$$

where δ is a vector of variance parameters for each level of the stratification variable S (the species in the study) and v_{ijkl} is a vector of variance covariates.

We tested the different fixed-effects covariates in the nested models using a stepwise backward approach and we evaluated the significance of a fixed parameter by using conditional t-tests (Pinheiro and Bates 2006). We compared the models fitted by maximum likelihood with a different number of fixed parameters by means of likelihood ratio tests including, in the final stage, models with the variance function and the auto-correlation structure. All models were also evaluated based on the distribution of the residuals, the RMSE, the RMSE of the cross-sections at 1.3 m only

($\text{RMSE}_{130} = \sqrt{(1/n_k) \sum_1^{n_k} (\widehat{D}_{\text{area}130,k} - D_{\text{area}130,k})^2}$) and the AIC. In the case of the general taper models (Eqs. 2, 3), we also included the mean absolute error ($\text{MAE} = (1/n) \sum_1^n |\widehat{D}_{l,k} - D_{l,k}|$) as it is less sensitive to large individual errors than RMSE. Relative RMSE and MAE were computed by dividing them with the mean tree diameter D_{POM} of the data set. We finally selected the best models based on all covariates and on covariates commonly available in forest inventory data. Nonlinear mixed effects models were fitted with the nlme package in the R statistical environment (Pinheiro et al. 2012).

Effect of the H_{POM} harmonization

Tree-level AGB estimates.—In order to assess the relevance of the H_{POM} harmonization in biomass prediction, we compared the performance of AGB allometric models using as the main predictor, alternatively D_{POM} (with $H_{\text{POM}} \geq 1.3$ m) or DBH, the harmonized diameter at breast height (i.e., D_{POM} for trees with $H_{\text{POM}} = 1.3$ m or DBH', the equivalent DBH for trees with $H_{\text{POM}} > 1.3$ m). For this analysis, we used destructive measurements available for 140 trees (Appendix S1: Table S4) sampled in northern Congo in the frame of the PREREDD+ project (Fayolle et al. 2018) in a site close (18 km) to the second site of the taper study. Note that the basal area was indirectly measured on each stump by photographing the cross-sections of the stump covered with a graduated Plexiglas. The images were then orthorectified and the stump cross-sections were digitized in a GIS software allowing an accurate estimate of the stump area (Fayolle et al. 2013, Bauwens and Fayolle 2014, Bauwens et al. 2017). For trees with H_{POM} higher than the breast height, the equivalent diameter at breast height (DBH') was thus computed by back-transforming the $\log(\text{DBH}')$ from the linear interpolation of the couple of points

$(\log(D_{\text{area_stump}}) - \log(H_{\text{stump}}))$ and $(\log(D_{\text{POM}}) - \log(H_{\text{POM}}))$. In this destructive biomass data set, DBH' is thus interpolated and not estimated from a taper model and could then be assumed as a measurement.

Using the destructive biomass data set, we tested (1) the assumption that using the DBH instead of D_{POM} in the pantropical allometric model developed by Chave et al. (2014) reduced the negative bias encountered on large trees and (2) compared the quality of local biomass models fits based on D_{POM} or DBH.

The pantropical model tested here is the model 4 in Chave et al. (2014), m_{PAN} in Table 1. For local biomass models, we used the same functional form fitted on the destructive biomass data set using either D_{POM} (hereafter $m_{\text{LOC-DPOM}}$) or DBH (hereafter $m_{\text{LOC-DBH}}$) as the tree diameter predictor (Table 1).

The relevance of each of AGB estimates from the four approaches (i.e., $\text{AGB}_{\text{PAN-DPOM}}$, $\text{AGB}_{\text{PAN-DBH}}$, $\text{AGB}_{\text{LOC-DPOM}}$, and $\text{AGB}_{\text{LOC-DBH}}$) was assessed by the mean error

$$\left(\frac{1}{n} \times \sum_{i=1}^n (\widehat{\text{AGB}}_i - \text{AGB}_i) \right)$$

the mean relative error

$$\left(\frac{1}{n} \times \sum_{i=1}^n \left(\frac{\widehat{\text{AGB}}_i - \text{AGB}_i}{\text{AGB}_i} \right) \right)$$

and using a t test to gauge the presence of bias. The performances of the local AGB models (i.e., $m_{\text{LOC-DPOM}}$ and $m_{\text{LOC-DBH}}$) were also assessed with their respective AIC.

Plot-level estimates of AGB stock and stock change.—

Finally, we assessed the impact of the H_{POM} harmonization at the 1-ha plot scale using eight permanent sampling plots located in the second site in the north of the Republic of Congo (see Panzou et al. 2018, Forni et al. 2019 for further details of the site). For this assessment, we compared the plot AGB estimates from the four approaches: Pan- D_{POM} , Pan-DBH, Loc- D_{POM} , and Loc-DBH (Table 1). For the two approaches requiring DBH, we first estimated the equivalent DBH (i.e., DBH') of the trees with $H_{\text{POM}} > 1.3$ m. Then, we estimated the height of each tree in the plots using height-diameter allometry models calibrated on the destructive biomass data set. Two distinct height-diameter models were fitted and used depending on whether the approach required D_{POM} (TH- D_{POM} model) or DBH (TH-DBH model) as predictor. We then estimated total plot AGB by summing tree-level AGB estimates derived from the four approaches. The plot AGB estimated with the $m_{\text{LOC-DBH}}$ model was used as the reference, and compared with the three other sets of AGB estimates.

TABLE 1. Aboveground biomass (AGB) models retrieved from the literature (m_{PAN}) or fitted in this study ($m_{LOC-DPOM}$ and $m_{LOC-DBH}$).

Model and approach	Equation
m_{PAN}	
Pan- D_{POM}	$AGB_{PAN-DPOM} = 0.673 \times (\rho \times D_{POM}^2 \times TH)^{0.976}$
Pan-DBH	$AGB_{PAN-DBH} = 0.673 \times (\rho \times DBH^2 \times TH)^{0.976}$
$m_{LOC-DPOM}$	
Loc- D_{POM}	$AGB_{LOC-DPOM} = 0.043 \times (\rho \times D_{POM}^2 \times TH)^{1.018}$
$m_{LOC-DBH}$	
Loc-DBH	$AGB_{LOC-DBH} = 0.049 \times (\rho \times DBH^2 \times TH)^{1.001}$

Notes: Model predictors are the basic wood density (ρ , in g/cm^3), the total height of the tree (TH, in m) and, the reference stem diameter measured at 1.3 m or above any deformation (D_{POM} , in cm) or the diameter at breast height (DBH, in cm), which includes a mix of D_{POM} for trees measured at 1.3 m height and the equivalent diameter at breast height (DBH' , in cm) for diameter D_{POM} measured above any deformation ($H_{POM} > 1.3$ m).

Following the same procedure, we assessed the effect of H_{POM} harmonization on plot AGB stock changes using inventory data collected 4 yr after the first census.

RESULTS

Variability in the stem profile

We first fitted the taper model (Eq. 1) to each tree separately and thus obtained one taper parameter a_i for each of the 228 trees. The values of the taper parameter a were normally distributed around a mean of -0.123 ± 0.049 (Appendix S1: Fig. S1). The RMSE of

the predicted diameters was 3.8 cm for trees with a D_{POM} ranging from 17 cm to 249 cm.

There was a high intraspecific variation in a for most species (Fig. 3 and Appendix S1: Fig. S2) except Sapelli (*E. cylindricum*), Iroko (*M. excelsa*), and Emien (*A. boonei*). An interspecific variation of a was also noticed, with Iroko (highest mean value, $a = -0.062$) and Ako (lowest mean value, $a = -0.180$) being the species for which a deviated the most from the average. A virtual Iroko (resp. Ako) tree with $D_{POM} = 100$ cm and $H_{POM} = 3.3$ m (H_{POM} frequently encountered for these species, see Appendix S1: Table S1), would have a DBH' of 106 cm (resp. 118 cm). Note the average difference between D_{POM} and DBH' on the 228 trees is -12 cm.

Toward a general taper model

After assessing the potential of Eq. 1 to fit the taper of each of the 228 trees with 3D data, we generalized the model by fitting Eq. 2 using all the cross-sections of the 228 trees in one single model. We tested many covariates in Eq. 3 to accommodate for individual variations of the taper parameter $a_{i,j,k}$. Among all the fixed covariates tested, $h:d_c$ ($P = 0.003$, $F = 8.6$) and $h:d^2$ ($P = 0.0004$, $F = 12.7$) were found to be significant and kept in model $m1$ (RMSE = 6.9 cm, MAE = 3.7 cm, mean error = -0.9 cm, Table 2). To obtain an operational taper model that can be applied in any forest inventory plot in central Africa, despite their significance we removed some covariates such as $D_{convHull130}$ and metrics related to $D_{convHull130}$ (e.g., $h:d_c$), leading to the model $m2$ with only D_{POM} as significant covariate ($P < 0.001$, $F = 15.2$, Table 2). The parameters of the selected covariates for

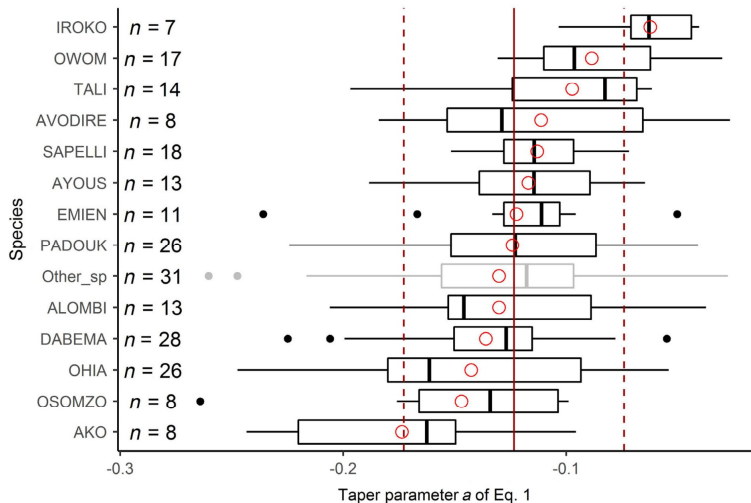


FIG. 3. Taper parameter a of each taper model fitted at the tree-level (Eq. 1) and grouped by species. Solid and dotted vertical red lines represent the mean and the mean \pm SD of a across all species, respectively.

TABLE 2. Goodness of fit of the general taper models (Eq. 2) with different fixed covariates used to predict the taper parameter $a_{i,j,k}$.

Models	Fixed covariates	RMSE (cm)		MAE (cm)		Mean error (cm)		df
		All	1.3	All	1.3	All	1.3	
<i>m1</i>	$a \sim h:d_c + h:d^2$	7.0 (7.0%)	7.0 (7.6%)	3.7 (3.7%)	4.2 (4.5%)	-0.9 (-0.9%)	-0.9 (-0.9%)	21
<i>m2</i>	$a \sim D_{\text{POM}}$	7.8 (7.8%)	8.0 (8.7%)	4.0 (4.0%)	4.7 (5.1%)	-1.5 (-1.5%)	-1.5 (-1.6%)	20

Notes: The root mean square error (RMSE), the mean absolute error (MAE), and the mean error were computed over all the cross-sections as well as for cross-sections at a 1.3 m height only. The model *m1* requires $h:d_c$ covariate (definitions in Appendix S1: Table S3), which is based on $D_{\text{convHull130}}$, a variable not routinely measured in forest inventory. For model *m2*, before the selection of the significant covariates in the fitting process, we only selected covariates that are based on conventional measurements in forest inventories.

TABLE 3. General fixed parameters for the two general taper models of the Table 2.

Parameter	Covariate	<i>m1</i>	<i>m2</i>
β_1	(Intercept)	-0.129	-0.156
β_2	D_{POM}		0.048
β_3	$h:d_c$	0.014	
β_4	$h:d^2$	-0.004	

Note: The parameters correspond to the equation $a_{ijk} = (\beta_1 + b_{1,j} + b_{1,j,j} + b_{1,j,j,k}) + \beta_2(D_{\text{POM}}) + \beta_3(h:d_c) + \beta_4(h:d^2)$ (Eq. 3).

m1 and *m2* are provided in Table 3. In comparison to the taper model fitted on individual trees (see section “Variability in the stem profile”, RMSE = 3.8 cm), using a general taper model increased the RMSE by 3.2–4 cm depending on the model, resulting in RMSE values of 7 and 7.8 cm for *m1* and *m2*, respectively (Table 2, Fig. 4).

The inclusion of the correlation structure (Eq. 4) in the final step of the model selection removed almost all the correlations (Appendix S1: Figs. S4, S5). Consequently, the number of significant covariates was reduced and overfitting avoided. Nevertheless, we additionally tested the site effect at the species level, for the three species having balanced sampling between second and third sites, namely Dabema, Ohia, and Padouk (Appendix S1: Fig. S2b). The Student *t* test performed on the taper parameter did not reveal any significant site effect for these three species, with, respectively, $P = 0.06$ (df = 10.2), $P = 0.4$ (df = 18.7), and $P = 0.8$ (df = 9.9). In addition, using nonlinear mixed models fitted for each species separately and including the site, $h:d_c$, and $h:d^2$ as covariates provided the same results. We also further investigated the species effect and found that including $D_{\text{convHull130}}$ (or derived metrics as $h:d_c$) can compensate, in addition to other metrics, the absence of the species covariate and even outperform models including the species factor in terms of RMSE and Bias (results not shown).

The estimated equivalent diameter DBH' with the models *m1* and *m2* have an RMSE of 7 cm and 8 cm, respectively (Table 2). DBH' predicted with model *m1* do not show any important bias (mean error = -0.9 cm) and, following Piñeiro et al. (2008), the comparison of

observed vs. predicted DBH' lead to a coefficient of determination of 0.98 with no significant deviance to the line 1:1 (Table 2 and Appendix S1: Fig. S6A). The DBH' predicted with model *m2* are, on average, slightly underestimated (mean error = -1.5 cm) and more specifically for very large trees (Table 2, Appendix S1: Fig. S6B).

Effect of D_{POM} harmonization on tree-level AGB estimates

Based on the destructive data available for 140 trees, we compared the prediction error associated with the use of DBH and D_{POM} in AGB models following four approaches (Pan- D_{POM} , Pan-DBH, Loc- D_{POM} , and Loc-DBH, Table 4). The mean prediction error for $\text{AGB}_{\text{PAN-DPOM}}$ estimates was slightly different from zero across all trees sizes (mean = -0.348 Mg, $P = 0.017$) and significantly different from zero for large trees (i.e., $D_{\text{POM}} \geq 70$ cm, mean = -1.430 Mg, $P = 0.009$, Table 4 and Appendix S1: Fig. S7). The relative error was positive for all the four approaches with a mean relative error of almost 10% for $\text{AGB}_{\text{PAN-DBH}}$. The unbalanced numbers of trees along the diameter range lead to a positive mean relative error for all the four approaches. Indeed, this positive mean relative error was mostly driven by the high number of trees with $D_{\text{POM}} < 70$ cm, which had an overall systematic positive error (Table 4 and Appendix S1: Fig. S7).

When fitting local AGB models, we found that tree AGB was better predicted by the model $m_{\text{LOC-DBH}}$ (AIC = -50.4) than by $m_{\text{LOC-DPOM}}$ (AIC = -37.9) with lower mean errors occurring across all trees sizes (Table 4 and Appendix S1: Fig. S7). The Akaike weights (AICw) of these models were, respectively, 0.002 and 0.998, meaning that the local AGB model fitted with DBH is 0.998/0.002 = 499 times more likely to be the best model in terms of Kullback-Leibler discrepancy than the model fitted with D_{POM} (Wagenmakers and Farrell 2004). We thus considered the $m_{\text{LOC-DBH}}$ model as our reference model in the plot-level analysis. Note that the AIC (and AICw) of TH-DBH and TH- D_{POM} models are 836 (0.72) and 838 (0.28) respectively. Allometry relationships relating either AGB or TH to the tree diameter thus show better fits with DBH than with D_{POM} .

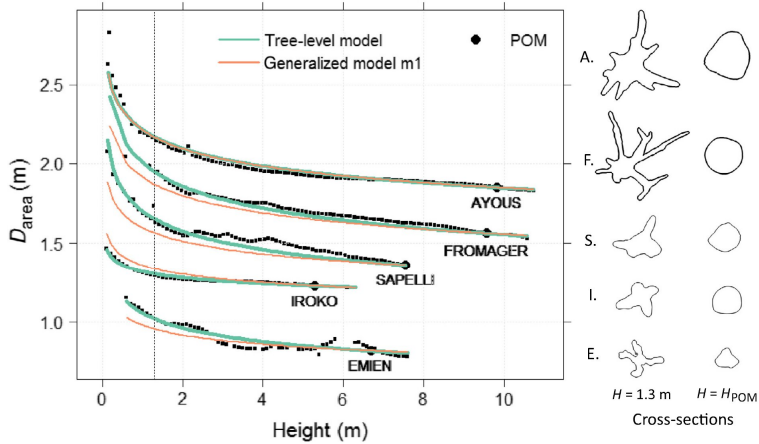


FIG. 4. Equivalent diameters $D_{area,i}$ along the stem. $D_{area,i}$ is predicted from (1) the taper models fitted on each tree separately (green curves) and (2) the general model m1 fitted on all trees (orange curves). Curves represent $D_{area,i}$ predictions from the two approaches for five individual trees from species showing contrasted stem shapes. Ayous (*Triplochiton scleroxylon*) and Fromager (*Ceiba pentandra*) are species with well-developed buttresses. Sapelli (*Entandrophragma cylindricum*) is known to develop irregularities at the base of the stem with sometimes buttresses. Emien (*Alstonia boonei*) is a fluted species and Iroko (*Milicia excelsa*) has a more circular stem with some irregularities at the base of the stem for the largest individuals. On the right, the cross-sections of the five trees for two reference heights: the breast height (1.3 m) and the height of the point of measurement (H_{POM}) of the reference diameter (D_{POM}) located 50 cm above the irregularities. The sizes of the cross-sections are proportional within trees but not among trees.

TABLE 4. Prediction error of the four approaches tested to tree-level AGB estimates with destructive AGB measurements available for 140 trees.

AGB prediction approach	Mean error (Mg)		Mean relative error (%)		MAE (Mg)	
	All sizes	$D_{POM} \geq 70$ cm	All sizes	$D_{POM} \geq 70$ cm	All sizes	$D_{POM} \geq 70$ cm
PAN- D_{POM}	-0.35*	-1.430**	6.2**	-5.7 ^{ns}	0.87	2.56
PAN-DBH	0.016 ^{ns}	-0.120 ^{ns}	9.8***	3.0 ^{ns}	0.83	2.41
LOC- D_{POM}	0.074 ^{ns}	0.250 ^{ns}	4.4*	1.3 ^{ns}	0.85	2.49
LOC-DBH	0.019 ^{ns}	0.111 ^{ns}	4.0*	3 ^{ns}	0.82	2.41

Notes: The significance of a bias in the mean error was assessed with *t* test (***) for $P < 0.001$, ** for $P < 0.01$, * for $P < 0.05$, and ns for not significant). MAE is the mean absolute error.

Effect of H_{POM} harmonization on plot-level AGB stock and stock change estimates

First, we used the taper model m2 to estimate the DBH' of trees with a raised POM in the forest inventory data. Then we predicted tree AGB with the reference model (i.e., $m_{LOC-DBH}$) and summed AGB for all trees within a plot. We found, AGB stocks to equal 401 ± 96 Mg/ha on average (\pm SD) and, the annual AGB stock changes to 6.2 ± 0.8 Mg·ha⁻¹·yr⁻¹ on average (\pm SD). The average contribution of large trees ($D_{POM} \geq 70$ cm) to AGB stock and stock changes were $46\% \pm 13\%$ and $26\% \pm 7\%$, respectively. For very large trees ($D_{POM} > 140$ cm), these contributions decreased to $20\% \pm 13\%$ and $7\% \pm 3\%$ (Appendix S1: Fig. S8).

Using D_{POM} to estimate tree AGB (i.e., LOC- D_{POM} and Pan- D_{POM} approaches) led to an underestimation of

AGB stocks at the plot level in comparison with the reference approach. The magnitude of this underestimation increased with the proportion of (large) trees with trunk irregularities (Fig. 5A and Appendix S1: Figs. S9, S10). Depending on the approach used with D_{POM} , the underestimation reached -10% to -15% in the plots with the highest abundance of trees with H_{POM} superior to 1.3 m height.

The estimates of AGB stock changes obtained when using approaches with D_{POM} were not, on average, significantly different from those obtained with the reference approach ($P = 0.052$ and $P = 0.745$ for LOC- D_{POM} and Pan- D_{POM} , respectively). For some plots, deviations between the two estimates were, however, larger than 5%, and tended to be increasingly negative as the plot basal area contribution of trees with H_{POM} superior to 1.3 m height increased (Fig. 5B). This negative deviation disappeared when using DBH (i.e., Pan-DBH, the

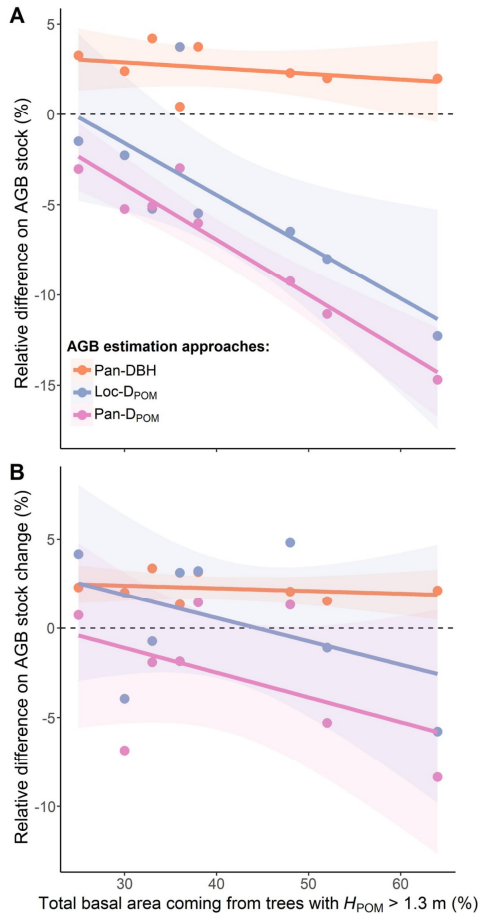


FIG. 5. The 1-ha plot-scale relative difference on AGB stock and stock change between the reference approach Loc-DBH and approaches using D_{POM} (Loc- D_{POM} and Pan- D_{POM}) or the pantropical approach with DBH (Pan-DBH). The basal area was computed with DBH; stock was measured as Mg/ha. The stock change estimates are based on a 4-yr-interval remeasurement; stock change as measured as $\text{Mg}\cdot\text{ha}^{-1}\cdot\text{yr}^{-1}$.

horizontal orange line in Fig. 5B). However, using Pan-DBH approach led to an average positive deviation of 2.2% ($P < 0.001$) compare to estimates derived from the reference AGB model.

DISCUSSION

The taper of irregularly shaped stems well captured by a simple taper model

In this study, we developed general taper models having RMSEs ranging from 7% to 7.8% for trees with

different types of stem irregularities (Table 2). These RMSE values are similar to the range of values (4.9–8.5%) obtained with species-specific taper models predicting tree diameter of the lower stem part of more regularly shaped boreal conifers species (Garber and Maguire 2003, Lejeune et al. 2009). Here, our data set mainly combined irregular tree stems from three sites in central Africa, including several species and notably covering a large range of diameters ($D_{POM} = 17\text{--}249$ cm). Our results thus suggest that simple taper models can be developed and be yet performant, even on mixes of tropical species with contrasted stem irregularities.

An improved AGB allometry when using equivalent diameter at breast height

We could expect that for trees with irregularities such as buttresses, using an equivalent diameter at breast height would have added noise to the relationship between stem lateral size (diameter, circumference or basal area) and tree AGB. Nevertheless, we found that power AGB models calibrated with DBH (i.e., D_{POM} for trees with regular stems and DBH' for irregular stems) was more accurate than the same model using the conventional D_{POM} of all the trees, confirming the results obtained by Bauwens et al. (2017) for one species. The improvement brought by DBH over D_{POM} should be further studied in other sites and forest types as the distribution of the model error vs. sampled tree size might not show the same pattern as the one observed in our study (see Fayolle et al. 2018 for examples of various AGB error pattern according to sites). Moreover, using DBH to improve the goodness of fit of other types of AGB models than the power model on the product $\rho \times D^2 \times \text{TH}$, should be further studied to ensure that DBH is a reliable predictor for tree AGB estimates of any tropical trees. More complex general allometries with non-power models or power models with more than one entry have been shown to provide better fits (Picard et al. 2015, Fayolle et al. 2018) and could be investigated with DBH.

H_{POM} harmonization to mitigate AGB estimation bias induced by the widely used pantropical AGB model

Using the equivalent diameter at breast height (DBH') in the published pantropical AGB model m_{PAN} reduced the negative bias on AGB estimates for large irregularly shaped tree stems (Chave et al. 2014). The reduction of this “allometric bias” has been earlier demonstrated on a smaller data set from Cameroon (Bauwens et al. 2017). At the plot level, using DBH' removed the increasing negative AGB prediction error observed with the increasing abundance of irregular tree stems. By removing this error pattern, the H_{POM} harmonization renders AGB estimates comparable between plots with different shares of irregular tree stems. However, the harmonization led to a systematic positive deviation of plot-level

AGB estimates of about 2% when compared to estimates obtained from our reference AGB model (Fig. 5). This systematic deviation is probably due to the high number of small trees within plots ($D < 70$ cm), for which the systematic overestimation of AGB is more important when using the pantropical AGB model whatever the type of diameter used (Pan- D_{POM} or Pan-DBH, see Table 4 and the local maxima in the loess curves in Appendix S1: Fig. S7B). The systematic overestimation of AGB for small trees could be avoided by segmenting the AGB power model (Picard et al. 2015). Therefore, in absence of an AGB model fitted with DBH', using the published pantropical AGB model of Chave et al. (2014) with DBH' is an efficient way to correct for plot-level AGB estimation bias associated with nonstandard H_{POM} , and the overall small positive bias of 2% resulting from this estimation approach could be corrected a posteriori.

A higher AGB growth for trees with $H_{\text{POM}} > 1.3$ m when taking into account the H_{POM} in AGB estimates

The displacement of the H_{POM} over time, because of the height growth of the buttresses, adds an additional source of uncertainty on tree growth (Cushman et al. 2014, Muller-Landau et al. 2014, Talbot et al. 2014). Different correction procedures can be used to account for this uncertainty on tree growth estimates and the choice of the appropriate correction procedure depends on the objective of the analysis, in particular, whether it focuses on among-plot or within-plot AGB changes (Cushman et al. 2014, Talbot et al. 2014). Nevertheless, the derivative of the AGB model (m_{PAN} or $m_{\text{LOC-DBH}}$) is higher when considering the equivalent diameter at breast height DBH' for trees with raised POM (see the slopes of the curves from $m_{\text{LOC-DBH}}$ in Appendix S1: Fig. S11). Therefore, tree AGB change between two censuses will be higher when using DBH' than a corrected D_{POM} , whatever the growth correction procedure. Harmonizing the H_{POM} would thus limit this growth underestimation. To prevent H_{POM} changes over time due to the buttress development, an alternative long-term solution would be to set a new standard height that remains above buttresses during the whole ontogeny of individuals belonging to species known to develop buttresses. Following this reasoning, Picard and Gourlet-Fleury (2008) recommended setting the H_{POM} at a standardized height of 4.5 m for all trees of such species. The development of new AGB models including this higher standard POM height for these species would then be necessary (Muller-Landau et al. 2014).

Reducing uncertainty on plot-level AGB stock change estimates

At the plot level, AGB stock changes are mainly driven by the small trees (Ligot et al. 2018), and the divergences in AGB stock changes based on our reference model and the pantropical model are mainly coming

from trees with $D_{\text{POM}} \leq 70$ cm (Appendix S1: Figs. S9, S10). The local positive bias for small trees in AGB power model on the product $\rho \times D^2 \times \text{TH}$ should be further investigated (Picard et al. 2015) in order to reduce as much as possible the AGB stock change uncertainty of small trees. In addition, for AGB stock changes comparison among plots, controlling the H_{POM} variation is required. Reducing the stock changes uncertainty from the two uncertainty sources described in this section would increase the overall carbon sink of structurally intact tropical forests for example. Note the analysis presented here looks at AGB stock change over a relatively short period (4 yr). The difference in AGB stock change estimates with and without harmonizing H_{POM} may show a different pattern over longer monitoring periods (higher negative trend or a positive trend) because of the change in H_{POM} distribution within a plot through time and the higher probability of mortality events including large trees with $H_{\text{POM}} > 1.3$ m.

Perspectives for improved AGB estimation

The H_{POM} distribution within forest inventory plots should be accounted for to avoid any local/regional AGB negative bias associated with spatial variation in the abundance of irregular tree stems. H_{POM} should thus be measured and reported in forest inventories, but also in destructive AGB data sets (Muller-Landau et al. 2014). For instance, the absence of the H_{POM} information, or any tree morphological characteristics besides D_{POM} , TH, and ρ , in the pantropical data set used by Chave et al. (2014), strongly limits the investigations on the error source.

In this study, we have shown that a simple, multi-specific taper model could be used to mitigate tree-level AGB estimation bias and its propagation to plot level. Since 3D data on tropical trees are becoming more available using TLS technology and the emergence of databases with thousands of trees already scanned and processed across the globe (e.g., Verbeeck et al. 2019), we believe there is an unprecedented opportunity to refine general taper models, or even develop species-specific models for the most important species. Indeed, while tropical forests are hyper-diverse, only a handful of "hyperdominant" species constitute the majority of the biomass stock (Bastin et al. 2015). Following the procedure presented here, general or specific taper models could be easily integrated into automatic biomass estimation routines, such as in the BIOMASS R package (Réjou-Méchain et al. 2017), to correct tree diameters from H_{POM} variation. The data required for this correction, H_{POM} and D_{POM} , is already available in many forest inventories and this correction procedure could thus be performed with no additional burden on AGB model end users. Furthermore, we could reduce the uncertainty related to H_{POM} harmonization by measuring, in addition to the H_{POM} and D_{POM} , the circumference around the stem irregularities at the reference 1.3 m height (the

equivalent to $D_{convHull130}$ in this study) in forest inventory plots. Indeed, the models having this additional measurement have better performances to estimate DBH' as demonstrated here and earlier (Ngomanda et al. 2012, Bauwens et al. 2017).

CONCLUSION

We showed that harmonizing tree diameter measurement height with taper models can reduce biomass underestimation for large trees by allometric models, and this correction can have large (up to 15%) implications for plot-level biomass estimates. Reducing biases in biomass estimates among tropical forest plots is important to improve our understanding and monitoring of the global carbon budget and has direct implications on the calibration/validation of space-borne biomass models.

ACKNOWLEDGMENTS

Our thanks go to the Fonds Français pour l'Environnement Mondial (FFEM) and the French Development Agency (AFD), which co-funded the DynAIFor project at the origin of this work (Conventions CZZ 1636.01 D and CZZ 1636.02 E). We thank the Center for International Forestry Research (CIFOR), Resources and Synergies Development (RS&D) and the University of Kisangani (UNIKIS), through the REFORCO project funded by the European Union, for their financial and logistic support in DRC, our thanks go more specifically F. Boyemba (UNIKIS), L. Ndjele (UNIKIS), C. Lomba (UNIKIS), and Q. Ducenne (RS&D). We thank the DynAIFor team for their logistic support and their assistance in the fieldwork in Congo and the CIB-Olam company, partner of the DynAIFor project, who hosts the PSP of Lououndougou, our thanks go more specifically E. Forni (CIRAD) and V. Istace (CIB). We thank the Institut de Recherche pour le développement (IRD) and the Alpicam company for their logistic support and their assistance in the fieldwork in Cameroon. S. Bauwens' time was partially supported with funds (i) from the DynAIFor Project and, (ii) from the World Bank throughout the Pre-REDD+ Project. We also thank the NGO Nature + for their administrative support and the PDR research fund *3D-stand* (C-15/50/P5224) that supported the purchase of the laser scanning used in the study. Authors' contributions: S. Bauwens, S. Gourlet-Fleury, and P. Lejeune conceived the ideas and designed methodology; S. Bauwens, P. Ploton, and J. Loumeto collected the data; S. Bauwens, G. Ligot, and P. Ploton analyzed and interpreted the data; S. Bauwens, A. Fayolle, and P. Ploton led the writing of the manuscript. S. Gourlet-Fleury, P. Lejeune, and A. Fayolle secured funding for the study. All authors contributed critically to the drafts and gave final approval for publication.

LITERATURE CITED

- Bastin, J.-F., et al. 2015. Seeing Central African forests through their largest trees. *Scientific Reports* 5:1–8.
- Bauwens, S., and A. Fayolle. 2014. Protocole de collecte des données sur le terrain et au laboratoire nécessaires pour quantifier la biomasse aérienne des arbres et pour l'établissement d'équations allométriques (No. 029/COMIFAC/SE/PREREDD+/SPM/2013). *Nature +*. 39p. <http://hdl.handle.net/2268/170397>
- Bauwens, S., A. Fayolle, S. Gourlet-Fleury, L. M. Ndjele, C. Mengal, and P. Lejeune. 2017. Terrestrial photogrammetry: a non-destructive method for modelling irregularly shaped tropical tree trunks. *Methods in Ecology and Evolution* 8:460–471.
- Brown, S., A. J. Gillespie, and A. E. Lugo. 1989. Biomass estimation methods for tropical forests with applications to forest inventory data. *Forest Science* 35:881–902.
- Burkhardt, H. E., and M. Tomé. 2012. Tree form and stem taper. Pages 9–41 in H. E. Burkhardt and M. Tomé, editors. *Modeling forest trees and stands*. Springer Netherlands, Dordrecht, The Netherlands.
- Chave, J., et al. 2005. Tree allometry and improved estimation of carbon stocks and balance in tropical forests. *Oecologia* 145:87–99.
- Chave, J., et al. 2014. Improved allometric models to estimate the aboveground biomass of tropical trees. *Global Change Biology* 20:3177–3190.
- Chave, J., R. Condit, S. Aguilar, A. Hernandez, S. Lao, and R. Perez. 2004. Error propagation and scaling for tropical forest biomass estimates. *Philosophical Transactions of the Royal Society B* 359:409–420.
- Chen, Q., R. E. McRoberts, C. Wang, and P. J. Radtke. 2016. Forest aboveground biomass mapping and estimation across multiple spatial scales using model-based inference. *Remote Sensing of Environment* 184:350–360.
- Clark, D. B., and J. R. Kellner. 2012. Tropical forest biomass estimation and the fallacy of misplaced concreteness. *Journal of Vegetation Science* 23:1191–1196.
- Cushman, K. C., H. C. Muller-Landau, R. S. Condit, and S. P. Hubbell. 2014. Improving estimates of biomass change in buttressed trees using tree taper models. *Methods in Ecology and Evolution* 5:573–582.
- Fayolle, A., et al. 2018. A regional allometry for the Congo basin forests based on the largest ever destructive sampling. *Forest Ecology and Management* 430:228–240.
- Fayolle, A., J. L. Doucet, J. F. Gillet, N. Bourland, and P. Lejeune. 2013. Tree allometry in Central Africa: testing the validity of pantropical multi-species allometric equations for estimating biomass and carbon stocks. *Forest Ecology and Management* 305:29–37.
- Forni, E., et al. 2019. Dispositifs permanents de nouvelle génération pour le suivi de la dynamique forestière en Afrique centrale: bilan en République du Congo. *Bois et Forêts des Tropiques* 341:55–70.
- Garber, S. M., and D. A. Maguire. 2003. Modeling stem taper of three central Oregon species using nonlinear mixed effects models and autoregressive error structures. *Forest Ecology and Management* 179:507–522.
- Gibbs, H. K., S. Brown, J. O. Niles, and J. A. Foley. 2007. Monitoring and estimating tropical forest carbon stocks: making REDD a reality. *Environmental Research Letters* 2:045023.
- Gonzalez de Tanago, J., et al. 2018. Estimation of aboveground biomass of large tropical trees with terrestrial LiDAR. *Methods in Ecology and Evolution* 9:223–234.
- Goodman, R. C., O. L. Phillips, and T. R. Baker. 2014. The importance of crown dimensions to improve tropical tree biomass estimates. *Ecological Applications* 24:680–698.
- Higuchi, N., J. dos Santos, R. J. Ribeiro, L. Minette, and Y. Biot. 1998. Biomassa da parte aérea da vegetação da Floresta Tropical úmida de terra-firme da Amazônia Brasileira. *Acta Amazonica* 28:153.
- Lau, A., K. Calders, H. Bartholomeus, C. Martius, P. Raumanen, M. Herold, M. Vicari, H. Sukhdeo, J. Singh, and R. C. Goodman. 2019. Tree biomass equations from terrestrial LiDAR: a case study in Guyana. *Forests* 10:527.
- Lejeune, G., C.-H. Ung, M. Fortin, X. J. Guo, M.-C. Lambert, and J.-C. Ruel. 2009. A simple stem taper model with mixed effects for boreal black spruce. *European Journal of Forest Research* 128:505–513.

- Ligot, G., S. Gourlet-Fleury, D. Y. Ouédraogo, X. Morin, S. Bauwens, F. Baya, Y. Brostaux, J. L. Doucet, and A. Fayolle. 2018. The limited contribution of large trees to annual biomass production in an old-growth tropical forest. *Ecological Applications* 28:1273–1281.
- Lutz, J. A., A. J. Larson, M. E. Swanson, and J. A. Freund. 2012. Ecological importance of large-diameter trees in a temperate mixed-conifer forest. *PLoS ONE* 7:e36131.
- McRoberts, R. E. 2010. Probability- and model-based approaches to inference for proportion forest using satellite imagery as ancillary data. *Remote Sensing of Environment* 114:1017–1025.
- McRoberts, R. E., E. O. Tomppo, and E. Næsset. 2010. Advances and emerging issues in national forest inventories. *Scandinavian Journal of Forest Research* 25:368–381.
- Mitchard, E. T., T. R. Feldpausch, R. J. Brienen, G. Lopez-Gonzalez, A. Monteagudo, T. R. Baker, S. L. Lewis, J. Lloyd, C. A. Quesada, and M. Gloor. 2014. Markedly divergent estimates of Amazon forest carbon density from ground plots and satellites. *Global Ecology and Biogeography* 23:935–946.
- Mitchard, E. T., S. S. Saatchi, A. Baccini, G. P. Asner, S. J. Goetz, N. L. Harris, and S. Brown. 2013. Uncertainty in the spatial distribution of tropical forest biomass: a comparison of pantropical maps. *Carbon Balance and Management* 8:10.
- Molto, Q., V. Rossi, and L. Blanc. 2013. Error propagation in biomass estimation in tropical forests. *Methods in Ecology and Evolution* 4:175–183.
- Muller-Landau, H. C., M. Detto, R. A. Chisholm, S. P. Hubbell, and R. I. C. H. A. R. D. Condit. 2014. Detecting and projecting changes in forest biomass from plot data. *Forests and Global Change* 17:381–416.
- Ngomanda, A., Q. M. Mavouroulou, N. L. E. Obiang, D. M. Iponga, J.-F. Mavoungou, N. Lépengué, N. Picard, and B. Mbatshi. 2012. Derivation of diameter measurements for buttressed trees, an example from Gabon. *Journal of Tropical Ecology* 28:299–302.
- Nogueira, E. M., P. M. Fearnside, B. W. Nelson, R. I. Barbosa, and E. W. H. Keizer. 2008. Estimates of forest biomass in the Brazilian Amazon: New allometric equations and adjustments to biomass from wood-volume inventories. *Forest Ecology and Management* 256:1853–1867.
- Overman, J. P. M., H. J. L. Witte, and J. G. Saldarriaga. 1994. Evaluation of regression models for above-ground biomass determination in Amazon rainforest. *Journal of Tropical Ecology* 10:207–218.
- Pan, Y., et al. 2011. A large and persistent carbon sink in the world's forests. *Science* 333:988–993.
- Panzou, G. J. L., G. Ligot, S. Gourlet-Fleury, J.-L. Doucet, E. Forni, J.-J. Loumeto, and A. Fayolle. 2018. Architectural differences associated with functional traits among 45 coexisting tree species in Central Africa. *Functional Ecology* 32:2583–2593.
- Phillips, O. L., and S. L. Lewis. 2014. Evaluating the tropical forest carbon sink. *Global Change Biology* 20:2039–2041.
- Picard, N., and S. Gourlet-Fleury. 2008. Manuel de référence pour l'installation de dispositifs permanents en forêt de production dans le bassin du Congo. Page 265. COMIFAC, Yaounde, Cameroon. <http://hal.cirad.fr/cirad-00339816>
- Picard, N., E. Rutishauser, P. Ploton, A. Ngomanda, and M. Henry. 2015. Should tree biomass allometry be restricted to power models? *Forest Ecology and Management* 353:156–163.
- Piñeiro, G., S. Perelman, J. P. Guerschman, and J. M. Paruelo. 2008. How to evaluate models: observed vs. predicted or predicted vs. observed? *Ecological Modelling* 216:316–322.
- Pinheiro, J., and D. Bates. 2006. *Mixed-effects models in S and S-PLUS*. Springer Science & Business Media. Springer, New York, USA.
- Pinheiro, J., D. Bates, S. DebRoy, D. Sarkar, and R. C. Team. 2012. nlme: linear and nonlinear mixed effects models. R package version 3. <https://cran.r-project.org/web/packages/nlme/index.html>
- Ploton, P., et al. 2016. Closing a gap in tropical forest biomass estimation: taking crown mass variation into account in pantropical allometries. *Biogeosciences* 13:1571–1585.
- Ploton, P., et al. 2020. A map of African humid tropical forest aboveground biomass derived from management inventories. *Scientific Data* 7:221.
- Réjou-Méchain, M., A. Tanguy, C. Piponiot, J. Chave, and B. Hérault. 2017. biomass: an r package for estimating above-ground biomass and its uncertainty in tropical forests. *Methods in Ecology and Evolution* 8:1163–1167.
- Slik, J. W. F., et al. 2013. Large trees drive forest aboveground biomass variation in moist lowland forests across the tropics. *Global Ecology and Biogeography* 22:1261–1271.
- Talbot, J., et al. 2014. Methods to estimate aboveground wood productivity from long-term forest inventory plots. *Forest Ecology and Management* 320:30–38.
- Tasissa, G., and H. E. Burkhart. 1998. An application of mixed effects analysis to modeling thinning effects on stem profile of loblolly pine. *Forest Ecology and Management* 103:87–101.
- Verbeeck, H., M. Bauters, T. Jackson, A. Shenkin, M. Disney, and K. Calders. 2019. Time for a plant structural economics spectrum. *Frontiers in Forests and Global Change* 2:43.
- Wagenmakers, E.-J., and S. Farrell. 2004. AIC model selection using Akaike weights. *Psychonomic Bulletin & Review* 11:192–196.
- West, P. W., D. A. Ratkowsky, and A. W. Davis. 1984. Problems of hypothesis testing of regressions with multiple measurements from individual sampling units. *Forest Ecology and Management* 7:207–224.
- Zhao, F., Q. Guo, and M. Kelly. 2012. Allometric equation choice impacts lidar-based forest biomass estimates: A case study from the Sierra National Forest, CA. *Agricultural and Forest Meteorology* 165:64–72.

SUPPORTING INFORMATION

Additional supporting information may be found online at: <http://onlinelibrary.wiley.com/doi/10.1002/eap.2451/full>

OPEN RESEARCH

Data are available in the Open Repository and Bibliography (ORBI): <http://hdl.handle.net/2268/262867>.

5

Discussion

5.1. The major findings

The main objective of our thesis was to improve the monitoring of large tropical trees with stem irregularities by exploring direct 3D measuring tools and a model-based approach for broader uses.

5.1.1 The effectiveness of direct 3D measuring tools in tropical forests

The low-cost close-range terrestrial photogrammetric approach (CRTP) is an effective 3D measurement tool for irregularly shaped stems encountered in tropical forests. The main limitations of CRTP are the maximum height reached (10-13 m, Bauwens et al., 2017; Fang and Strimbu, 2017) and the light conditions that might limit the success of the 3D point cloud generation. Besides good camera quality and wide-angle lens, adding artificial targets is highly recommended to help the SfM process and increase the success of tree stem point cloud generation. Good field protocol and camera gear increase the success of point cloud generation from around 30-40% to 70-80% of the sampled trees (Bauwens et al., 2017; Cushman et al., 2021).

Personal laser scanning, as the handheld mobile laser scanning (HMLS), gives new insight for direct 3D measurements at the plot and tree scales. HMLS could remove some limitations of the more conventional static terrestrial laser scanning (TLS) tools in the tropical dense forest since walking with HMLS through the plot results in a theoretically unlimited number of scan positions. The occlusion effect (part of the stems not scanned due to the surrounding vegetation) is then reduced. The lower spatial precision of the resulting point cloud of this type of device compared to conventional TLS is compensated by a lower occlusion rate, an important issue in the case of stems with irregularities.

In the case of TLS point cloud, the issue of occluded stem parts is solved by fitting geometrical primitives as a cylinder that completes the occluded parts. This modelling approach is not adapted for irregular shapes. Meshing (Bauwens et al., 2017; Nölke et al., 2015; Takoudjou et al., 2018) or fitting free-form curves (Gollob et al., 2020; Pfeifer and Winterhalder, 2004) are alternative modelling methods in this latter case. Nevertheless, these alternative methods require a low level of occlusion which is hardly obtained with conventional tropical TLS plot setups (Martin-Ducup et al., 2021; Tao et al., 2021; Wilkes et al., 2017). The HMLS reduces significantly occluded parts of the stems. Nevertheless, the quality of the HMLS point cloud for accurate reconstruction of the cross-section of irregular stems needs to be tested as well as the effect of the dense undergrowth encountered in tropical forests on the overall consistency of the HMLS point cloud.

5.1.2 The model-based approach to overcome the current limits of 3D measuring tools

A simple taper model fitted on 3D data significantly improves the monitoring of tropical forest biomass. We first showed that harmonizing the height of stem diameter measurement (H_{POM}) in tree biomass data used for fitting AGB models improves the relationship and removes allometric negative bias for large trees. We then found an increasing negative difference between conventional plot AGB estimates and corrected AGB estimates with the increasing share of irregularly shaped stems within the plot (up to -15%). Harmonizing H_{POM} in forest inventory plots data before using AGB models allows comparing plot AGB stocks by removing the negative error trend.

Additionally, we noticed that i) the stem basis taper more slowly in trees with larger diameters (the taper is lower in large tree diameter than lower ones) and, ii) due to the taper, the AGB growth of trees with $H_{POM} > 1.3$ m was previously underestimated both on trees with a constant H_{POM} and those with an arise H_{POM} over time (Figure 5.1).

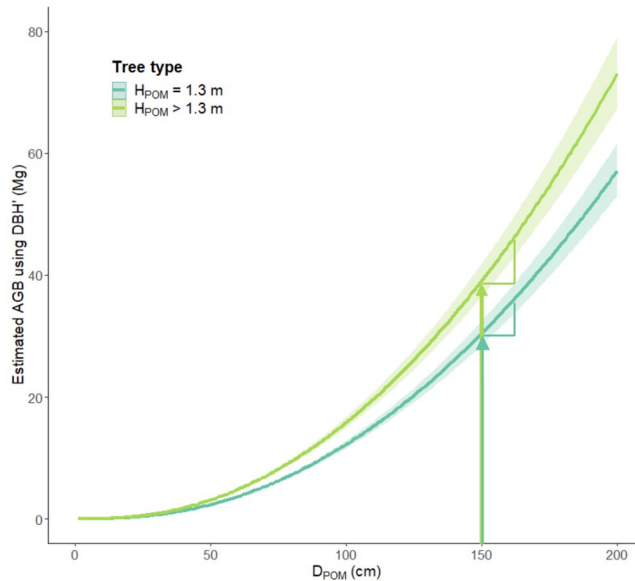


Figure 5.1: The increasing AGB of two virtual trees with the same D_{POM} according to the increasing size of the tree diameters D_{POM} over time. The first virtual tree has a constant 1.3m H_{POM} , D_{POM} is then equal to the so-called diameter at breast height, DBH (dark blue-green) and, the second virtual tree has its POM raised through the time (light green). For this later virtual tree, the equivalent diameter at breast height (DBH') is 12 % higher than D_{POM} (slope of the linear regression DBH'- D_{POM} without intercept fitted on the trees with $H_{POM} > 1.3$ m of the Congolese plots of the study in chapter 4). AGB estimates are based on the same D_{POM} corrected (DBH') AGB model and with a basic wood density of 0.57 g.m^{-3} for both (Supplementary information of Bauwens et al., 2021). The tree with $H_{POM} > 1.3$ has a higher AGB growth than the tree with $H_{POM} = 1.3$ for the same D_{POM} (e.g., $D_{POM} = 150$ cm).

5.2. The perspectives

5.2.1 Which 3D measurement tool in which case for permanent forest inventory plots?

Some considerations in field data acquisition

A minimum standard in the field data acquisition protocol is required to ensure optimal 3D measurements of the trees and data interoperability between campaigns (Wilkes et al., 2017). The field data acquisition protocol will first depend on the scale (tree-level vs plot-level), but the temptation would lead scientists and field operators to try to optimize their fieldwork by directly working at the plot level to increase the number of individuals measured at once and getting more area-based data to answer to forestry and ecological questions. Nevertheless, tree-level field data acquisition protocol is still recommended to ensure the best 3D modelling of the tree, more specifically for irregularly shaped tree stems.

Close-range terrestrial photogrammetry the low-cost approach

The use of close-range terrestrial photogrammetry will still be an important tree-level 3D measurement tool for irregular stems despite its range limit (Bauwens et al., 2021; Cushman et al., 2021). Indeed, its low cost and ease of use remove some current limits encountered in 3D measurement tools (**Table 5.1**). Multicopter UAV (unmanned aerial vehicle also known as drone) is an alternative to overcome the height limitation. Nevertheless, surrounding vegetation must be removed before flights and might be a limitation for studies within PSP.

TLS for the 3D description of the whole aboveground part of the trees (crown included)

TLS has been used with success in close dense tropical forests but often requires cleaning the surrounding vegetation to limit the occlusion of the laser pulses oriented to the focal tree and to ensure the visibility of the artificial target between the different locations of the scanner around the tree (Bauwens et al., 2021; Lau et al., 2019; Takoudjou et al., 2018). The artificial targets are used to co-register (align or merge) the pointclouds from the different scan locations. The time-of-flight TLS technology is recommended for scanning the leaf-on crown part as this type of device has a better signal-to-noise ratio (**Table 5.1**). Inversely, phase-shift (v.s. time of flight) technology has greater ranging ambiguity when intercepting multiple objects within the footprint of a single laser beam (i.e. a higher point cloud noise in branches and leaves areas, Bauwens et al., 2016; Calders et al., 2020). The cost of such device is decreasing but remains high and the need for artificial targets to co-register the scans reduces its effectiveness in the field (Bauwens et al., 2016). The time-of-flight TLS technology is nevertheless the gold standard for modelling the whole woody aboveground volume of a tree.

Personal laser scanning the most effective 3D measurement tool at the plot/stand level

We would recommend further research on the use of personal laser scanning (PLS), as the HMLS tested in chapter 3 in the context of tropical forests. Since our forerunner study, numerous study showed the great potential of PLS in temperate and boreal forests at the plot level (Balenović et al., 2021; Gollob et al., 2020; Jurjević et al., 2020), but are still note tested in tropical forests to our knowledge. These tools have wider operational perspectives than TLS by significantly reducing the field acquisition time and reducing the occlusion effect. The lower precision of the point clouds from PLS compared to TLS could be compensated by a higher number of stems scanned. Since our study, new devices are available and remove some limitations noticed with the ZEB1 device tested in the study of chapter 3. For example, the range of the laser (mainly coming from the VLP puck series) are now up to 100-200 m and the beam divergence is 3 mrad compared to 1.7x14 mrad for ZEB1(Balenović et al., 2021; Gollob et al., 2020; Jurjević et al., 2020).

Table 5.1: Advantages of the 3D measurement tools. CRTP: Close-range photogrammetry; TLS-TOF: Terrestrial laser scanning using the time-of-flight technology; TLS-PS: Terrestrial laser scanning using the phase-shift technology; PLS: Personal mobile laser scanning such as hand-held laser scanning.

Tool	Range	Acquisition time	Reduced occlusion	Price	Point cloud precision	Pre-processing time	Tree modelling		
							stem lower part	stem upper part	Crown
CRTP	-	+	+++	+++	++	---	+++	--	--
TLS TOF	+++	-	+	--	+++	--	*/+++	++	++
TLS PS	++	-	+	-	++	--	*/+++	++	+
PLS	+ /+++	+++	+++	--	+	+	+++	+++	-

**Due to the high probability of occlusion in the case of irregularly shaped tree stem*

Prospects for exploiting these new 3D data in tropical forest monitoring

A new metric standard might emerge from these measurement tools as the volume of the five first meters of the stem instead of the traditional DBH or D_{POM} as well as crown metrics. New allometric models including these measurements/metrics could then be used to estimate total stem volume or aboveground biomass with perhaps a higher precision than current allometric models (Goodman et al., 2014; Kankare et al., 2013; Ploton et al., 2016). For AGB estimates of the larger trees, tree-level scanning acquisition could be recommended to model the total aboveground volume and convert it into biomass using weighted basic wood density (Gonzalez de Tanago et al., 2018; Takoudjou et al., 2018). The high uncertainty and bias from the current pantropical allometric biomass model and the issue of the non-standard point of measurement of the diameter could thus be bypassed.

5.2.2 The close-range 3D measurement tools in operational Precision Forestry

Precision forestry leverages advanced technology sensing and analytical tools to support site-specific economic, environmental, and sustainable decision-making for the forestry sector (Bare and Dean, 2001; Moskal et al., 2009). The current main close-range 3D measurement tools such as terrestrial laser scanning, mobile laser scanning, personal laser scanning (e.g.: HMLS) or close-range terrestrial photogrammetry should be first seen as a precise scientific measurement tools. Operational uses of these tools in the forestry sector are still limited and absent in tropical forestry. Nevertheless, new smartphone devices combining SfM process with a build-in low-range LiDAR system bring new insights (**Figure 5.2**, [Gollob et al., 2021](#); [Mokroš et al., 2021](#)). Indeed, this current low-cost technology allows measuring the first three to five meters of the stems with a root mean square error of around 9 to 13 % and a bias of -2% (Gollob et al., 2021; Mokroš et al., 2021). In tropical forestry, the next generation of such device could be used, for example, to measure the diameter of standing irregularly shaped tree stems inventoried for logging but having a diameter above the buttresses close to the minimum logging diameter allowed by the law or the forest management plan. Measurements with such device will avoid a posteriori (after logging) check in the case of a H_{POM} not reachable by hand. A scaling allometric model could also be used to estimates the total stem volume based on the scanned volume of the first meters of the stem.

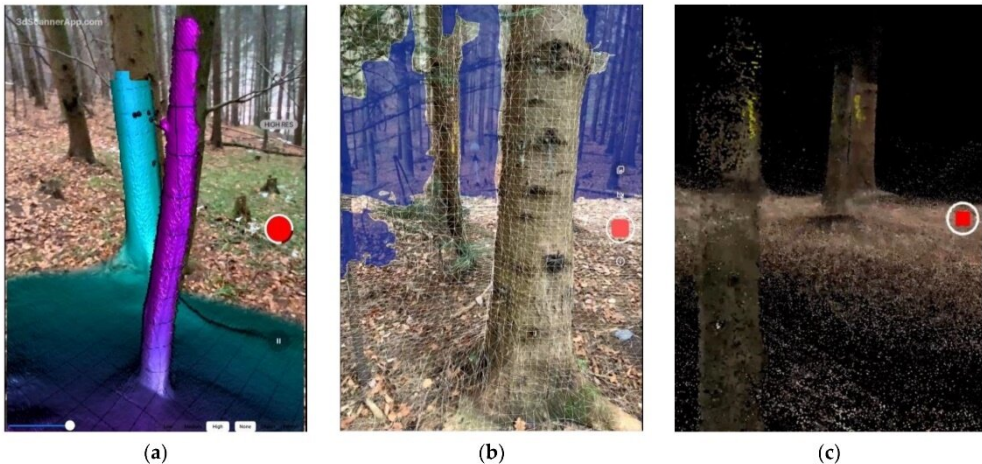


Figure 5.2: 3D measurement of stems with a smartphone using sfm process and build-in low-range LiDAR system. Screenshot of three applications built for 3D data acquisition: (a) 3D Scanner App. (b) Polycam. (c) SiteScape (Figure from Gollob et al., 2021).

5.2.3 The model-based approaches to overcome the current limits of 3D measuring tools

The model-based approaches (versus direct 3D measurements) have broader uses by using its on historical and current forest inventory data. The use of a taper model compared to empirical statistical models (Ngomanda et al., 2012) has the advantage to be less sensitive to field protocol for measuring the diameter of trees with irregularities at the standard height (e.g. of field protocols: D_{POM} measured 30 or 50 cm, 1 m, or even more above the buttresses). Moreover, simple multispecies taper models can be developed and be performant, even on mixes of tropical species with contrasted stem irregularities. The main improvements for taper model would be to test additional covariates related to functional traits of the irregularly shaped tree stems. For example, Cushman et al. (2021) show the significant effect of average species basic wood density on the parameter of their taper model. Nevertheless, the correlation between the covariates as well as between the cross-section measurements should be carefully considered to avoid overfitting effect and then keeping covariates that may appear statistically significant. Among the functional traits, the geometry of the cross-sections could also be further tested.

Following the model-based approach studied in this research, general or specific taper models could be easily integrated into automatic biomass estimation routines, such as in the BIOMASS R package (Réjou-Méchain et al., 2017), to correct tree diameters from H_{POM} variation. The data required for this correction, H_{POM} and D_{POM} , is already available in many forest inventories and this correction procedure could thus be performed with no additional burden on AGB model end-users. Furthermore, we could reduce the uncertainty related to H_{POM} harmonization by measuring, in addition to the H_{POM} and D_{POM} , the circumference around the stem irregularities at the reference 1.3 m height in forest inventory plots. Indeed, the models having this additional measurement have better performances to estimate DBH' (Ngomanda et al. 2012, Bauwens et al. 2017, 2021).

The error propagation from field forest inventory measurements and AGB destructive data to plot biomass stock and stock change estimates should be further investigated as well. Indeed, the better allometric relationship between AGB and DBH' than AGB and D_{POM} should be tested on other contrasted sites.

The tropical forest biomass stocks are underestimated in forest inventory plots with a high proportion of irregularly shaped tree stems and, additionally, the current remote sensing AGB models systematically underestimate the AGB stocks of most tropical forests. A caution on the use of such estimates in the context of IPCC reports should then be noticed and the sampling of tropical forest inventory plots should be improved.

Independently of the irregularly shaped tree stems problematic, research on allometric biomass models should be pursued to minimize biases in the range of variables and model predictions. For example, we have highlighted the problem of overestimating the AGB of small trees ($DBH < 70$ cm) when using the widely used pantropical geometrical power model with a local maximal relative AGB error around

25 cm of diameter. Picard et al. (2015b) already noticed this an error size-dependant allometry with a diameter breakpoint in allometry at also 25 cm. This issue has an important impact on plot AGB changes estimates and thus on the CO₂ fluxes related to it as small trees weight significantly in these biomass changes. Research in AGB allometry should then continue to focus on the size and ontogenic dependence of AGB allometry (Picard et al., 2015b; Pilli et al., 2006).

5.3. Practical recommendation for measuring irregularly shaped tree stems in permanent forest inventory plots

In the context of biomass monitoring of tropical forests, the gold standard would be to scan the whole forest plots, including regular and irregular tree stems. The main advantage would be to reduce the error propagation in plot biomass stock and stock change estimates by removing the current issues on AGB allometric model errors, including the non-standard point of measurement in the case of irregular stems. Currently, in complex multilayered tropical forests, such an approach consists in co-registering multiple TLS scans obtained over a systematic sampling grid covering an entire plot (Wilkes et al., 2017). However, this approach generates additional uncertainties, such as large zones of occlusion and co-registration errors (Demol et al., 2022) compared to the tree-centered scanning protocol. Unreliable tree volume estimations may result from QSM algorithms or other 3D modelling methods (Stovall et al., 2018) and more specifically for trees with irregularly shaped stem. In our opinion, the 1 ha plot size traditionally inventoried in tropical forest and scanned in once (Martin-Ducup et al., 2021; Wilkes et al., 2017) should be subdivided in subsample area which are independently scanned and personal mobile laser scanning should be considered to reduce the occlusion on the irregular stems. The processing workflow of plot TLS data still require numerous manual checks in different intermediate processing results (Martin-Ducup et al., 2021) and high technical skills. Note that scanning a 1 ha plot typically takes a team of 3 people between 3 and 8 days dependent upon topography and understorey conditions (Wilkes et al., 2017).

Tree-centered approaches have more effective operational results to better consider irregularly shaped tree stems in forest monitoring. The different tree-level approaches differ in the level of complexity of the data acquisition and processing (Figure 5.3).

The first approach to consider the non-standard measurement height of the diameter use the conventional forest inventory tree measurements H_{POM} and D_{POM} into a taper model to predict the equivalent diameter at breast height (DBH', Bauwens et al. 2021 and Cushman et al. 2021). The equivalent diameter is then used with an allometric biomass model calibrated on breast-height diameter measurements: AGB-DBH' allometric model (Approach A.I with the resulting AGB estimates 2 in Figure 5.3., Bauwens et al., 2021). In the absence of such an allometric model, the current existing allometric models, AGB- D_{POM} allometric model, as the Chave et al. 2014 allometric model will be used with the estimated DBH' instead of D_{POM} to reduce the magnitude of the systematic error in aboveground biomass estimates for this type of trees (Approach A.I with the resulting GB estimates 1 in Figure 5.3, see chapter 4). Additionally, measuring the convex hull of the stem at 1.3 m height ($D_{convhull130}$) by stretching the diameter tape at this height would guarantee a higher precision. DBH' is then predicted with a taper model including $D_{convhull130}$ as covariate. Fixing the H_{POM} at 4.5 m as recommended by Picard et Gourlet-Fleury (2008) would also increase the precision of the predicted DBH' by removing the H_{POM} effect in the parameter of the taper model.

In the second approach (approach *B*), The basal area at 1.3m height is directly measured by using Close Range Terrestrial Photogrammetry (CRTP) or another laser scanning tool (TLS, PLS, or next generation of smartphone with built-in LiDAR sensor). The equivalent breast height diameter (DBH') is then deduced and used in either current AGB- D_{POM} allometric model (AGB estimate 1 in **Figure 5.3**) or AGB-DBH' allometric model (AGB estimate 2 in **Figure 5.3**).

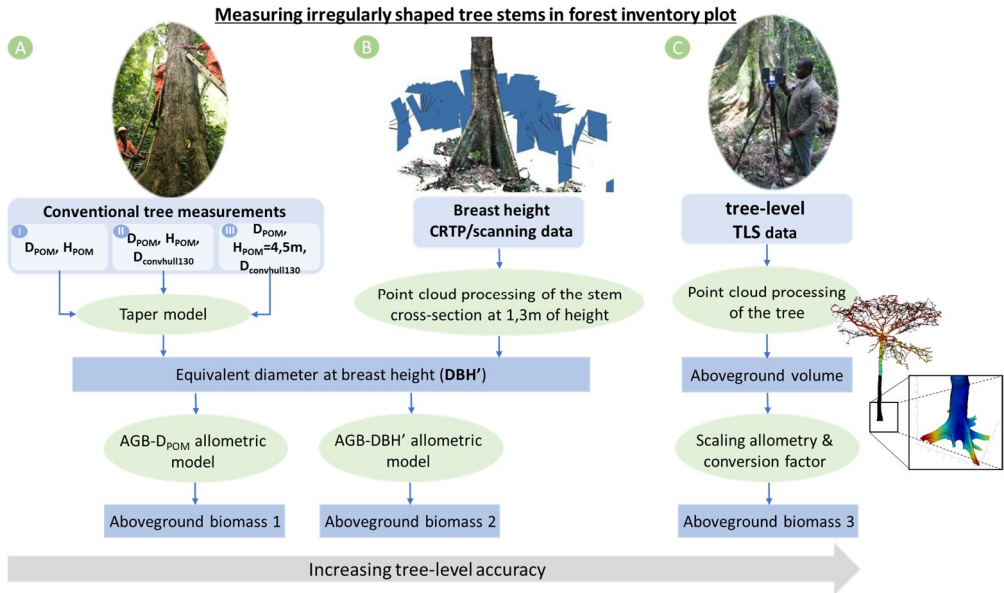


Figure 5.3: Tree-centered approaches to manage the issue of irregularly shaped tree stems in aboveground biomass monitoring in tropical forest inventory plots. The approach *A* is based on conventional tree measurements and, optionally, with an additional measurement: $D_{convhull130}$ (the equivalent diameter of the convex hull at 1.3m height, see text for further details) in the case of A.II and A.III. AGB- D_{POM} allometric model is the current conventional allometric model requiring the stem diameter D_{POM} as one predictor in the model. AGB-DBH' model is as model calibrated on DBH or equivalent DBH measurement instead of D_{POM} . The approach *B* is based on close-range terrestrial photogrammetry (CRTP) or other scanning methods to extract the DBH' of the focal tree. In *C*, the whole tree is scanned with TLS and the whole aboveground woody volume is modelled and converted into aboveground biomass using conversion factor based on basic wood density. The accuracy of the aboveground biomass estimates increases from the approach *A* to *C*.

In the approach *C*, the whole tree is scanned with TLS, the current gold standard 3D measurement tool in that case (Table 5.1). The TLS point cloud is then processed and modelled to get the aboveground woody volume (Du et al., 2019; Hackenberg et al., 2015; Raumonon et al., 2013; Trochta et al., 2017). This woody volume is then scaled (extrapolated) if some woody parts are not modelled due to the limitation of the TLS

measurements (e.g., small branches (diameter inferior to 5 – 7 cm) and leaves). The woody volume is then converted into biomass using basic wood density model (Demol et al., 2021; Momo et al., 2020). This third approach should be applied on all the trees superior to a definite diameter threshold whatever the morphology of the stem (e.g. : 70 cm). Focusing on only some large buttressed trees will lead to inconsistent plot-level biomass estimates as some trees of similar diameter size would be estimated by an AGB allometric model and other by this third approach. The mix of different approaches for biomass estimate of trees with similar diameters may lead to a biased sampling strategy as predictions with AGB allometric models are reliable at the plot-scale and not at the tree scale (Chen et al., 2015).

The approach *A* does not require highly qualified personnel in the field. Compared to current forest inventory campaign, the extra time required to measure an irregular shaped stems is not very significant if a ladder was already used in the field, i.e. less than five extra minutes per tree. Extra time and one highly qualified personnel are nevertheless required to develop taper models with 3D data and to standardize AGB model from existing destructive data. In the opposite, the approach *C* would require one highly skilled personnel for field data acquisition and for processing the data of each field measurement campaigns. Two additional persons will be required for the field campaigns to carry the equipment and for preparing the scan and target locations. The time required to scan one tree with stem irregularities is around one hour (Bauwens, personal comment) and the human assisted processing time for 3D modelling is around one hour per tree (Martin-Ducup et al., 2021). In the approach *B*, less than 20 min would be required to takes the images of one stem and, the required human assisted processing time would also be around 20 minutes to clean the pointcloud and to extract the cross-section area at 1.3 m height. We strongly recommend processing the images of the approach *B* during the field campaign to start over if the SfM process of the images failed.

Finally, the approach *C* or scanning the whole plot would be suggested in specific site, such as the so-called supersite (Chave et al., 2019) to retrieve precise tree-level measurements and plot biomass estimates for remote sensing AGB model calibration.

References

- Achard, F., DeFries, R., Eva, H., Hansen, M., Mayaux, P., Stibig, H.-J., 2007. Pan-tropical monitoring of deforestation. *Environ. Res. Lett.* 2, 045022. <https://doi.org/10.1088/1748-9326/2/4/045022>
- Alder, D., Synnott, T.J., 1992. Permanent sample plot techniques for mixed tropical forest.
- Avery, T.E., Avery, T.E., 1975. Natural resources measurements.
- Avitabile, V., Herold, M., Heuvelink, G.B.M., Lewis, S.L., Phillips, O.L., Asner, G.P., Armston, J., Ashton, P.S., Banin, L., Bayol, N., Berry, N.J., Boeckx, P., Jong, B.H.J. de, DeVries, B., Girardin, C.A.J., Kearsley, E., Lindsell, J.A., Lopez-Gonzalez, G., Lucas, R., Malhi, Y., Morel, A., Mitchard, E.T.A., Nagy, L., Qie, L., Quinones, M.J., Ryan, C.M., Ferry, S.J.W., Sunderland, T., Laurin, G.V., Gatti, R.C., Valentini, R., Verbeeck, H., Wijaya, A., Willcock, S., 2016. An integrated pan-tropical biomass map using multiple reference datasets. *Glob. Change Biol.* 22, 1406–1420. <https://doi.org/10.1111/gcb.13139>
- Baccini, A., Goetz, S.J., Walker, W.S., Laporte, N.T., Sun, M., Sulla-Menashe, D., Hackler, J., Beck, P.S.A., Dubayah, R., Friedl, M.A., Samanta, S., Houghton, R.A., 2012. Estimated carbon dioxide emissions from tropical deforestation improved by carbon-density maps. *Nat. Clim. Change* 2, 182–185. <https://doi.org/10.1038/nclimate1354>
- Balenović, I., Liang, X., Jurjević, L., Hyyppä, J., Seletković, A., Kukko, A., 2021. Hand-Held Personal Laser Scanning: Current Status and Perspectives for Forest Inventory Application. *Croat. J. For. Eng.* 42, 165–183. <https://doi.org/10.5552/crojfe.2021.858>
- Banin, L., Lewis, S.L., Lopez-Gonzalez, G., Baker, T.R., Quesada, C.A., Chao, K.-J., Burslem, D.F., Nilus, R., Abu Salim, K., Keeling, H.C., others, 2014. Tropical forest wood production: a cross-continental comparison. *J. Ecol.* 102, 1025–1037.
- Bare, B.B., Dean, A., 2001. Opening remarks and welcome to the first international precision forestry symposium. *Precis. For.* 1.
- Bastin, J.-F., Barbier, N., Réjou-Méchain, M., Fayolle, A., Gourlet-Fleury, S., Maniatis, D., De Haulleville, T., Baya, F., Beekman, H., Beina, D., 2015. Seeing Central African forests through their largest trees. *Sci. Rep.* 5, 13156.
- Bauwens, S., Bartholomeus, H., Calders, K., Lejeune, P., 2016. Forest Inventory with Terrestrial LiDAR: A Comparison of Static and Hand-Held Mobile Laser Scanning. *Forests* 7, 127.
- Bauwens, S., Fayolle, A., Gourlet-Fleury, S., Ndjele, L.M., Mengal, C., Lejeune, P., 2017. Terrestrial photogrammetry: a non-destructive method for modelling irregularly shaped tropical tree trunks. *Methods Ecol. Evol.* 8, 460–471.
- Bauwens, S., Ploton, P., Fayolle, A., Ligot, G., Loumeto, J.J., Lejeune, P., Gourlet-Fleury, S., 2021. A 3D approach to model the taper of irregular tree stems: making plots biomass estimates comparable in tropical forests. *Ecol. Appl.* 31, e02451.
- Belyea, H.C., 1931. Forest measurement. New York.

- Brienen, R.J.W., Phillips, O.L., Feldpausch, T.R., Gloor, E., Baker, T.R., Lloyd, J., Lopez-Gonzalez, G., Monteagudo-Mendoza, A., Malhi, Y., Lewis, S.L., Vásquez Martínez, R., Alexiades, M., Álvarez Dávila, E., Alvarez-Loayza, P., Andrade, A., Aragão, L.E.O.C., Araujo-Murakami, A., Arets, E.J.M.M., Arroyo, L., C, G.A.A., Bánki, O.S., Baraloto, C., Barroso, J., Bonal, D., Boot, R.G.A., Camargo, J.L.C., Castilho, C.V., Chama, V., Chao, K.J., Chave, J., Comiskey, J.A., Cornejo Valverde, F., da Costa, L., de Oliveira, E.A., Di Fiore, A., Erwin, T.L., Fauset, S., Forsthofer, M., Galbraith, D.R., Grahame, E.S., Groot, N., Hérault, B., Higuchi, N., Honorio Coronado, E.N., Keeling, H., Killeen, T.J., Laurance, W.F., Laurance, S., Licona, J., Magnussen, W.E., Marimon, B.S., Marimon-Junior, B.H., Mendoza, C., Neill, D.A., Nogueira, E.M., Núñez, P., Pallqui Camacho, N.C., Parada, A., Pardo-Molina, G., Peacock, J., Peña-Claros, M., Pickavance, G.C., Pitman, N.C.A., Poorter, L., Prieto, A., Quesada, C.A., Ramírez, F., Ramírez-Angulo, H., Restrepo, Z., Roopsind, A., Rudas, A., Salomão, R.P., Schwarz, M., Silva, N., Silva-Espejo, J.E., Silveira, M., Stropp, J., Talbot, J., ter Steege, H., Teran-Aguilar, J., Terborgh, J., Thomas-Caesar, R., Toledo, M., Torello-Raventos, M., Umetsu, R.K., van der Heijden, G.M.F., van der Hout, P., Guimarães Vieira, I.C., Vieira, S.A., Vilanova, E., Vos, V.A., Zagt, R.J., 2015. Long-term decline of the Amazon carbon sink. *Nature* 519, 344–348. <https://doi.org/10.1038/nature14283>
- Bruce, D., Schumacher, F.X., 1950. *Forest mensuration*. McGraw-Hill Book Co., New York, NY.
- Bruggeman, D., Meyfroidt, P., Lambin, E.F., 2015. Production forests as a conservation tool: Effectiveness of Cameroon’s land use zoning policy. *Land Use Policy* 42, 151–164. <https://doi.org/10.1016/j.landusepol.2014.07.012>
- Butsic, V., Baumann, M., Shortland, A., Walker, S., Kuemmerle, T., 2015. Conservation and conflict in the Democratic Republic of Congo: The impacts of warfare, mining, and protected areas on deforestation. *Biol. Conserv.* 191, 266–273. <https://doi.org/10.1016/j.biocon.2015.06.037>
- Cailliez, F., Alder, D., 1980. *Forest volume estimation and yield prediction Vol 1- Volume estimation*, F.A.O. forestry paper.
- Calders, K., Adams, J., Armston, J., Bartholomeus, H., Bauwens, S., Bentley, L.P., Chave, J., Danson, F.M., Demol, M., Disney, M., Gaulton, R., Krishna Moorthy, S.M., Levick, S.R., Saarinen, N., Schaaf, C., Stovall, A., Terry, L., Wilkes, P., Verbeeck, H., 2020. Terrestrial laser scanning in forest ecology: Expanding the horizon. *Remote Sens. Environ.* 251, 112102. <https://doi.org/10.1016/j.rse.2020.112102>
- Chapman, C.A., Kaufman, L., Chapman, L.J., 1998. Buttress formation and directional stress experienced during critical phases of tree development. *J. Trop. Ecol.* 14, 341–349.
- Chave, J., Andalo, C., Brown, S., Cairns, M.A., Chambers, J.Q., Eamus, D., Fölster, H., Fromard, F., Higuchi, N., Kira, T., others, 2005. Tree allometry and

- improved estimation of carbon stocks and balance in tropical forests. *Oecologia* 145, 87–99.
- Chave, J., Condit, R., Aguilar, S., Hernandez, A., Lao, S., Perez, R., 2004. Error propagation and scaling for tropical forest biomass estimates. *Philos. Trans. R. Soc. Lond. B. Biol. Sci.* 359, 409–420.
- Chave, J., Réjou-Méchain, M., Búrquez, A., Chidumayo, E., Colgan, M.S., Delitti, W.B., Duque, A., Eid, T., Fearnside, P.M., Goodman, R.C., 2014. Improved allometric models to estimate the aboveground biomass of tropical trees. *Glob. Change Biol.*
- Chen, Q., McRoberts, R.E., Wang, C., Radtke, P.J., 2016. Forest aboveground biomass mapping and estimation across multiple spatial scales using model-based inference. *Remote Sens. Environ.* 184, 350–360. <https://doi.org/10.1016/j.rse.2016.07.023>
- Chen, Q., Vaglio Laurin, G., Valentini, R., 2015. Uncertainty of remotely sensed aboveground biomass over an African tropical forest: Propagating errors from trees to plots to pixels. *Remote Sens. Environ.* 160, 134–143. <https://doi.org/10.1016/j.rse.2015.01.009>
- Clark, D.A., 2002. Are tropical forests an important carbon sink? Reanalysis of the long-term plot data. *Ecol. Appl.* 12, 3–7.
- Clark, D.A., Clark, D.B., 1999. Assessing the growth of tropical rain forest trees: issues for forest modeling and management. *Ecol. Appl.* 9, 981–997.
- Condit, R., Hubbell, S.P., Condit, R., 1998. Tropical forest census plots.
- Coomes, D.A., Burslem, D.F., Simonson, W.D., 2014. *Forests and Global Change*. Cambridge University Press.
- Cushman, K.C., Bunyavejchewin, S., Cárdenas, D., Condit, R., Davies, S.J., Duque, Á., Hubbell, S.P., Kiratiprayoon, S., Lum, S.K.Y., Muller-Landau, H.C., 2021. Variation in trunk taper of buttressed trees within and among five lowland tropical forests. *Biotropica* 53, 1442–1453. <https://doi.org/10.1111/btp.12994>
- Cushman, K.C., Muller-Landau, H.C., Condit, R.S., Hubbell, S.P., 2014. Improving estimates of biomass change in buttressed trees using tree taper models. *Methods Ecol. Evol.*
- Dean, C., Roxburgh, S., 2006. Improving visualisation of mature, high-carbon-sequestering forests. *For. Biometry Model. Inf. Sci.* 1, 48–69.
- Dean, C., Roxburgh, S., Mackey, B.G., 2003. Growth modelling of Eucalyptus regnans for carbon accounting at the landscape scale. *Model. For. Syst.* 27–39.
- Demol, M., Calders, K., Krishna Moorthy, S.M., Van den Bulcke, J., Verbeeck, H., Gielen, B., 2021. Consequences of vertical basic wood density variation on the estimation of aboveground biomass with terrestrial laser scanning. *Trees* 35, 671–684. <https://doi.org/10.1007/s00468-020-02067-7>
- Demol, M., Wilkes, P., Raumonon, P., Krishna Moorthy, S., Calders, K., Gielen, B., Verbeeck, H., 2022. Volumetric overestimation of small branches in 3D

- reconstructions of *Fraxinus excelsior*. *Silva Fenn.* 56. <https://doi.org/10.14214/sf.10550>
- Du, S., Lindenbergh, R., Ledoux, H., Stoter, J., Nan, L., 2019. AdTree: Accurate, Detailed, and Automatic Modelling of Laser-Scanned Trees. *Remote Sens.* 11, 2074. <https://doi.org/10.3390/rs11182074>
- Fang, R., Strimbu, B.M., 2017. Stem Measurements and Taper Modeling Using Photogrammetric Point Clouds. *Remote Sens.* 9, 716. <https://doi.org/10.3390/rs9070716>
- Fayolle, A., Doucet, J.-L., Gillet, J.-F., Bourland, N., Lejeune, P., 2013a. Tree allometry in Central Africa: Testing the validity of pantropical multi-species allometric equations for estimating biomass and carbon stocks. *For. Ecol. Manag.* 305, 29–37.
- Fayolle, A., Rondeux, J., Doucet, J.-L., Ernst, G., Bouissou, C., Quevauvillers, S., Bourland, N., Feteke, F., Lejeune, P., 2013b. Réviser les tarifs de cubage pour mieux gérer les forêts du Cameroun. *Bois For. Trop.* 317, 35–49.
- Forbes, R.D., Meyer, A.B., 1955. *Forestry handbook*. For. Handb.
- Friedlingstein, P., Jones, M.W., O’Sullivan, M., Andrew, R.M., Hauck, J., Peters, G.P., Peters, W., Pongratz, J., Sitch, S., Quéré, C.L., Bakker, D.C.E., Canadell, J.G., Ciais, P., Jackson, R.B., Anthoni, P., Barbero, L., Bastos, A., Bastrikov, V., Becker, M., Bopp, L., Buitenhuis, E., Chandra, N., Chevallier, F., Chini, L.P., Currie, K.I., Feely, R.A., Gehlen, M., Gilfillan, D., Gkritzalis, T., Goll, D.S., Gruber, N., Gutekunst, S., Harris, I., Haverd, V., Houghton, R.A., Hurtt, G., Ilyina, T., Jain, A.K., Joetzjer, E., Kaplan, J.O., Kato, E., Klein Goldewijk, K., Korsbakken, J.I., Landschützer, P., Lauvset, S.K., Lefèvre, N., Lenton, A., Lienert, S., Lombardozzi, D., Marland, G., McGuire, P.C., Melton, J.R., Metzl, N., Munro, D.R., Nabel, J.E.M.S., Nakaoka, S.-I., Neill, C., Omar, A.M., Ono, T., Peregon, A., Pierrot, D., Poulter, B., Rehder, G., Resplandy, L., Robertson, E., Rödenbeck, C., Séférian, R., Schwinger, J., Smith, N., Tans, P.P., Tian, H., Tilbrook, B., Tubiello, F.N., Werf, G.R. van der, Wiltshire, A.J., Zaehle, S., 2019. Global Carbon Budget 2019. *Earth Syst. Sci. Data* 11, 1783–1838. <https://doi.org/10.5194/essd-11-1783-2019>
- Gollob, C., Ritter, T., Kraßnitzer, R., Tockner, A., Nothdurft, A., 2021. Measurement of Forest Inventory Parameters with Apple iPad Pro and Integrated LiDAR Technology. *Remote Sens.* 13, 3129. <https://doi.org/10.3390/rs13163129>
- Gollob, C., Ritter, T., Nothdurft, A., 2020. Forest Inventory with Long Range and High-Speed Personal Laser Scanning (PLS) and Simultaneous Localization and Mapping (SLAM) Technology. *Remote Sens.* 12, 1509. <https://doi.org/10.3390/rs12091509>
- Gonzalez de Tanago, J., Lau, A., Bartholomeus, H., Herold, M., Avitabile, V., Raumonon, P., Martius, C., Goodman, R.C., Disney, M., Manuri, S., 2018. Estimation of above-ground biomass of large tropical trees with terrestrial LiDAR. *Methods Ecol. Evol.* 9, 223–234.
- Gourlet-Fleury, S., Mortier, F., Fayolle, A., Baya, F., Ouédraogo, D., Bénédet, F., Picard, N., 2013. Tropical forest recovery from logging: a 24 year silvicultural

- experiment from Central Africa. *Philos. Trans. R. Soc. B Biol. Sci.* 368, 20120302.
- Hackenberg, J., Spiecker, H., Calders, K., Disney, M., Raunonen, P., 2015. SimpleTree—an efficient open source tool to build tree models from TLS clouds. *Forests* 6, 4245–4294.
- Henry, M., Besnard, A., Asante, W.A., Eshun, J., Adu-Bredu, S., Valentini, R., Bernoux, M., Saint-Andre, L., 2010. Wood density, phytomass variations within and among trees, and allometric equations in a tropical rainforest of Africa. *For. Ecol. Manag.* 260, 1375–1388.
- Hubau, W., Lewis, S.L., Phillips, O.L., Affum-Baffoe, K., Beeckman, H., Cuní-Sanchez, A., Daniels, A.K., Ewango, C.E.N., Fauset, S., Mukinzi, J.M., Sheil, D., Sonké, B., Sullivan, M.J.P., Sunderland, T.C.H., Taedoumg, H., Thomas, S.C., White, L.J.T., Abernethy, K.A., Adu-Bredu, S., Amani, C.A., Baker, T.R., Banin, L.F., Baya, F., Begne, S.K., Bennett, A.C., Benedet, F., Bitariho, R., Bocko, Y.E., Boeckx, P., Boundja, P., Brienen, R.J.W., Brncic, T., Chezeaux, E., Chuyong, G.B., Clark, C.J., Collins, M., Comiskey, J.A., Coomes, D.A., Dargie, G.C., de Haulleville, T., Kamdem, M.N.D., Doucet, J.-L., Esquivel-Muelbert, A., Feldpausch, T.R., Fofanah, A., Foli, E.G., Gilpin, M., Gloor, E., Gonmadje, C., Gourlet-Fleury, S., Hall, J.S., Hamilton, A.C., Harris, D.J., Hart, T.B., Hockemba, M.B.N., Hladik, A., Ifo, S.A., Jeffery, K.J., Jucker, T., Yakusu, E.K., Kearsley, E., Kenfack, D., Koch, A., Leal, M.E., Levesley, A., Lindsell, J.A., Lisingo, J., Lopez-Gonzalez, G., Lovett, J.C., Makana, J.-R., Malhi, Y., Marshall, A.R., Martin, J., Martin, E.H., Mbayu, F.M., Medjibe, V.P., Mihindou, V., Mitchard, E.T.A., Moore, S., Munishi, P.K.T., Bengone, N.N., Ojo, L., Ondo, F.E., Peh, K.S.-H., Pickavance, G.C., Poulsen, A.D., Poulsen, J.R., Qie, L., Reitsma, J., Rovero, F., Swaine, M.D., Talbot, J., Taplin, J., Taylor, D.M., Thomas, D.W., Toirambe, B., Mukendi, J.T., Tuagben, D., Umunay, P.M., van der Heijden, G.M.F., Verbeeck, H., Vleminckx, J., Willcock, S., Wöll, H., Woods, J.T., Zemagho, L., 2020. Asynchronous carbon sink saturation in African and Amazonian tropical forests. *Nature* 579, 80–87. <https://doi.org/10.1038/s41586-020-2035-0>
- Hummel, F.C., 1959. Code of sample plot procedure. H.M.S.O., London.
- Jia, G., Shevliakova, E., Artaxo, P., De Noblet-Ducoudré, N., Houghton, R., House, J., Kitajima, K., Lennard, C., Popp, A., Sirin, A., 2019. Land–Climate Interactions. *Climate Change and Land: An IPCC Special Report on Climate Change, Desertification, Land Degradation, Sustainable Land Management, Food Security, and Greenhouse Gas Fluxes in Terrestrial Ecosystems*. Springer, Berlin.
- Jurjević, L., Liang, X., Gašparović, M., Balenović, I., 2020. Is field-measured tree height as reliable as believed – Part II, A comparison study of tree height estimates from conventional field measurement and low-cost close-range remote sensing in a deciduous forest. *ISPRS J. Photogramm. Remote Sens.* 169, 227–241. <https://doi.org/10.1016/j.isprsjprs.2020.09.014>

- Kankare, V., Holopainen, M., Vastaranta, M., Puttonen, E., Yu, X., Hyypä, J., Vaaja, M., Hyypä, H., Alho, P., 2013. Individual tree biomass estimation using terrestrial laser scanning. *ISPRS J. Photogramm. Remote Sens.* 75, 64–75. <https://doi.org/10.1016/j.isprsjprs.2012.10.003>
- Lau, A., Calders, K., Bartholomeus, H., Martius, C., Raunonen, P., Herold, M., Vicari, M., Sukhdeo, H., Singh, J., Goodman, R.C., 2019. Tree Biomass Equations from Terrestrial LiDAR: A Case Study in Guyana. *Forests* 10, 527.
- Le Quéré, C., Andrew, R.M., Friedlingstein, P., Sitch, S., Pongratz, J., Manning, A.C., Korsbakken, J.I., Peters, G.P., Canadell, J.G., Jackson, R.B., Boden, T.A., Tans, P.P., Andrews, O.D., Arora, V.K., Bakker, D.C.E., Barbero, L., Becker, M., Betts, R.A., Bopp, L., Chevallier, F., Chini, L.P., Ciais, P., Cosca, C.E., Cross, J., Currie, K., Gasser, T., Harris, I., Hauck, J., Haverd, V., Houghton, R.A., Hunt, C.W., Hurtt, G., Ilyina, T., Jain, A.K., Kato, E., Kautz, M., Keeling, R.F., Klein Goldewijk, K., Körtzinger, A., Landschützer, P., Lefèvre, N., Lenton, A., Lienert, S., Lima, I., Lombardozzi, D., Metzl, N., Millero, F., Monteiro, P.M.S., Munro, D.R., Nabel, J.E.M.S., Nakaoka, S., Nojiri, Y., Padín, X.A., Peregon, A., Pfeil, B., Pierrot, D., Poulter, B., Rehder, G., Reimer, J., Rödenbeck, C., Schwinger, J., Séférian, R., Skjelvan, I., Stocker, B.D., Tian, H., Tilbrook, B., van der Laan-Luijkx, I.T., van der Werf, G.R., van Heuven, S., Viovy, N., Vuichard, N., Walker, A.P., Watson, A.J., Wiltshire, A.J., Zaehle, S., Zhu, D., 2017. Global Carbon Budget 2017. *Earth Syst. Sci. Data Discuss.* 1–79. <https://doi.org/10.5194/essd-2017-123>
- Le Quéré, C., Andrew, R. M., Friedlingstein, P., Sitch, S., Pongratz, J., Manning, A. C., Korsbakken, J. I., Peters, G. P., Canadell, J. G., Jackson, R. B., Boden, T. A., Tans, P. P., Andrews, O. D., Arora, V. K., Bakker, D. C. E., Barbero, L., Becker, M., Betts, R. A., Bopp, L., Chevallier, F., Chini, L. P., Ciais, P., Cosca, C. E., Cross, J., Currie, K., Gasser, T., Harris, I., Hauck, J. ORCID: <https://orcid.org/0000-0003-4723-9652> <<https://orcid.org/0000-0003-4723-9652>>, Haverd, V., Houghton, R. A., Hunt, C. W., Hurtt, G., Ilyina, T., Jain, A. K., Kato, E., Kautz, M., Keeling, R. F., Klein Goldewijk, K., Körtzinger, A., Landschützer, P., Lefèvre, N., Lenton, A., Lienert, S., Lima, I., Lombardozzi, D., Metzl, N., Millero, F., Monteiro, P. M. S., Munro, D. R., Nabel, J. E. M. S., Nakaoka, S. i., Nojiri, Y., Padín, X. A., Peregon, A., Pfeil, B., Pierrot, D., Poulter, B., Rehder, G., Reimer, J., Rödenbeck, C., Schwinger, J., Séférian, R., Skjelvan, I., Stocker, B. D., Tian, H., Tilbrook, B., van der Laan-Luijkx, I. T., van der Werf, G. R., van Heuven, S., Viovy, N., Vuichard, N., Walker, A. P., Watson, A. J., Wiltshire, A. J., Zaehle, S. and Zhu, D. (2017) Global Carbon Budget 2017, *Earth System Science Data Discussions*, pp. 1-79. [doi:https://doi.org/10.5194/essd-2017-123](https://doi.org/10.5194/essd-2017-123) <<https://doi.org/10.5194/essd-2017-123>>, [hdl:10013/epic.26a49935-0a4e-4ab3-a7a9-384bbb489d89](https://doi.org/10.5194/essd-2017-123)
- Letouzey, R., 1982. Manuel de botanique tropicale—Afrique tropicale. Nogent Sur Marne Cent. Tech. For. Trop. Tomes 1.

- Lewis, S.L., Lopez-Gonzalez, G., Sonké, B., Affum-Baffoe, K., Baker, T.R., Ojo, L.O., Phillips, O.L., Reitsma, J.M., White, L., Comiskey, J.A., 2009. Increasing carbon storage in intact African tropical forests. *Nature* 457, 1003–1006.
- Lewis, S.L., Maslin, M.A., 2015. Defining the Anthropocene. *Nature* 519, 171–180. <https://doi.org/10.1038/nature14258>
- Ligot, G., Gourlet-Fleury, S., Ouédraogo, D.-Y., Morin, X., Bauwens, S., Baya, F., Brostaux, Y., Doucet, J.-L., Fayolle, A., 2018. The limited contribution of large trees to annual biomass production in an old-growth tropical forest. *Ecol. Appl.* 28, 1273–1281. <https://doi.org/10.1002/eap.1726>
- Lutz, J.A., Larson, A.J., Swanson, M.E., Freund, J.A., 2012. Ecological Importance of Large-Diameter Trees in a Temperate Mixed-Conifer Forest. *PLOS ONE* 7, e36131. <https://doi.org/10.1371/journal.pone.0036131>
- Martin-Ducup, O., Mofack, G., II, Wang, D., Raunonen, P., Ploton, P., Sonké, B., Barbier, N., Couteron, P., Péliissier, R., 2021. Evaluation of automated pipelines for tree and plot metric estimation from TLS data in tropical forest areas. *Ann. Bot.* 128, 753–766. <https://doi.org/10.1093/aob/mcab051>
- McDowell, N.G., Allen, C.D., Anderson-Teixeira, K., Aukema, B.H., Bond-Lamberty, B., Chini, L., Clark, J.S., Dietze, M., Grossiord, C., Hanbury-Brown, A., 2020. Pervasive shifts in forest dynamics in a changing world. *Science* 368.
- Metcalf, C.J.E., Clark, J.S., Clark, D.A., 2009. Tree growth inference and prediction when the point of measurement changes: modelling around buttresses in tropical forests. *J. Trop. Ecol.* 25, 1–12.
- Mitchard, E.T., Saatchi, S.S., Baccini, A., Asner, G.P., Goetz, S.J., Harris, N.L., Brown, S., 2013. Uncertainty in the spatial distribution of tropical forest biomass: a comparison of pan-tropical maps. *Carbon Balance Manag.* 8, 10.
- Mitchard, E.T.A., 2018. The tropical forest carbon cycle and climate change. *Nature* 559, 527–534. <https://doi.org/10.1038/s41586-018-0300-2>
- Mokroš, M., Mikita, T., Singh, A., Tomaščík, J., Chudá, J., Wężyk, P., Kuželka, K., Surový, P., Klimánek, M., Zięba-Kulawik, K., Bobrowski, R., Liang, X., 2021. Novel low-cost mobile mapping systems for forest inventories as terrestrial laser scanning alternatives. *Int. J. Appl. Earth Obs. Geoinformation* 104, 102512. <https://doi.org/10.1016/j.jag.2021.102512>
- Molto, Q., Rossi, V., Blanc, L., 2013. Error propagation in biomass estimation in tropical forests. *Methods Ecol. Evol.* 4, 175–183.
- Momo, S.T., Ploton, P., Martin-Ducup, O., Lehnebach, R., Fortunel, C., Sagang, L.B.T., Boyemba, F., Couteron, P., Fayolle, A., Libalah, M., Loumeto, J., Medjibe, V., Ngomanda, A., Obiang, D., Péliissier, R., Rossi, V., Yongo, O., Sonké, B., Barbier, N., 2020. Leveraging Signatures of Plant Functional Strategies in Wood Density Profiles of African Trees to Correct Mass Estimations From Terrestrial Laser Data. *Sci. Rep.* 10, 2001. <https://doi.org/10.1038/s41598-020-58733-w>

- Moskal, L.M., Erdody, T., Kato, A., Richardson, J., Zheng, G., Briggs, D., 2009. Lidar applications in precision forestry. *Proc. Silvilaser* 154–163.
- Moutinho, P., Guerra, R., Azevedo-Ramos, C., 2016. Achieving zero deforestation in the Brazilian Amazon: What is missing? *Elem Sci Anth* 4, 000125. <https://doi.org/10.12952/journal.elementa.000125>
- Muller-Landau, H.C., Detto, M., Chisholm, R.A., Hubbell, S.P., Condit, R., 2014. Detecting and projecting changes in forest biomass from plot data. *For. Glob. Change Coomes Burslem DFRP Simonsen WDEds Camb. Univ. Press Camb.* 381–416.
- Ngomanda, A., Mavouroulou, Q.M., Obiang, N.L.E., Iponga, D.M., Mavoungou, J.-F., Lépengué, N., Picard, N., Mbatchi, B., 2012. Derivation of diameter measurements for buttressed trees, an example from Gabon. *J. Trop. Ecol.* 28, 299–302.
- Nogueira, E.M., Nelson, B.W., Fearnside, P.M., 2006. Volume and biomass of trees in central Amazonia: influence of irregularly shaped and hollow trunks. *For. Ecol. Manag.* 227, 14–21.
- Nölke, N., Fehrmann, L., I Nengah, S.J., Tiryan, T., Seidel, D., Kleinn, C., 2015. On the geometry and allometry of big-buttressed trees—a challenge for forest monitoring: new insights from 3D-modeling with terrestrial laser scanning. *IForest-Biogeosciences For.* 681.
- Pan, Y., Birdsey, R.A., Fang, J., Houghton, R., Kauppi, P.E., Kurz, W.A., Phillips, O.L., Shvidenko, A., Lewis, S.L., Canadell, J.G., 2011. A large and persistent carbon sink in the world's forests. *Science* 333, 988–993.
- Pfeifer, N., Winterhalder, D., 2004. Modelling of tree cross sections from terrestrial laser scanning data with free-form curves. *Int. Arch. Photogramm. Remote Sens. Spat. Inf. Sci.* 36, W2.
- Phillips, O.L., Aragão, L.E., Lewis, S.L., Fisher, J.B., Lloyd, J., López-González, G., Malhi, Y., Monteagudo, A., Peacock, J., Quesada, C.A., 2009. Drought sensitivity of the Amazon rainforest. *Science* 323, 1344–1347.
- Phillips, O.L., Baker, T.R., Brienen, R., Feldpausch, T.R., 2010. Field manual for plot establishment and remeasurement. URL <http://www.Geog.Leeds.Ac.Uk/projects/rainfor>.
- Phillips, O.L., Lewis, S.L., 2014. Evaluating the tropical forest carbon sink. *Glob. Change Biol.* 20, 2039–2041.
- Picard, N., Boyemba Bosela, F., Rossi, V., 2015a. Reducing the error in biomass estimates strongly depends on model selection. *Ann. For. Sci.* 72, 811–823. <https://doi.org/10.1007/s13595-014-0434-9>
- Picard, N., Gourlet-Fleury, S., 2008. Manuel de référence pour l'installation de dispositifs permanents en forêt de production dans le Bassin du Congo.
- Picard, N., Rutishauser, E., Ploton, P., Ngomanda, A., Henry, M., 2015b. Should tree biomass allometry be restricted to power models? *For. Ecol. Manag.* 353, 156–163. <https://doi.org/10.1016/j.foreco.2015.05.035>

- Pilli, R., Anfodillo, T., Carrer, M., 2006. Towards a functional and simplified allometry for estimating forest biomass. *For. Ecol. Manag.* 237, 583–593. <https://doi.org/10.1016/j.foreco.2006.10.004>
- Plumptre, A.J., 1995. The importance of "seed trees" for the natural regeneration of selectively logged tropical forest. *Commonw. For. Rev.* 253–258.
- Quééré, C.L., Raupach, M.R., Canadell, J.G., Marland, G., Bopp, L., Ciais, P., Conway, T.J., Doney, S.C., Feely, R.A., Foster, P., Friedlingstein, P., Gurney, K., Houghton, R.A., House, J.I., Huntingford, C., Levy, P.E., Lomas, M.R., Majkut, J., Metzl, N., Ometto, J.P., Peters, G.P., Prentice, I.C., Randerson, J.T., Running, S.W., Sarmiento, J.L., Schuster, U., Sitch, S., Takahashi, T., Viovy, N., Werf, G.R. van der, Woodward, F.I., 2009. Trends in the sources and sinks of carbon dioxide. *Nat. Geosci.* 2, 831–836. <https://doi.org/10.1038/ngeo689>
- Raumonen, P., Kaasalainen, M., Åkerblom, M., Kaasalainen, S., Kaartinen, H., Vastaranta, M., Holopainen, M., Disney, M., Lewis, P., 2013. Fast Automatic Precision Tree Models from Terrestrial Laser Scanner Data. *Remote Sens.* 5, 491–520. <https://doi.org/10.3390/rs5020491>
- Réjou-Méchain, M., Tanguy, A., Piponiot, C., Chave, J., Hérault, B., 2017. biomass: an r package for estimating above-ground biomass and its uncertainty in tropical forests. *Methods Ecol. Evol.* 8, 1163–1167.
- Rondeux, J., 1993. La mesure des arbres et des peuplements forestiers. Les presses agronomiques de Gembloux.
- Rowland, L., da Costa, A.C.L., Galbraith, D.R., Oliveira, R.S., Binks, O.J., Oliveira, A. a. R., Pullen, A.M., Doughty, C.E., Metcalfe, D.B., Vasconcelos, S.S., Ferreira, L.V., Malhi, Y., Grace, J., Mencuccini, M., Meir, P., 2015. Death from drought in tropical forests is triggered by hydraulics not carbon starvation. *Nature* 528, 119–122. <https://doi.org/10.1038/nature15539>
- Saatchi, S.S., Harris, N.L., Brown, S., Lefsky, M., Mitchard, E.T., Salas, W., Zutta, B.R., Buermann, W., Lewis, S.L., Hagen, S., 2011. Benchmark map of forest carbon stocks in tropical regions across three continents. *Proc. Natl. Acad. Sci.* 108, 9899–9904.
- Slik, J.W., Paoli, G., McGuire, K., Amaral, I., Barroso, J., Bastian, M., Blanc, L., Bongers, F., Boundja, P., Clark, C., 2013. Large trees drive forest aboveground biomass variation in moist lowland forests across the tropics. *Glob. Ecol. Biogeogr.* 22, 1261–1271.
- Stovall, A.E.L., Anderson-Teixeira, K.J., Shugart, H.H., 2018. Assessing terrestrial laser scanning for developing non-destructive biomass allometry. *For. Ecol. Manag.* 427, 217–229. <https://doi.org/10.1016/j.foreco.2018.06.004>
- Swaine, M.D., Lieberman, D., Putz, F.E., 1987. The dynamics of tree populations in tropical forest: a review. *J. Trop. Ecol.* 3, 359–366.
- Takoudjou, S.M., Ploton, P., Sonké, B., Hackenberg, J., Griffon, S., Coligny, F. de, Kamdem, N.G., Libalah, M., Mofack, G.I., Moguédec, G.L., Péliissier, R., Barbier, N., 2018. Using terrestrial laser scanning data to estimate large tropical trees biomass and calibrate allometric models: A comparison with

- traditional destructive approach. *Methods Ecol. Evol.* 9, 905–916. <https://doi.org/10.1111/2041-210X.12933>
- Talbot, J., Lewis, S.L., Lopez-Gonzalez, G., Brienen, R.J., Monteagudo, A., Baker, T.R., Feldpausch, T.R., Malhi, Y., Vanderwel, M., Murakami, A.A., 2014. Methods to estimate aboveground wood productivity from long-term forest inventory plots. *For. Ecol. Manag.* 320, 30–38.
- Tao, S., Labrière, N., Calders, K., Fischer, F.J., Rau, E.-P., Plaisance, L., Chave, J., 2021. Mapping tropical forest trees across large areas with lightweight cost-effective terrestrial laser scanning. *Ann. For. Sci.* 78, 103. <https://doi.org/10.1007/s13595-021-01113-9>
- Thompson, J., Proctor, J., Viana, V., Milliken, W., Ratter, J.A., Scott, D.A., 1992. Ecological studies on a lowland evergreen rain forest on Maraca Island, Roraima, Brazil. I. Physical environment, forest structure and leaf chemistry. *J. Ecol.* 689–703.
- Trochta, J., Krůček, M., Vrška, T., Král, K., 2017. 3D Forest: An application for descriptions of three-dimensional forest structures using terrestrial LiDAR. *PLOS ONE* 12, e0176871. <https://doi.org/10.1371/journal.pone.0176871>
- Vitousek, P.M., 1992. Global environmental change: an introduction. *Annu. Rev. Ecol. Syst.* 23, 1–14.
- Vitousek, P.M., Ehrlich, P.R., Ehrlich, A.H., Matson, P.A., 1986. Human appropriation of the products of photosynthesis. *BioScience* 36, 368–373.
- Wilkes, P., Lau, A., Disney, M., Calders, K., Burt, A., Gonzalez de Tanago, J., Bartholomeus, H., Brede, B., Herold, M., 2017. Data acquisition considerations for Terrestrial Laser Scanning of forest plots. *Remote Sens. Environ.* 196, 140–153. <https://doi.org/10.1016/j.rse.2017.04.030>
- Zarin, D.J., Harris, N.L., Baccini, A., Aksenov, D., Hansen, M.C., Azevedo-Ramos, C., Azevedo, T., Margono, B.A., Alencar, A.C., Gabris, C., Allegretti, A., Potapov, P., Farina, M., Walker, W.S., Shevade, V.S., Loboda, T.V., Turubanova, S., Tyukavina, A., 2016. Can carbon emissions from tropical deforestation drop by 50% in 5 years? *Glob. Change Biol.* 22, 1336–1347. <https://doi.org/10.1111/gcb.13153>
- Zhao, F., Guo, Q., Kelly, M., 2012. Allometric equation choice impacts lidar-based forest biomass estimates: A case study from the Sierra National Forest, CA. *Agric. For. Meteorol.* 165, 64–72. <https://doi.org/10.1016/j.agrformet.2012.05.019>
- Zhiyuan, H., Yong, T., Xiaobao, D., Min, C., 2013. Buttress trees in a 20-hectare tropical dipterocarp rainforest in Xishuangbanna, SW China. *J. Plant Ecol.* 6, 187–192.
- Zolkos, S.G., Goetz, S.J., Dubayah, R., 2013. A meta-analysis of terrestrial aboveground biomass estimation using lidar remote sensing. *Remote Sens. Environ.* 128, 289–298. <https://doi.org/10.1016/j.rse.2012.10.017>

Appendices

Appendix 1 – Supplementary information of scientific paper of chapter 2: *Terrestrial photogrammetry: a non-destructive method for modelling irregularly shaped tropical tree trunks*

SI 1: Description of the Loundoungou site (Republic of Congo).

The methodology was extended to 34 trees located in one of 400 ha of the two DynAfFor Permanent Sample Plots (PSP) of Loundoungou. The PSP are in the logging concession of CIB in the north of the Republic of Congo (Figure S1). Following Köppen–Geiger classification, the region is in the Am-type tropical rainforest climate. Annual rainfall is between 1365 mm per year and 1685 mm per year following the two closest weather stations (Gillet, 2013). There is one dry season between December and February (monthly precipitation inferior to 60 mm). Temperatures are high and constant throughout the year with a minimum of 24.2 ± 0.4 °C in July and a maximum of 25.5 ± 0.6 °C in March. The altitude in Loundoungou PSP's varies from 395 m to 470m and the soil is mainly a Xanthic Acrisol (Freycon, 2014). Vegetation in the region of Loundoungou is characterized by a moist forest of transition between evergreen forest and semi-deciduous forests and with fragments of swamp forest (Fayolle et al., 2014a, 2014b).

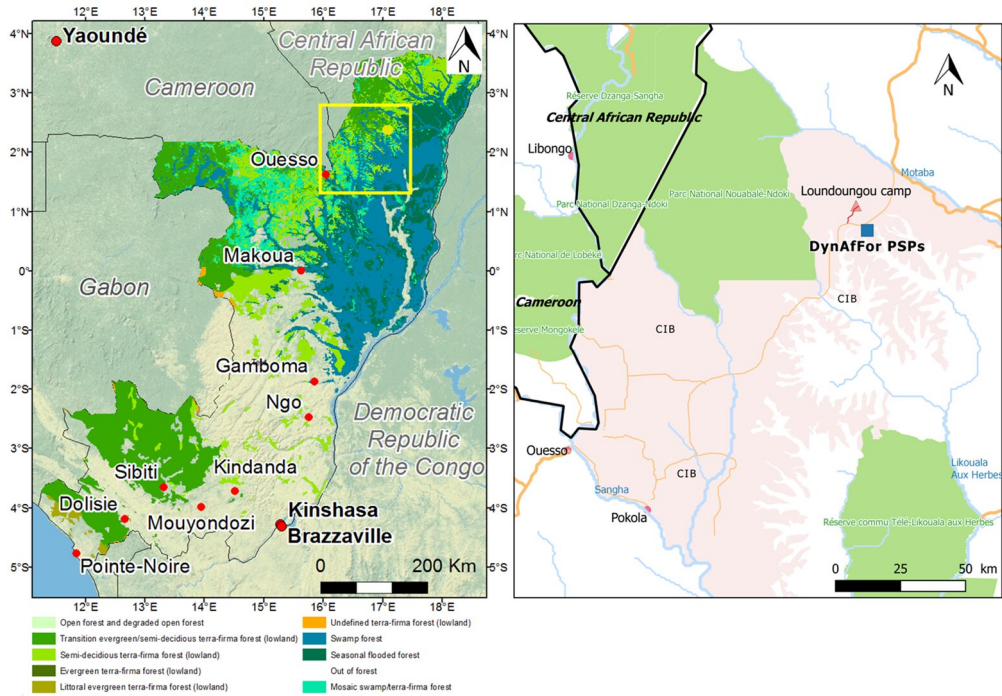


Fig. S1. Location of the two adjacent DynAffFor Permanent Sample of Loundougou in the North of the Republic of Congo (Vegetation map source: Fayolle et al. (2014a)).

References:

La mise à jour automatique des citations est désactivée. Pour voir la bibliographie, cliquez sur Actualiser dans l'onglet Zotero.

SI 2: Methodology and validation of the photogrammetric process.

Additional information on the photogrammetric methodology: image acquisition in the field



Fig. S2.1: Focal buttressed trees with surrounding vegetation that limits the photogrammetric process. The white panel is a panel with coded targets which are automatically detected by the photogrammetric software Photoscan.



Fig. S2.2: Focal buttressed tree with the small vegetation and the liana removed. Four panels with coded targets were positioned in the four cardinal points to add artificial tie-points in the photogrammetric process. The panel from the south was used as the metric reference (one vertical line of the coded target was considered as the z axis). The distance between the highest coded targets of the reference panel and the ground was measured to deduce the height of the coded targets.

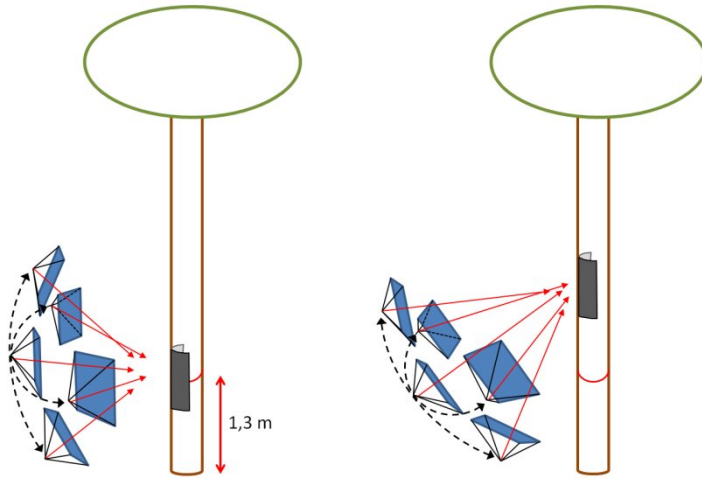


Fig. S2.3: Cross-convergent image acquisition

Validation method: rectified images of the cross sections

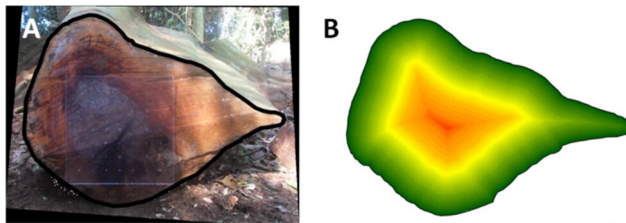


Fig. S2.4: Cross sections of irregular stems. **A:** Rectified image overlapped with the digitized contour of the cross section. The rectification of the image is a projective transformation based on the 40 cm x 40 cm Plexiglas grid with 5 cm x 5 cm graduations positioned on the cross section; **B:** Center computed by extracting the farthest location within the polygon (red in the cross sections).

Quality analysis of the destructive validation method

A comparison between two perpendicular lengths (diameters) measured with a tape in the field and the measurement of the same distance on the rectified image was carried out to estimate the accuracy of the destructive method. The distances measured on the rectified images were within the precision of the tape used for distance measurement (bias of -0.47 cm and RMSE of 0.92 cm). The destructive method was found to be consistent as a reference for the quality evaluation of the 3D model.

Results of the calibration trees

A.

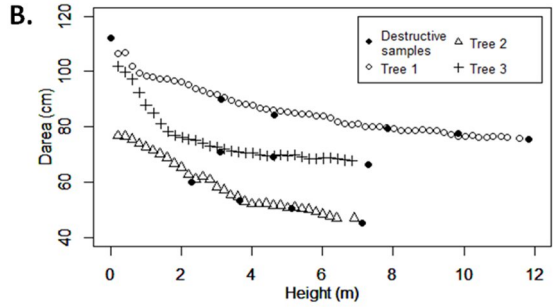
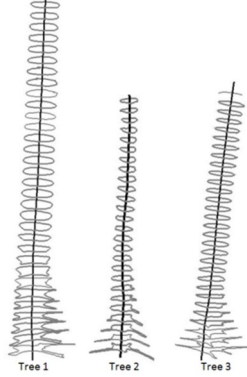


Fig. S2.5. A. Cross sections along the stem of the three calibration trees. B. Diameter variation along the stem, with the diameter expressed as the diameter of a circular disc with the same area as the basal area of the cross section (Darea). Black points were measured from the cross section digitized on rectified images of log sections (destructive samples).

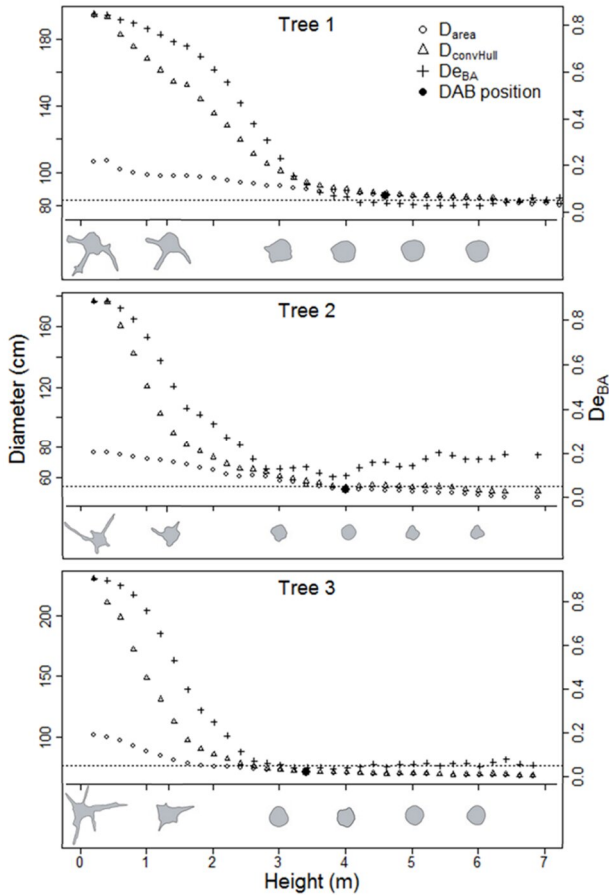


Fig. S2.6. Diameter variation along the stem of the three trees studied, according to different diameter measurement methods: diameters deduced from the area of the cross sections (D_{area}), and diameters estimated with the convex hull of the cross sections ($D_{convHull}$). The fractional basal area deficit is also displayed with height ($DeBA$). Black dots represent the position of the reference diameter DAB. Cross sections with a $DeBA$ below the 0.05 reference value (horizontal dotted line) is considered as a circular cross section. Cross sections along the stem are also illustrated.

SI 3: POM definition, formatting biomass data and $D_{area130}$ (ie DBH')-field variable relationships

Quantitative definition of the point of measurement (POM)

The relative difference between $D_{ConvHull}$ and $D_{area130}$ decreases with the height of the buttressed trees. The threshold of 3% for the relative difference between $D_{ConvHull}$ and $D_{area130}$ leads to a mean height of 23 cm under the highest buttress measured in the field and with a mean De_{BA} of 0.07 (93% of the trees reached this threshold). The threshold of 2% leads to a similar height than the buttress height (mean difference of 9 cm) with a mean De_{BA} of 0.05, but only 72 % of the trees reached this last threshold. The 5 % threshold is encountered for all the trees and on average, De_{BA} is equal to 0.12.

Table S3.1: Definition of the POM by varying the threshold: ie varying the relative difference between the $D_{ConvHull}$ and $D_{area130}$ to: 1%, 2%, 3%, 4%, 5%, 7%, 10%. De_{BA130} is the De_{BA} at 1.3 m height, De_{BAbut} is the De_{BA} encountered just above the highest buttress, De_{BAPOM} is the De_{BA} at the point of measurement of the DAB, De_{BAi} is the De_{BA} at the height where difference between $D_{ConvHull}$ and $D_{area130}$ is i %, H_{but} is the height of the highest buttress (m), $HDAB$ is the height where DAB is measured, dH_i is the difference between H_{but} (measured in the field) and the height where difference between $D_{ConvHull}$ and D_{area} is i %.

	<i>Celtis mildbraedii</i>				<i>Entandophragma cylindricum</i>				Both species			
	n	Min-max	Mean	CV (%)	n	Min-max	mean	CV (%)	n	Min-max	Mean	CV (%)
DeBA130	13	0.05-0.79	0.50	58	16	0.03-0.72	0.35	62	29	0.03-0.79	0.42	62
DeBAbut	13	0.04-0.54	0.17	94	16	0.01-0.25	0.08	88	29	0.01-0.54	0.12	102
DeBAPOM	13	0.05-0.22	0.11	60	16	0.01-0.13	0.06	68	29	0.01-0.22	0.08	70
DeBA1	1	0.54-0.54	0.54	NA	8	0.02-0.04	0.02	30	9	0.02-0.54	0.08	214
DeBA2	7	0.04-0.15	0.06	73	14	0.03-0.11	0.05	40	21	0.03-0.15	0.05	56
DeBA3	12	0.05-0.14	0.07	35	15	0.05-0.11	0.07	21	27	0.05-0.14	0.07	28
DeBA4	12	0.06-0.17	0.10	35	16	0.07-0.25	0.10	46	28	0.06-0.25	0.10	41
DeBA5	13	0.09-0.2	0.12	28	16	0.08-0.21	0.12	29	29	0.08-0.21	0.12	28
DeBA7	13	0.12-0.18	0.14	13	16	0.12-0.29	0.15	27	29	0.12-0.29	0.15	23
DeBA10	13	0.15-0.57	0.23	48	16	0.12-0.31	0.21	20	29	0.12-0.57	0.22	36
Hbut	13	1-5	3.2	44	16	1.6-7.2	4.2	42	29	1-7.2	3.7	45
HDAB	13	1.6-5.5	3.7	37	16	2.0-7.8	5.0	36	29	1.6-7.8	4.4	39
dH1	1	1.6-1.6	1.60	NA	8	-0.7-2.2	0.53	165	9	-0.7-2.2	0.64	137
dH2	7	-0.7-1.4	0.63	116	14	-1.4-1.4	-0.19	-382	21	-1.4-1.4	0.09	935
dH3	12	-0.9-1.4	0.36	187	15	-1.8-0.3	-0.71	-91	27	-1.8-1.4	-0.23	-360
dH4	12	-1.1-1.3	-0.04	-1456	16	-2--0.1	-0.94	-63	28	-2-1.3	-0.55	-134
dH5	13	-1.2-1.4	-0.08	-961	16	-2.1-0.4	-1.17	-45	29	-2.1-1.4	-0.68	-122
dH7	13	-1.4-0.6	-0.45	-122	16	-2.5-0.7	-1.48	-41	29	-2.5-0.6	-1.02	-76
dH10	13	-1.8-0.2	-0.83	-63	16	-2.8--1	-1.90	-33	29	-2.8-0.2	-1.42	-55

Analysis on the best tree size predictor

Formatting the biomass data

The analysis of the standardized predictors is based on the biomass measurements of 15 *Entandophragma cylindricum* from the Fayolle et al. (2013) dataset. The equivalent diameter to the basal area and the perimeter of the convex hull at 1.3 m high (respectively $D_{\text{area}130}$ and $D_{\text{convHull}130}$) were not measured for the trees with buttresses at 1.3m height, but these measurements were available at the stump height (mean stump height: 99 cm). The cross sections of the stumps were photographed with a plexiglas grid of 5 cm x 5 cm graduations as we performed to validate our photogrammetric cross sections measurements (data S2). $D_{\text{area}130}$ and $D_{\text{convHull}130}$ of the biomass trees were estimated on the basis of the stump measurements and the modified taper model of Metcalf et al., 2009 (equation SI 3.1).

$$D_i = (D_{130} - DAB) \cdot e^{-b_2(h_i - 1.3)} + DAB \quad (\text{Eq. SI3.1})$$

with D_i the equivalent diameter (D_{area} or D_{convHull}) (in cm) at height h_i of the buttressed part of the stem (in m), D_{130} the equivalent diameter at 1.3 m height in cm ($D_{\text{area}130}$ or $D_{\text{convHull}130}$) (in cm), DAB , the diameter above the buttresses and b_2 is a parameter.

The modified taper model of Metcalf et al. (2009) does not intend to be a taper model for the whole stem, but a model to estimate $D_{\text{area}130}$ and $D_{\text{convHull}130}$ on the basis of the stump measurements of the 15 *Entandophragma cylindricum* with biomass measurements (Fig. S3.1).

The parameter b_2 has been estimated with the 34 photogrammetrics data from Congo by fitting a nonlinear mixed-effects model with the species as fixed effect and the individual trees as random factor (package nlme of R). With the D_{area} photogrammetric dataset, we found a significant effect of the species for the parameter b_2 (*C. mildbraedii* has an intercept with $p=0$ and *E. cylindricum* with $p=10^{-3}$) and a considerable intraspecific variation (Fig. S3.2). The same procedure was performed with the D_{convHull} data.

As the estimation of the parameter b_2 for D_{area} data is significantly different for the two species, we only analyzed the relationship between b_2 and the measurable parameters DAB , $HDAB$ and $D_{\text{convHull}130}$ for *Entandophragma cylindricum*. The variation of b_2 was best explained by a model mb3 that includes the equivalent diameter of the convex hull around the buttresses at 1.3 height ($D_{\text{convHull}130}$) and the height where DAB is measured ($HDAB$). As the convex hull around the buttresses at 1.3 height was not measured but estimated for the reference biomass trees, we preferred to use the model mb5 with only one variable which was measured: $HDAB$. mb5 is the second model with the lowest AIC and all the coefficient significantly different to zero. The same procedure was performed with the D_{convHull} data.

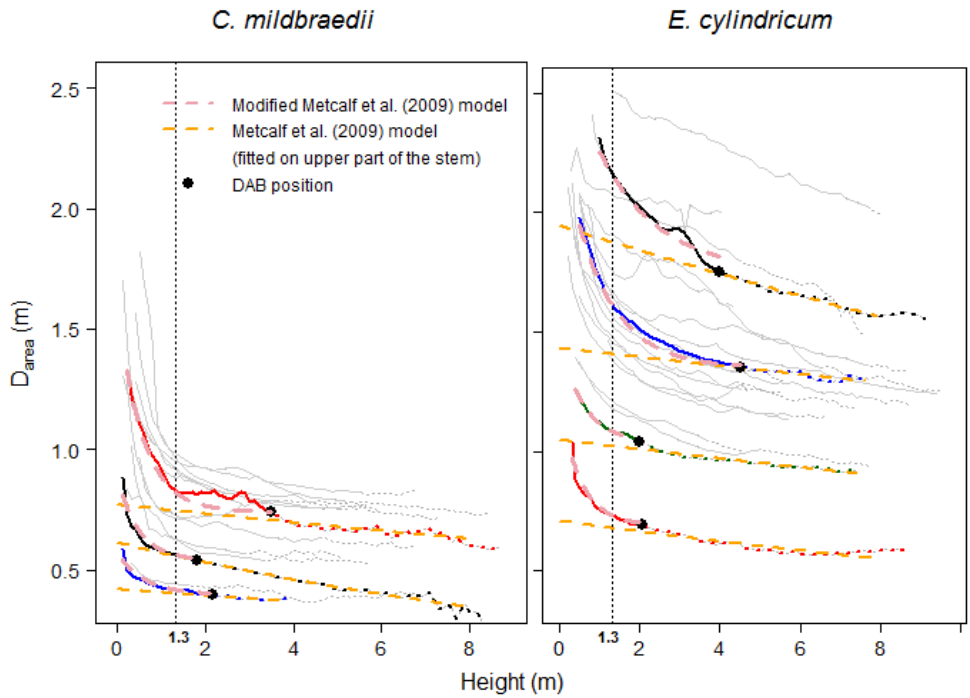


Fig S3.1. Taper data from the 3D models for the 14 *C. mildbraedii* and 20 *E. cylindricum* trees. The modified taper model of Metcalf et al. (2009) was fitted with D_{area} of the buttressed part of the stem (dark pink dashed lines) and the taper model of Metcalf et al. (2009) was fitted with a subset of D_{area} data above buttresses, between H_{DAB} and 8 m (orange dashed lines) following the field protocol of Cushman et al. (2014) for the trees highlighted in Fig. 2. Black dots correspond to the position of the diameter above buttresses (DAB) as well as the intersection between the solid and dotted lines.

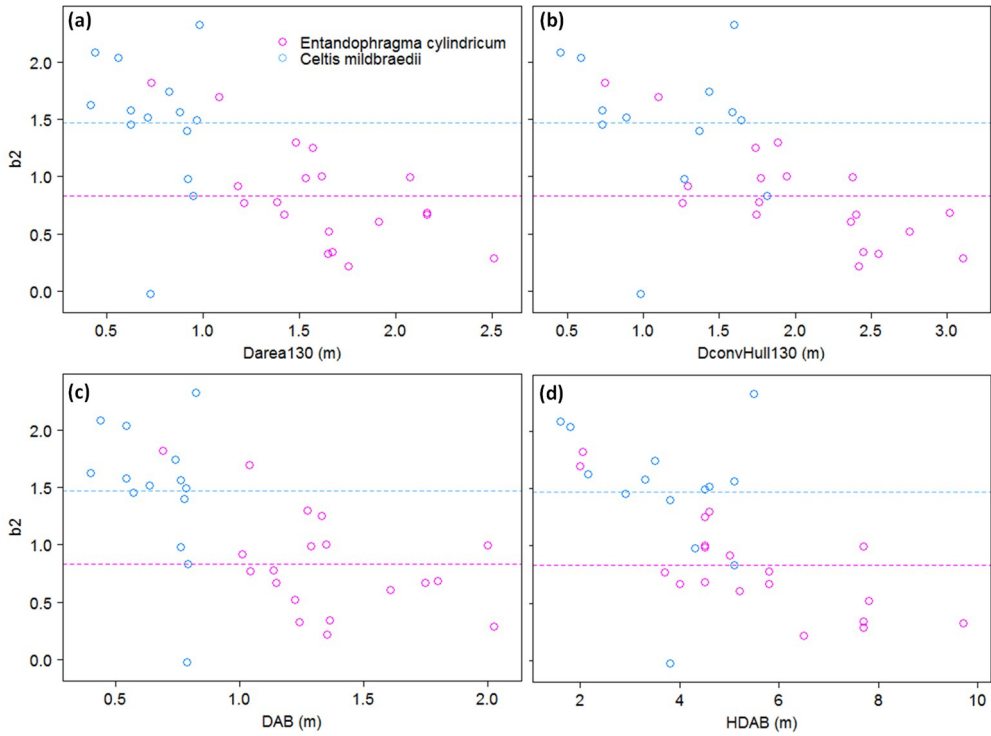


Fig. S3.5: Scatterplot between the taper parameter b_2 for D_{area} estimates and (a) the equivalent diameter of the basal area at 1.3 m height: $D_{area130}$, (b) the equivalent diameter of the convex hull around the buttresses at 1.3 m height: $D_{convHull130}$, (c) the diameter above the buttresses: DAB , and (d) the height of measurement of the DAB : $HDAB$. The horizontal blue dashed line, at $y=1.473$, is the mean value of b_2 for *Celtis mildbraedii* and the magenta dashed line, at $y=0.831$, is the mean value of b_2 for *Entandophragma cylindricum*.

Table S3.2: AIC values for alternative models for among-tree variation in taper parameter of all the 20 *E. Cylindricum* with photogrammetric measurements. The column “all param. $P < 0.05$ ” specifies if all the coefficients of the parameters of the models were statistically significant.

Models	Variables				AIC	df	All param. $P < 0.05$
	Species	DAB	HDAB	$D_{convHull130}$			
mb1		x	x	x	7.80	5	
mb2		x	x		11.28	4	
mb3			x	x	7.11	4	x
mb4		x		x	9.63	4	
mb5			x		10.61	3	x
mb6		x			23.74	3	x
mb7				x	10.86	3	x

Relationships between Darea130 and easy to measure field variables

Table S3.3: BIC values for the best models find with the leaps package of R.

Model	Nr of variables	D _{convHull130} :			D _{convHull130} :		D _{convHull130} :		BIC	R ² adj
		D _{convHull130}	DAB	H _{DAB}	DAB	HDAB	DAB:H _{DAB}	DAB:HDAB		
md1	3		X			X	X		-78.7	0.987
md2	4		X	X		X	X		-76.0	0.987
md3	4		X			X	X	X	-75.3	0.987
md4	4		X		X	X	X		-75.2	0.987
md5	2	X	X						-74.3	0.984
md6	5		X	X		X	X	X	-73.7	0.987
md7	5		X	X	X	X	X		-73.3	0.987
md8	5	X	X	X		X	X		-72.5	0.987
md9	3	X	X				X		-71.5	0.984
md10	6	X	X	X	X	X	X		-71.2	0.987
md11	3	X	X					X	-71.1	0.984
md12	6	X	X	X		X	X	X	-70.7	0.987
md13	6		X	X	X	X	X	X	-70.2	0.987
md14	7	X	X	X	X	X	X	X	-67.7	0.987
md15	2		X			X			-61.9	0.977
md16	2		X		X				-59.1	0.975
md17	1		X						-51.3	0.966
md18	1				X				-31.5	0.938
md19	1	X							-0.2	0.841

Appendix 2 - Supplementary information of the scientific paper of chapter 3: *Forest Inventory with Terrestrial LiDAR: A Comparison of Static and a Hand-Held Mobile Laser Scanning*

Plot 1: Coppice of hornbeam and birch



Plot 2: Even-aged of Beech



Plot 3: Uneven-aged of beech



Plot 4: Even-aged of douglas



Plot 5: Even-aged of spruce



Plot 6: Even-aged of oak and pine





Plot 7: Uneven-aged of beech



Plot 8: Even-aged of spruce



Plot 9: Even-aged of spruce



Plot 10: Uneven-aged of beech



No images

Figure SI. Images of the 10 forests plots studied.

Table S1. Summary of Experimental design, scanner settings and methodologies of previous studies on automatic stem detection and DBH extraction from TLS data for forest inventory. The number of trees in bracket in the column Tree is the number of trees used for DBH comparison (m = measured). The tree forest types are broadleaves (B), coniferous (C) and mixed (M). The shape of the plots is in bracket in the column Size (r: rectangle, s: square and c: circle). NHA is the number of trees per hectare. Mode is the scanning method (MS: multiscan, SS: single scan, PLS: personal mobile laser scanning and HMLS: hand-held mobile laser scanning). Occl. is the rate of trees detected without occlusion and Occl. + missed is the proportion of trees automatically detected.

Study	Plot (n)	Tree (n)	Forest Type	Terrain	Size (ha)	NHA	Mode	Detection			DBH		
								Process	Occl.	Occl+ Missed	Process	Bias (cm)	RMSE (cm)
Simonse et al., 2003	1	28	C	/	-0.12 (r.)	-233	4 MS	Filter + 2D-SliceHough transform + fitting circle	/	93	1.3 m circle fitting	1.7	/
Thies and Spiecker, 2004	1	50 (11 m)	B (UEA)	Slope (41%)	-0.09 (s)	555.6	SS 5 MS	Simonse et al. [6] method	/ /	22 52	Circle fitting	-0.75 0.32	3.48 3.22
Hopkinson et al., 2004	2	138	C & B	/	0.12 (s)	465-661	5 MS	2D-Slice between 1 and 7 m + manual detection	97.1	/	Manual extraction and cylinder fitting (1.25 & 1.75 m)	/	/
Bienert et al., 2006	/	65	/	/	/	/	2 MS	XY cluster at 1.3 m + fitting circle	97-100	/	1.3 m circle fitting	0.9	1.5
Bienert et al., 2007	21	547	M & B	/	0.07 (c.)	/	SS	Similar to [48] + point density raster analysis	/	97.4	/	/	/
Maas et al., 2008	4 1	82	B (1 C)	hilly/ flat slope	0.07 (c.)	212-410	SS 3 MS	Similar to [14]	/	97.5	Similar to [48]	-0.67-1.58	1.8-3.25
Murphy, 2008	9	220	C (EA)	Flat	0.04 (c.)	/	2 MS	Similar to [14]	93	93	Similar to [48]	-0.6	/
Strahler et al., 2008	1	102	C (EA)	/	0.79 (c.)	130	SS	Based on the range and intensity signal return	/	40.2	/	/	/
Brolly and Kiraly, 2009	1	213	M	/	0.28 (c.)	753	SS	2D-Slice clustering + Single circle fitting	81	72.3	Single circle fitting	-0.8	4.2
									81	72.3	Multy circle fitting	-1.6	3.4
									81	62.9	Cylinder fitting	0.5	7
Tansey et al., 2009	1	8 m	C	Flat	0.05 (r.)	1131	4 MS	XY cluster at 1.3 m + Hough transform detection	/	/	Hough transform	-1.6	2.3
									/	/	Cylinder least square fitting	-3.4	3.6
									/	/	Circle least square fitting	-1.7	1.9
Murphy et al., 2010	18 15	958 (~340 m)	C (EA)	Flat	0.1 (r.) 0.03-0.13 (c.)	207-570 153-326	SS 5 MS 2 MS	Similar to 14	68	59	1.3 m circle fitting or diameter profile	-0.3-1.9	/
									100	99			
									86	82			
Antonarakis,	2	261	B p (1 Co)	/	0.49 (s)	255-2340	5 MS	Similar to Hopkinson	80 (100)	/	Cylinder fitting	0.3-0.4	/

Biodiversity and ecosystem services in tropical forests: the role of forest allocations

Othmani et al., 2011	17	/	Co & EA	/	0.07 (c.)	56–3600	SS	Clustering + filetring + fitting circle	90.6	1.3 Circle fitting +cor. with local linear diam. profile	80% <5 cm	/	
Lovell et al., 2011	2	157	C	Flat	0.13 & 0.79 (c.)	124/477	SS	intensity thresholds + maximum intensity value	/	54/68	/	/	
Liang et al., 2012	9	/			0.03 (c.)	509–1432	SS	local 3D point density + flatness (eigenvalue) + vertical distribution	/	73	/	/	
Liang et al., 2013	5	128	C or M	/	0.03 (c.)	605–1210	SS	Similar to [53]	/	73.4	Cylinder fitting	0.35	0.74–2.41
							4 MSS	Similar to [53] + new registration method	/	95.3	Cylinder fitting	0.47	0.9–1.9
Pueschel et al., 2013	2	149	B & C	Slight slope (6 & 11%)	-0.5 (s)	579–1032	SS	Similar to Forsman and Alme, 2005 (neighboring difference in range image)	/	84–85	Circle fitting (+cor. with local linear diam. profile)	-0.07–0.51	1.39–2.43
							6 MS		/	/		0–0.32	0.64–1.15
Trochta et al., 2013	8	/	/	/	0.03–0.07 (p)	/	SS	Manual	88	/	/	/	/
							4 MS		94	/	/	/	/
Schilling et al., 2014	18	995	B p	/	0.07 (c.)	452–1160	>3 MS	Hough transform with disc + clustering + row filtering	/	/	/	/	
Mengesha et al., 2014	7	268	C	Slope (15%–25%)	0.07 (c.)	538–707	3 MS	Similar to [14]	/	80.7	/	/	/
	9	388				468–637	3 MS		/	86.2	/	/	/
Liang et al., 2014	1	46	C	Slope (15%)	0.2 (r.)	250	PLS	Similar to [54] for MSS	96	82.6	Cylinder fitting	1.1	5.06
Ryding et al., 2015	3	171	B	/	0.01 (s)	(2700–7900)	3 MS	Manual	/	/	Cylinder fitting	0.5	1.5
							HMLS		/	/			
This study	10	331 (202 m)	B & C (Co, EA & UEA)	Flat & slope	0.07 (c.)	113–1344	SS	Similar to [19]	83	75	Similar to [19]	-1.16	3.26
							5 MS		99.5	92.8		-0.17	1.16
							HMLS		99.5	89		-0.05	1.07

Appendix 3 – Supplementary information of the scientific paper of chapter 3: *A 3D approach to model the taper of irregular tree stems: making plots biomass estimates comparable in tropical forests*

Table S1: Characteristics of the species sampled for the 3D scanning (terrestrial photogrammetry or terrestrial laser scanning) in the three sites including the vernacular and scientific names, the number of trees (n), the mean and the range of the diameters (DBH¹, Dconvhull130, DPOM) and the height of measurement of the DPOM (HPOM). Bolded lines are the focal species. Apart from focal species, species with more than 5 sampled trees have the number of trees n in bold.

n° site	Site	Ver. name	Sc. name	n	Darea130 (cm)		DconvHull130 (cm)		Drom (cm)		Hrom (cm)	
					Mean	Range	Mean	Range	Mean	Range	Mean	Range
1	ALP	ALEP	<i>Desborderesia glaucescens</i>	1	34	[34-34]	119	[119-119]	32	[32-32]	158	[158-158]
1	ALP	AYOUS	<i>Triplochiton scleroxylon</i>	13	166	[78-229]	335	[224-462]	138	[66-203]	644	[400-983]
1	ALP	BETE	<i>Mansonia altissima</i>	2	62	[61-64]	171	[169-172]	60	[57-63]	229	[190-269]
1	ALP	CELTIS SP	<i>Celtis sp.</i>	2	78	[53-103]	232	[177-286]	69	[43-95]	552	[379-725]
1	ALP	DABEMA	<i>Piptadeniastrum africanum</i>	2	138	[123-153]	322	[302-342]	113	[103-123]	711	[597-824]
1	ALP	FRAKE	<i>Terminalia superba</i>	4	117	[98-137]	316	[292-376]	93	[77-105]	588	[470-791]
1	ALP	FROMAGER	<i>Ceiba pentandra</i>	3	194	[170-238]	394	[360-421]	166	[156-186]	793	[702-957]
1	ALP	ILOMBA	<i>Pycnanthus angolensis</i>	1	115	[115-115]	216	[216-216]	102	[102-102]	540	[540-540]
1	ALP	IROKO	<i>Milicia excelsa</i>	6	108	[87-129]	219	[190-257]	101	[81-123]	412	[282-529]
1	ALP	LONGHI	<i>Gambeya sp.</i>	1	91	[91-91]	199	[199-199]	85	[85-85]	260	[260-260]
1	ALP	MVANA	<i>Hyloidendron gabunense</i>	2	79	[51-107]	244	[171-318]	69	[43-96]	383	[288-478]
1	ALP	OHIA	<i>Celtis mildbraedii</i>	1	71	[71-71]	186	[186-186]	54	[54-54]	461	[461-461]
1	ALP	OKAN	<i>Cylicodiscus gabunensis</i>	1	124	[124-124]	226	[226-226]	119	[119-119]	253	[253-253]
1	ALP	PADOUK	<i>Pterocarpus sayauxii</i>	1	58	[58-58]	160	[160-160]	58	[58-58]	237	[237-237]
2	CIB	DABEMA	<i>Piptadeniastrum africanum</i>	20	110	[26-249]	187	[27-454]	91	[25-157]	506	[178-925]
2	CIB	OHIA	<i>Celtis mildbraedii</i>	15	77	[42-103]	110	[45-191]	68	[40-90]	371	[144-529]
2	CIB	OWOM	<i>Manilkara mabokeensis</i>	17	78	[44-136]	81	[44-151]	75	[44-115]	203	[128-503]
2	CIB	PADOUK	<i>Pterocarpus sayauxii</i>	18	65	[19-137]	89	[19-275]	57	[19-95]	362	[126-748]
2	CIB	SAPELLI	<i>Entandrophragma cylindricum</i>	18	148	[73-205]	180	[75-267]	126	[69-180]	494	[199-914]
2	CIB	TALI	<i>Erythrophloeum ivorense</i>	14	100	[74-135]	109	[76-143]	92	[71-123]	383	[224-550]
3	BIA	ACAJOU	<i>Khaya anthotheca</i>	1	62	[62-62]	64	[64-64]	61	[61-61]	147	[147-147]
3	BIA	AKO	<i>Antiaris toxicarpa</i>	8	64	[23-115]	78	[23-190]	54	[23-94]	296	[126-649]
3	BIA	ALOMBI	<i>Julbernardia seretii</i>	13	74	[17-124]	92	[17-204]	64	[17-102]	289	[127-557]
3	BIA	AVODIRE	<i>Turraeanthus africanus</i>	8	52	[38-71]	54	[39-75]	51	[38-69]	147	[129-201]
3	BIA	BOKONGOLA	<i>Pteleopsis hyloidendron</i>	1	44	[44-44]	45	[45-45]	44	[44-44]	127	[127-127]
3	BIA	DABEMA	<i>Piptadeniastrum africanum</i>	6	103	[58-137]	196	[73-307]	84	[55-113]	453	[169-603]
3	BIA	EMIEN	<i>Alstonia boonei</i>	11	73	[34-115]	110	[39-174]	62	[31-96]	578	[190-1170]
3	BIA	ESSESSANGE	<i>Ricinodendron heudelotii</i>	1	113	[113-113]	120	[120-120]	112	[112-112]	164	[164-164]
3	BIA	EVEUS	<i>Klainedoxa gabonensis</i>	1	47	[47-47]	57	[57-57]	44	[44-44]	176	[176-176]
3	BIA	IROKO	<i>Milicia excelsa</i>	1	77	[77-77]	77	[77-77]	77	[77-77]	212	[212-212]
3	BIA	KOSIPO	<i>Entandrophragma candollei</i>	2	143	[142-144]	208	[173-242]	122	[112-132]	398	[237-558]
3	BIA	KOTIBE	<i>Nesogordonia kabingaensis</i>	1	72	[72-72]	91	[91-91]	52	[52-52]	582	[582-582]
3	BIA	LONGHI	<i>Chrysophyllum lacourtauianum</i>	1	34	[34-34]	39	[39-39]	33	[33-33]	191	[191-191]
3	BIA	LUBOKO	<i>Parkia filicoidea</i>	2	90	[71-109]	157	[74-241]	85	[69-101]	324	[193-455]
3	BIA	OHIA	<i>Celtis mildbraedii</i>	10	68	[36-126]	91	[41-256]	59	[35-91]	383	[133-897]
3	BIA	OLOVONGO	<i>Zanthoxylum gillettii</i>	1	115	[115-115]	133	[133-133]	96	[96-96]	510	[510-510]
3	BIA	OSOMZO	<i>Trilepishum madagascariense</i>	8	40	[26-53]	45	[26-66]	36	[25-49]	219	[138-364]
3	BIA	PADOUK	<i>Pterocarpus sayauxii</i>	7	69	[38-120]	99	[38-282]	65	[38-98]	242	[129-568]
3	BIA	PENTACLETHRA	<i>Pentaclethra macrophylla</i>	1	41	[41-41]	41	[41-41]	38	[38-38]	191	[191-191]
3	BIA	STERCULIA t	<i>Sterculia tragacantha</i>	1	47	[47-47]	53	[53-53]	43	[43-43]	420	[420-420]
3	BIA	TOLA	<i>Prioria balsamifera</i>	1	140	[140-140]	140	[140-140]	139	[139-139]	135	[135-135]

Table S2: Taper models tested on irregular stems. The model selected as the reference model m in the study corresponds to Eq. 4.

Model	Formula	Comments
Eq. SI1	$Log(D_{Area,i}) = a \cdot (log(H_i) - log(H_{POM})) + log(D_{POM})$	Linear adjustment on the log-transformed variables $D_{Area,i}$ and height (H_i). The line is forced to cross the point $(log(H_{POM}), log(D_{POM}))$.
Eq. SI2	1) $D_{Area,i} = \frac{A}{(B+H_i)^b}$; 2) $D_{Area,i} = D_{ref} - K \cdot (L_i - H_{POM})$ With, $b = \frac{(B-H_{POM})K}{D_{POM}}$; $A = D_{ref} (B - H_{POM})^{\frac{(B-H_{POM})K}{D_{POM}}}$	A segmented equation with a rational function for the butt region of the stem and a linear function for the rest of the stem. The intersection between the two segments is the point (H_{POM}, D_{POM}) and the derivatives of the two equations are equals in this point. The vertical asymptote is located at $x=-B$ and the slope of the linear equation is K (i.e. the taper of the regular part of the trunk and expressed in m/m).
Eq. SI3	$D_{Area,i} = \frac{D_{POM}(H_{POM} + d)}{(H_i + d)}$	An homographic function $((ax+b)/(cx+d))$ with $a=0$ and $c=1$ and going through the point (H_{POM}, D_{POM}) .
Eq. SI4	$D_{Area,i} = \frac{D_{POM} H_i^a}{H_{POM}^a}$	The back-transformed equation of the log model Eq. SI1.

Table S3: Trunk metrics tested to predict the taper parameter a of the selected taper model (Eq. 2 and 3). The coefficients are unitless and have the advantage to include two measurements in one variable.

Trunk metric	Formula	Comments
Buttresses convex taper	$bct = \frac{(D_{conv hull 130} - D_{POM})}{(H_{POM})}$	We did not subtract the reference height of 1.3 m to H_{POM} in the denominator as it would lead to a division by zero for trees with $H_{POM} = 1.3$ m. A convex hull almost cylindrical at the stem base will have a bct close to zero and more the convex hull is conic more the value of the coefficient will be higher.
Slenderness coefficients	$h:d = \frac{H_{POM}}{D_{POM}}$	For the same H_{POM} , the coefficient decrease with higher D_{POM} while for the same D_{POM} , the coefficient increase with higher H_{POM} .
	$h:d^2 = \frac{H_{POM}}{D_{POM}^2}$	The coefficient decrease or increase less strongly than $h:d$.
	$h:d_c = \frac{H_{POM}}{D_{convHull 130}}$	For the same H_{POM} , the coefficient decrease with higher $D_{convHull 130}$ while for the same $D_{convHull 130}$, the coefficient increase with higher H_{POM} .
	$h:d_c^2 = \frac{H_{POM}}{D_{convHull 130}^2}$	The coefficient decrease or increase less strongly than $h:d_c$.
Hardiness coefficient	$hdn = \frac{\sqrt{D_{POM}}}{H_{POM}}$	Coefficient based on the hardiness coefficient concept of Vallet et al. (2007).
Deficit basal area index	$De_{BA} = 1 - \left(\frac{DBH'}{D_{perim 130}} \right)^2$	De_{BA} is equal to zero for a circular disc and tends to one as the cross-section becomes more irregular (Ngomanda et al., 2012)

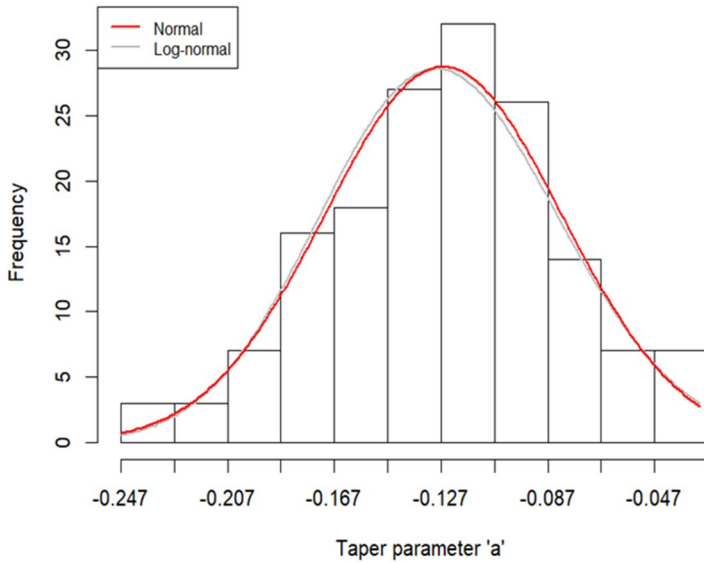
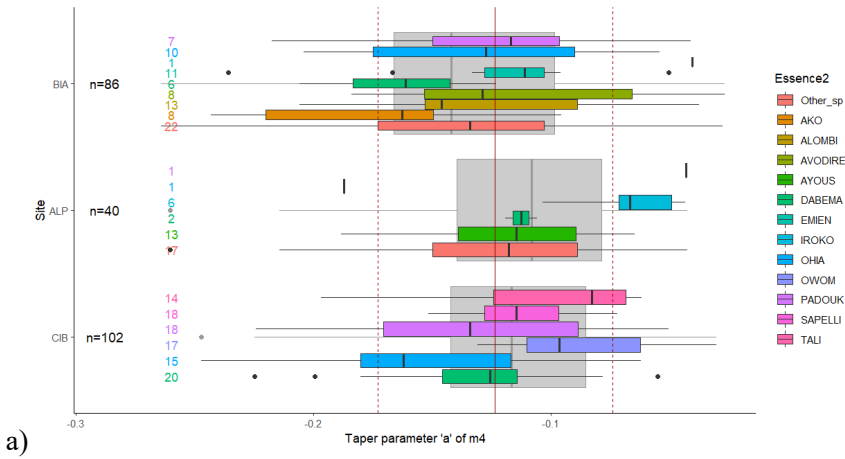
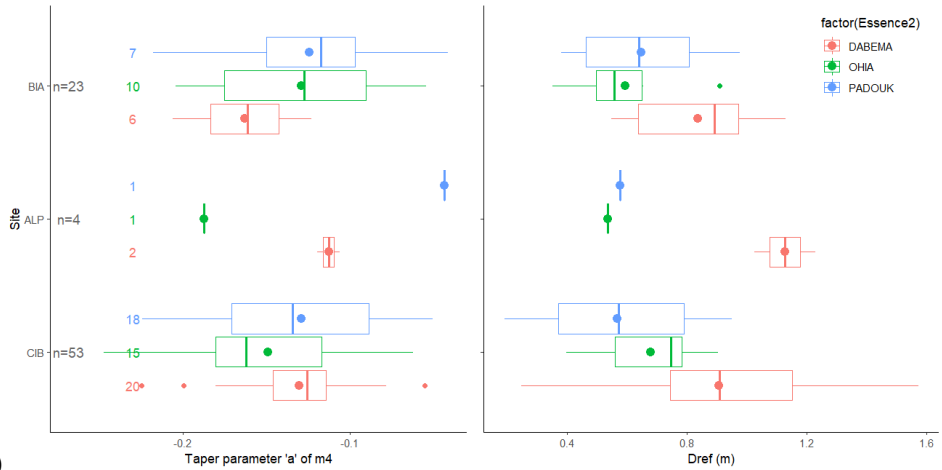


Figure S1: Distribution of the taper parameter a of the model based on Eq. 1. The null hypothesis of a distribution not normally distributed is rejected from the Shapiro–Wilk test.



a)



b)

Figure S2: Taper parameter 'a' of the model m (Eq. 1) among the species and sites (panel a). The vertical red line is the mean of 'a' for all sites and species and the vertical dotted lines are the standard deviation around the mean 'a'. Among the three common species of sampling Site BIA and CIB (panel b), no significant difference appears in the taper parameter ($P=0.06$, $df=10.2$ for Dabema; $P=0.4$, $df=18.7$ for Ohia and, $P=0.8$, $df=9.9$ for Padouk).

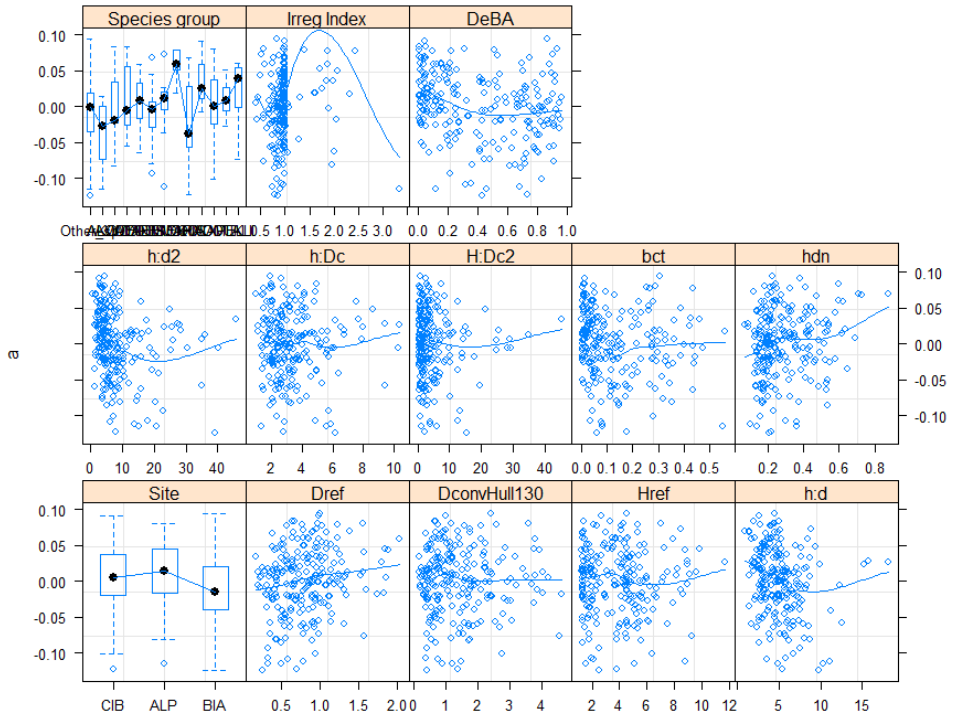


Figure S3: Estimated Random effects of different covariates in Eq. SI4 (or Eq. 2) adjusted without fixed effects. A loess smoother is included in the scatter plots of the continuous covariates to aid in visualizing possible trends.

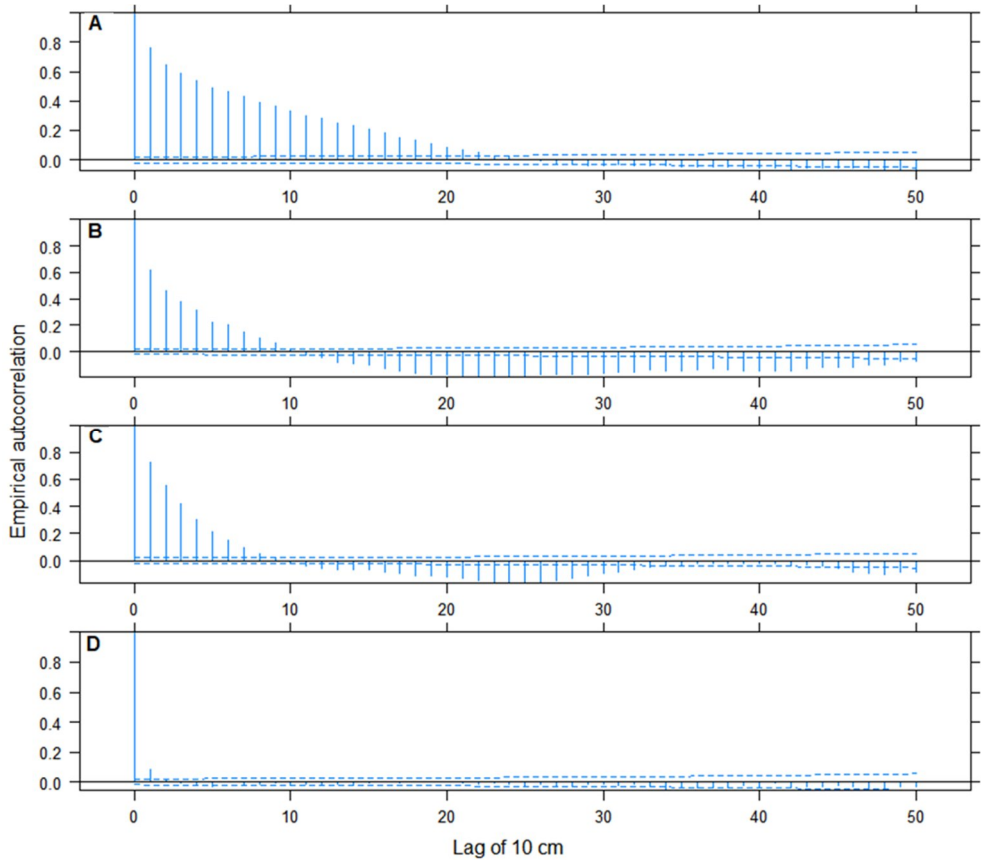


Figure S4: Empirical correlations against distance classes between height sections along the stem base for the four different runs of Eq2:

A. a nonlinear mixed-effects model run with no fixed effect, one random effect on tree, no variance weights and no correlation structure;

B. nonlinear mixed-effects model run with fixed effects and two nested random effects, no variance weights and no correlation structure;

C. nonlinear mixed-effects model run with fixed effects and two nested random effects, with variance weights and no correlation structure;

D. nonlinear mixed-effects model run with fixed effects and two nested random effects, with variance weights and an autoregressive correlation structure of order one.

Estimates of the parameters for each run were obtained using the method of maximum likelihood. Dashed lines represent the 95% confidence intervals under the null hypothesis H_0 : Autocorrelation is null.

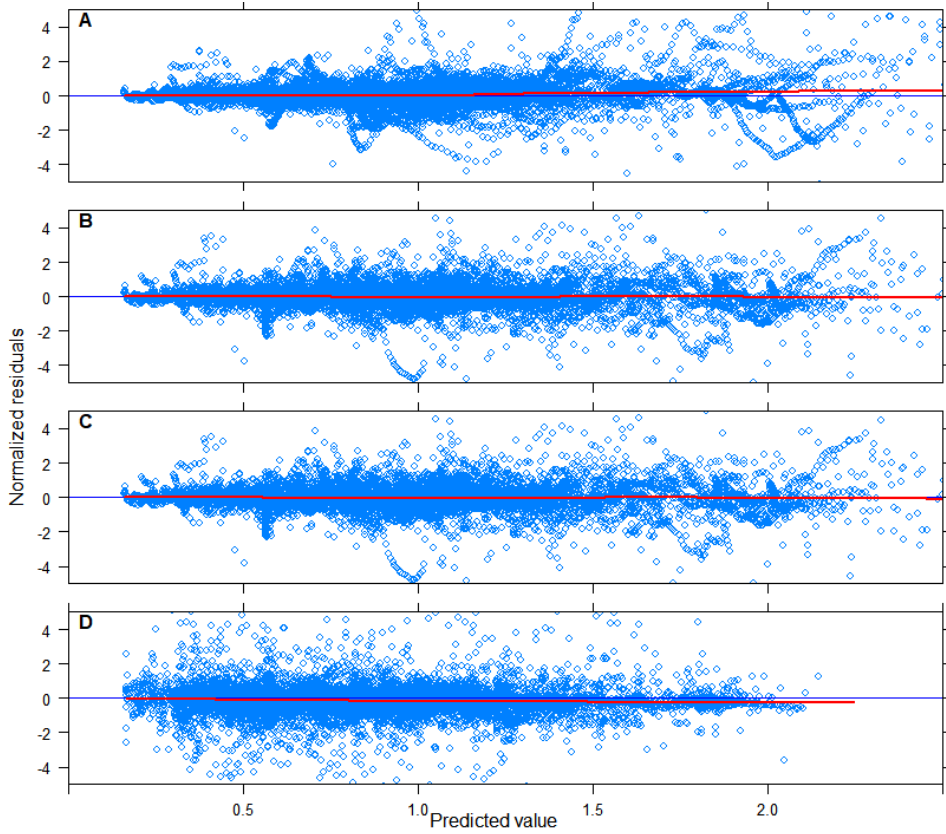


Figure S5: Residuals of the four different runs of models based on Eq.2.

A. a nonlinear mixed-effects model run with no fixed effect, one random effect on tree, no variance weights and no correlation structure;

B. nonlinear mixed-effects model run with fixed effects and two nested random effects, no variance weights and no correlation structure;

C. nonlinear mixed-effects model run with fixed effects and two nested random effects, with variance weights and no correlation structure;

D. nonlinear mixed-effects model run with fixed effects and two random effects, with variance weights and an autoregressive correlation structure of order one.

Estimates of the parameters for each run were obtained using the method of maximum likelihood. Note that the 99 percentile of the diameters Darea in the dataset is 2.2 meters.

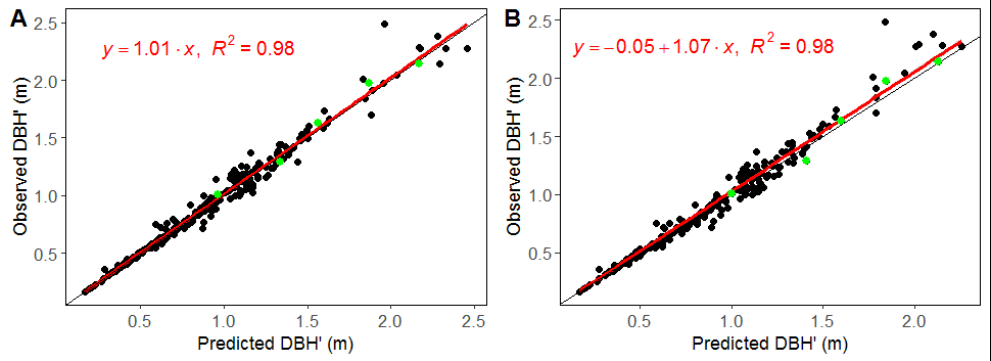


Figure S6: Comparison of the equivalent diameter at breast height (DBH') observed versus predicted for the model m1 (A) and m2 (B). The green dots are the five sample trees displayed in Fig. 4.

Table S4: Characteristics of destructively sampled species, including vernacular and scientific names, number (n) of sampled trees, mean and the range of the diameters (DBH/DBH' and D_{POM}), the height of measurement of the D_{POM} (H_{POM}), the total height (TH) and the basic wood density (ρ).

Ver. name	Sc. Name	n	DBH/DBH' (cm)		D _{POM} (cm)		H _{POM} (cm)		TH (m)		ρ (g/cm ³) ¹	
			Mean	Range	Mean	Range	Mean	Range	Mean	Range	Mean	Range
Angueuk	<i>Ongokea gore</i>	1	36	[36-36]	36	[36-36]	130	[130-130]	24	[24-24]	0.684	[0.684-0.684]
Assas	<i>Macaranga spp</i>	7	38	[15-54]	37	[15-53]	152	[130-236]	27	[18-36]	0.359	[0.314-0.423]
Ayous	<i>Triplochiton scleroxylon</i>	8	92	[25-215]	88	[25-208]	274	[130-597]	39	[24-53]	0.369	[0.315-0.43]
Diana_AF	<i>Celtis adolfi-friderici</i>	9	44	[18-74]	43	[18-70]	147	[130-230]	31	[20-37]	0.594	[0.544-0.666]
Ebom	<i>Anonidium mannii</i>	7	43	[19-72]	43	[19-72]	130	[130-130]	20	[0-27]	0.321	[0.292-0.357]
Fraké	<i>Terminalia superba</i>	9	56	[17-120]	50	[17-100]	248	[130-591]	32	[18-48]	0.446	[0.379-0.499]
Ilomba	<i>Pycnanthus angolensis</i>	8	48	[15-88]	47	[15-88]	137	[130-188]	27	[13-38]	0.406	[0.349-0.441]
Iroko	<i>Milicia excelsa</i>	3	72	[58-93]	70	[54-91]	178	[130-214]	38	[32-42]	0.59	[0.537-0.626]
Limbali	<i>Gilbertiodendron dewevrei</i>	30	50	[12-154]	50	[12-154]	130	[130-130]	31	[14-46]	0.673	[0.62-0.731]
Mubala	<i>Pentaclethra macrophylla</i>	8	52	[20-107]	52	[20-106]	158	[130-251]	29	[15-44]	0.75	[0.692-0.828]
Mukulungu	<i>Autranella congolensis</i>	6	118	[63-200]	118	[63-200]	145	[130-201]	45	[39-50]	0.75	[0.703-0.827]
Niové	<i>Staudtia kamerunensis</i>	8	54	[13-119]	54	[13-119]	130	[130-130]	33	[15-47]	0.627	[0.499-0.729]
Olen	<i>Iringia grandifolia</i>	8	58	[10-140]	56	[10-134]	189	[130-300]	30	[0-51]	0.756	[0.677-0.797]
Otungui	<i>Polyalthia suaveolens</i>	6	33	[14-50]	33	[14-50]	130	[130-130]	28	[14-39]	0.604	[0.541-0.649]
Padouk	<i>Pterocarpus soyauxii</i>	11	53	[18-110]	48	[18-101]	229	[110-600]	30	[17-41]	0.588	[0.496-0.661]
Sapelli	<i>Entandrophragma cylindricum</i>	11	80	[15-176]	76	[15-169]	198	[130-600]	38	[15-52]	0.531	[0.488-0.598]

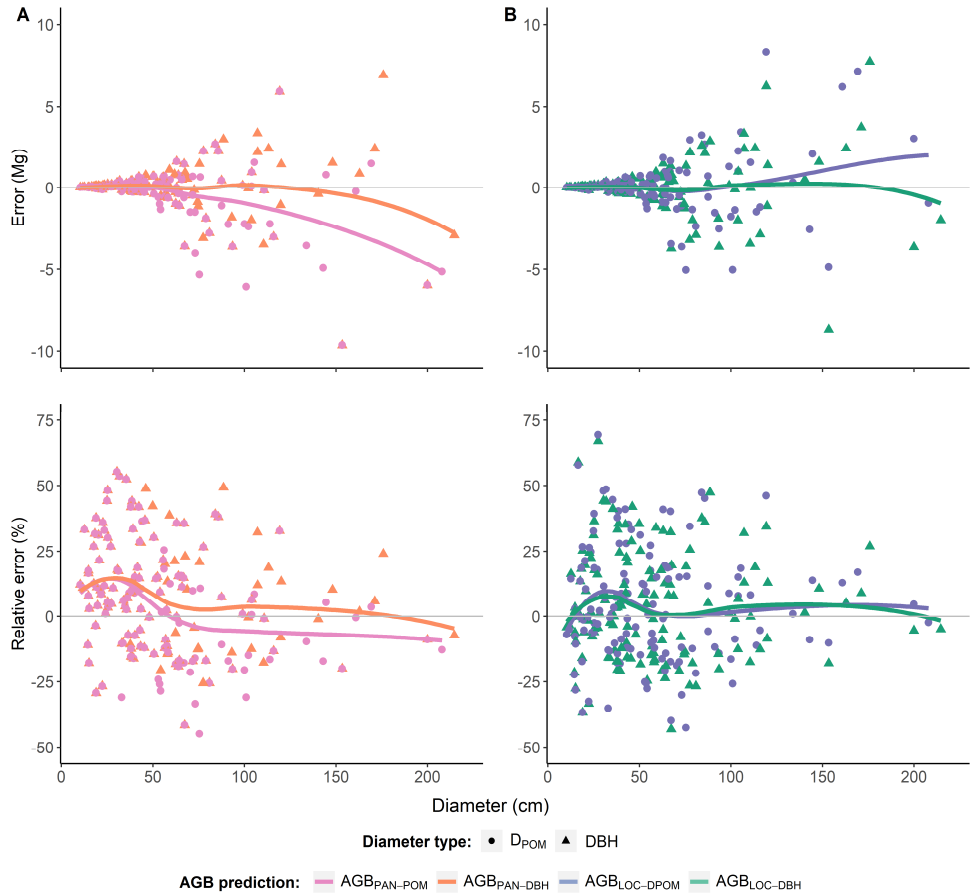


Figure S7: AGB predictions error from the two approaches with the PanTropical model m_{PAN} (A) and the two approaches with the local models $m_{LOC-DPOM}$ and $m_{LOC-DBH}$ (B) on 140 trees from Congo. Tree AGB predictions and associated errors were computed using D_{POM} (pink) or DBH (orange) as the diameter predictor in the PanTropical model. Local AGB models were fitted with D_{POM} for the model $m_{LOC-DPOM}$ and with DBH for $m_{LOC-DBH}$. Tree AGB predictions and associated errors were computed using D_{POM} (blue) or DBH (green) as the diameter predictor for respectively $m_{LOC-DPOM}$ and $m_{LOC-DBH}$.

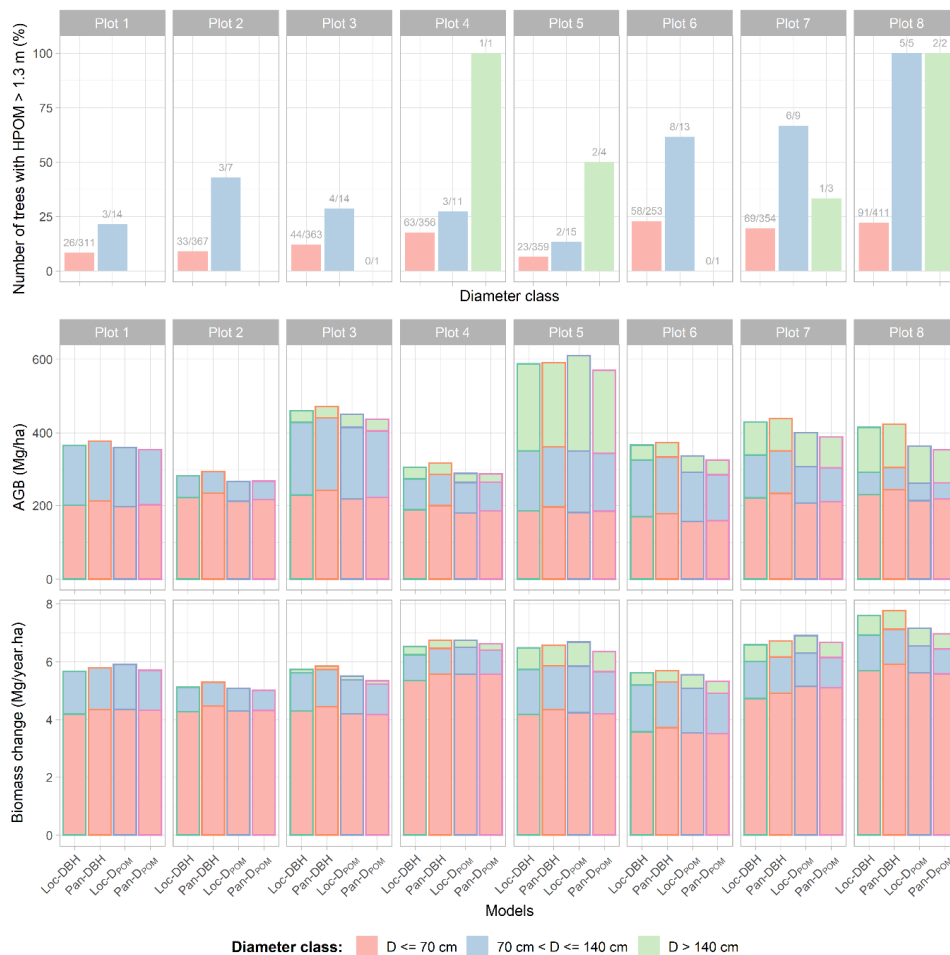


Figure S8: Characteristics of the eight forest inventory plots ordered by increasing contribution of trees with $H_{POM} > 1.3$ m to total plot basal area.

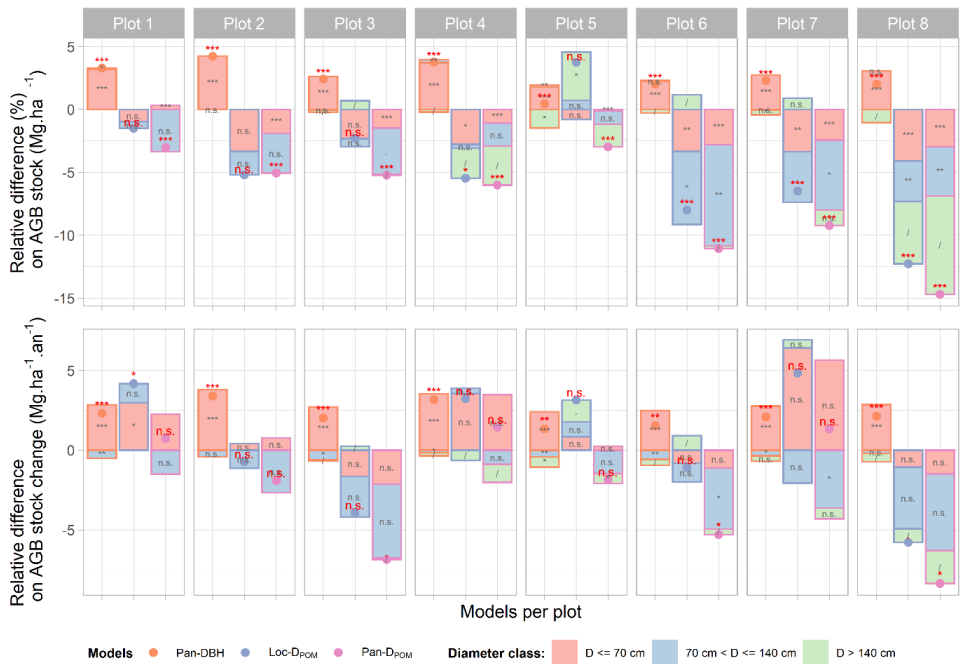


Figure S9: Relatives error of the three alternative approaches in comparison to the reference approach (i.e., Loc-DBH). In red, the results of the paired tree-level t-test at the plot level and in grey, the t-test results per diameter class. The colors of the border of the bars are related to the approach: Orange, for the model Loc-DBH; Blue, for the model Loc-D_{POM} and; Pink, for the model Pan-D_{POM}.

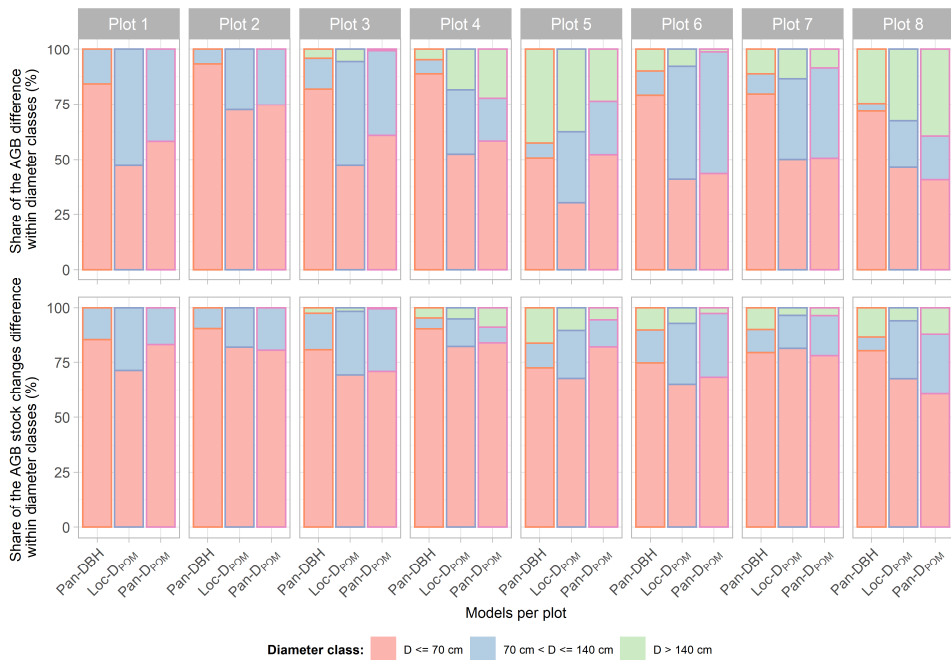


Figure S10: The share of the total absolute difference between the diameter classes for AGB estimates with the three alternative approaches compare to the reference approach Loc-DBH.

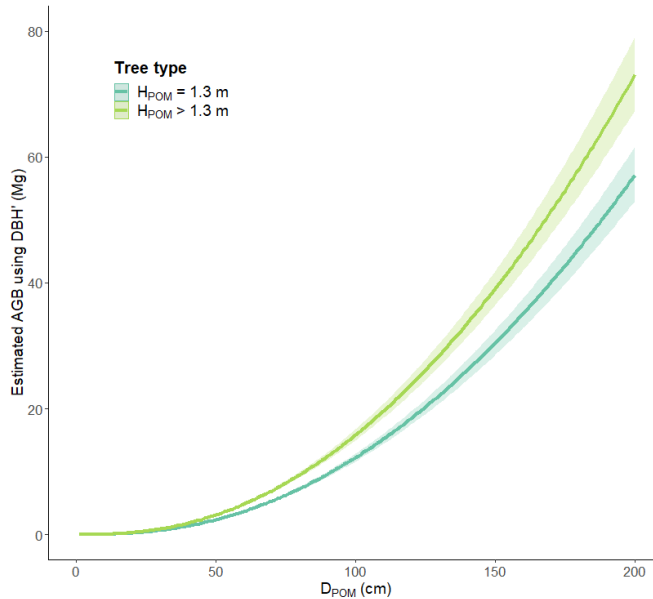


Figure S11: The increasing AGB of two virtual trees with the same D_{POM} according to the increasing size of the tree diameters D_{POM} over time. The first virtual tree has a constant POM at 1.3m height, D_{POM} is then equal to the diameter at breast height, DBH (dark blue- green) and, the second virtual tree have its POM raised through the time (light green). For this later virtual tree, the equivalent diameter at breast height (DBH') is 12 % higher than D_{POM} (slope of the linear regression DBH'- D_{POM} without intercept fitted on the trees with $H_{POM}>1.3.m$ of the Congolese plots of this study). The AGB are estimated with the mLoc-DBH model with a basic wood density of 0.57 g.m^{-3} for both.

